COMMERCIAL IN CONFIDENCE

Foundation Loads and Performance of Different Flap Widths

Document No: AMPL-OY02-H5006-RPT-R01

REVISION RECORD SHEET

Rev	Date		Prepared by	Checked by	Approved by
1.0	25-11-2008	Name	APL	APL	APL
X1	15-02-2021				WES
		Signature			

Table of Contents

1. Preliminaries 4
2. Performance 8
3. Foundation Loads 12
4. Extreme Value Analysis 20
5. Summary 22
Bibliography 23
APPENDIX A: Scatter plots-9 meter wide flap 24
APPENDIX B: Scatter plots-12 meter wide flap 31
APPENDIX C: Scatter plots-18 meter wide flap 37
APPENDIX D: Scatter plots-24 meter wide flap 43
APPENDIX 1: Return Period-9 meter wide flap 49
APPENDIX 2: Return Period-12 meter wide flap 55
APPENDIX 3: Return Period-18 meter wide flap 61
APPENDIX 4: Return Period-24 meter wide flap 67

1. Preliminaries

This document reports on the results obtained from tank test experiments performed in QUB on the foundation loads and performance of a 40th scale Oyster device of varying width. Four widths were investigated which are 9, 12, 18 and 24 meters. The information in this document primarily reports the results of the experiment. However, some issues relating to the behaviour of the model device and experimental events are discussed so that the results are interpreted correctly. A report on the calibration and accuracy of the foundation load rig can be found in (1).

For all four flap widths the remaining dimensions are as follows (Full Scale (FS) dimensions):

- Flap thickness = 1.8 meters.
- Flap height = 10.58 meters.
- Hinge height = 4 meters.
- Water depth = 13 meters.

Note: Froude Scaling is employed to convert from FS dimensions to Model Scale (MS). The model is situated on a flat "sea bed" which is at the end of a 1:24 slope and in all tests the model is orientated perpendicular to the direction of the incident waves.

It is important to know the pitch stiffness k_p, of each flap as it has a strong influence on the flaps dynamics. Pitch stiffness is a measure of the restoring moment acting on a flap due to the combined effects of buoyancy and weight. There are variations in how the pitch stiffness is determined and applied when modelling the device motion. In general, this restoring moment is a nonlinear effect which varies with the sine of the rotation angle (in a similar manner to the restoring effect of gravity on a standard pendulum). However, one way of simplifying the equation the motion of the device is to model the flap as a linear spring/pendulum, i.e $\sin(\theta) \approx \theta$, which holds valid for small angles of rotation. This expression is accurate to within 5% for an angle of 30° which is often taken as cut-off point for this assumption. By modelling the restoring moment in this way (i.e $ksin(\theta) \approx k_p\theta$) the pitch stiffness acts like a spring constant and is measured in Nm/radian. Beyond the small angle approximation the units and application of pitch stiffness must be modified. Even with the small angle approximation imposed, complications still arise in determining a value for pitch stiffness due to varying freeboard (portion of the flap above the water level) over a wave/flap rotation cycle. Equation (1) is a general expression for the pitch stiffness of an Oyster device where the small angle approximation is not assumed

$$k_p = \frac{1}{2} g(\rho w t(h - f(\theta))^2 - mh)\frac{\sin(\theta)}{\theta} \quad (1)$$

Here, m, w, t and h denote the flaps mass, width, thickness and height from the pivot respectively. The density of water and gravitational acceleration are given by ρ and g and $f(\theta)$ is the variable freeboard which is given by

$$f(\theta) = h - \frac{d}{\cos(\theta)} \quad (2)$$

where d is the still water depth above the pivot. For simplicity it has been assumed that the flap is a rectangular box and the mass and buoyancy are distributed uniformly so that the centre of mass and buoyancy are located at half the flap height and submerged height respectively. The expression for pitch stiffness given in equation (1) is not entirely valid. The reason for this is that pitch stiffness measured in Nm/radian is only applicable to a linear spring/pendulum model whereas equation (1) describes different nonlinear dynamics. Thus the small angle approximation must be imposed which gives

$$k_p = \frac{1}{2} g(\rho w t(h - f(\theta))^2 - mh) \tag{3}$$

Note, equation (3) is not modified by the small angle assumption, as a simple approximation for $\cos(\theta)$ cannot be achieved to the same accuracy for the same range of angles.

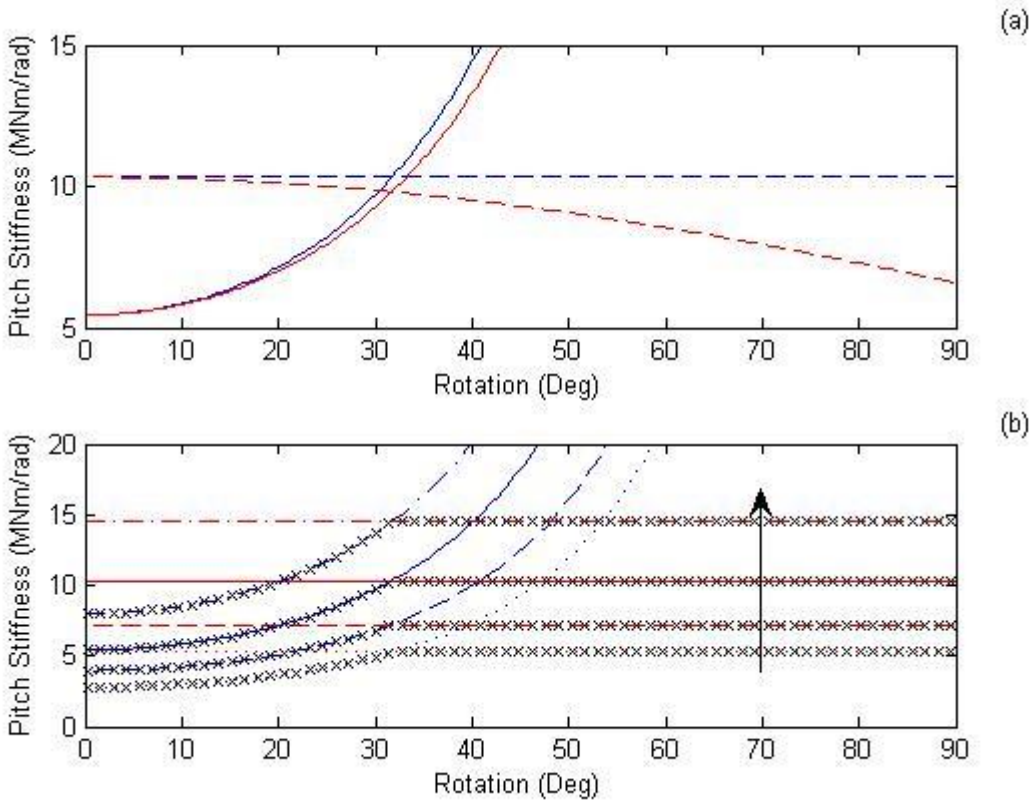

Figure (a): Linear (blue) and nonlinear (red) pitch stiffness for the 18 meter wide device. (b) Linear pitch stiffness for the four flap widths where the arrow indicates increasing flap width.

Figure (a) shows the difference between equations (1) (red) and (3) (blue) for an 18 meter wide flap. The solid lines are for a water depth of 13 meters which results in a freeboard of $f(0) = 1.58$ meters for this particular device configuration. The dashed lines are obtained by assuming that the device is completely submerged. As would be expected, these two scenarios coincide at the critical angle of $\theta_{crit} = cos^{-1}\left(\frac{d}{h}\right)$ beyond which the freeboard is held fixed at $f(\theta) = 0$, (negative freeboard is

irrelevant). It is interesting to note that for this particular device configuration the critical angle is $\theta_{crit} \approx 31^o$ which is close to the estimated limit of the small angle approximation. The maximum pitch stiffness achieved when fully submerged is 10.33 MNm/rad which compares well with actual pitch stiffness of 9.779 Mnm/rad, calculated from each component of the MS flap and is documented in the Excel spread sheet (2). In the nonlinear fully submerged case (red-dashed line) the reason why the pitch stiffness decreases is due to the $\frac{\sin(\theta)}{\theta}$ term in equation (1) which, as highlighted earlier, should not be interpreted in the same way as linear pitch stiffness. Figure (b) shows the pitch stiffness (linear) behaviour for the four different flap widths. The black crosses (x) indicate the pitch stiffness experienced by the device making the transition from a flap with nonzero freeboard to fully submerged.

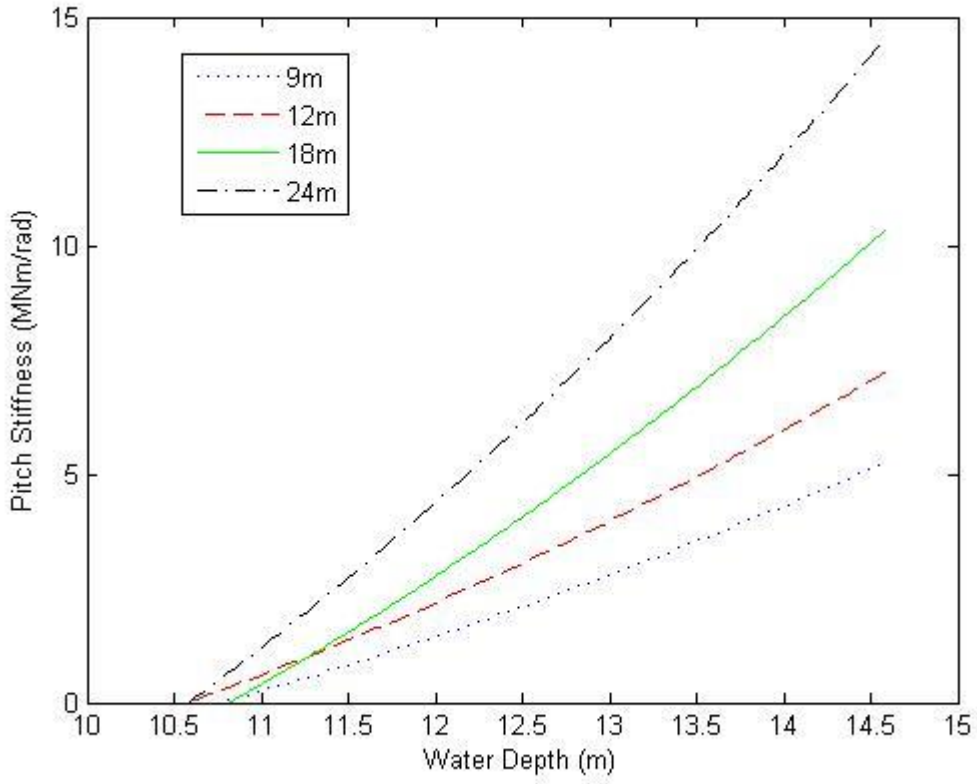

Figure (c): Variation of pitch stiffness with water depth for an approximately vertical flap.

An interesting feature of the pitch stiffness behaviour is the large difference between a flap which is fully submerged and one with maximum nonzero free board. This motivates the investigation of how the pitch stiffness varies with water depth, where a very small angle ($\theta \ll 1$) is assumed so that equation (3) holds valid. Figure(c) shows the variation of pitch stiffness with water depth for each of the four flap widths. Each flap is fully submerged just over 14.5 meters water depth giving the maximum pitch stiffness. If the water depth drops below 10.5 meters the weight of each device actually starts to dominate. Finally it can be seen that the curves associated with the 24 and 18 meters wide flaps actually cross over the narrower 12 and 9 meter ones. This is due to the relative difference in displaced volume and weight of each flap as the moment arm is the same for each flap for a particular water depth.

Pitch Stiffness (MNm/rad)	9m	12m	18m	24m
13 m mean water depth	2.8	4.0	5.5	8.0
Flap fully submerged	5.3	7.2	10.3	14.5

Table 1. Pitch stiffness for each of the four flap widths at a water depth of 13m and fully submerged > 14.58m.

When analytically/numerically modelling the motion of the Oyster device, constant pitch stiffness is often assumed which is usually defined for either the mean water depth or fully submerged scenarios, see Table 1. However, this is quite an over-simplification of the dynamics and care must be taken when interpreting results based on such an assumption.

2. Performance

Firstly the performance of each flap width is investigated. Six performance sea states are used in the tests which are derived in (3). These are based on the 9 year wave climate given in the RPS report (4). The performance seas used are

	Sea State	Energy Period T(s)	Wave Height H_s (m)	Incident Wave Power (kW/m)	Weighting Factor
Performance	1	6.7	1.18	5.43	0.25
	2	8.8	2.85	40.67	0.09
	3	9	1.13	6.53	0.3
	4	9	3.7	69.61	0.05
	5	11.4	1.64	15.6	0.24
	6	11.5	3.25	61.16	0.07

Table 2. Six Performance sea states.

For each sea state, a device will have an optimum damping torque (which is produced on the 40th scale model by a clutch brake) where the power captured is maximum. However, during the analysis only one constant global damping value was used for all six sea states. This global damping is determined from a weighted average of the optimal damping values, where the weighting factors are those given in Table 2. Six Performance sea states. The damping values and power capture calculations are given in the Excel spread sheet (5). Note that all damping torque values reported are RMS values, thus the actual damping torque amplitude will be larger. Figure 1 gives the global RMS damping values calculated for the four different flap widths.

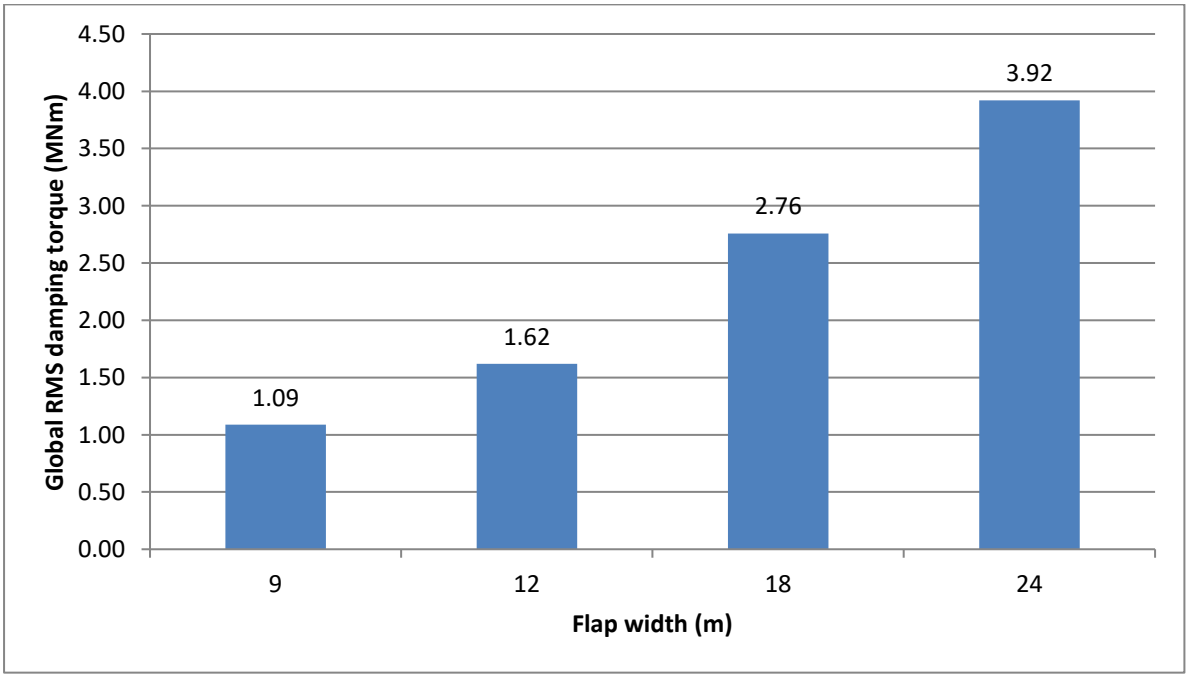

Figure 1. Global RMS damping values.

For the 40th scale model the damping torque is applied on the 9 and 12 meter flaps by a single clutch brake and on the 18 and 24 meter flap by a pair of clutch brakes. There is a limit as to how tight these

brakes can be adjusted, thus there is a limit on the damping which can be achieved. Also, for a fixed "clutch tightness" there is a slight variation in the actual damping torque achieved in different sea states. Thus it is difficult to achieve a required constant global damping value in all sea states.

Another issue which should be highlighted before the results are given is an effect called backlash. This is where the flap can rotate freely before the clutch brake engages. There are two possible sources of this effect. The first is a slight looseness in the clutch brakes used (which is intrinsic property of their design) which results in a backlash of about 2°. A second source of backlash is from the connection between the clutch brake and torque transducer. The effect of backlash is hard to eradicate completely and can increase causing free rotation of up to 6°-8° if the model is consistently used in large seas. During the testing this second source of backlash was resolved by pinning the clutch brake and torque transducer. Figure 2 shows the typical effect of backlash on the damping torque signal. This shows that when the flap changes direction it actually rotates freely (zero torque signal) for a period of time before the clutch brake engages, which creates a step the square wave profile expected from a constant damping system. This effect will be reflected in a smaller RMS damping torque value than an equivalent square wave profile. In larger sea states the effect of backlash on the results is diminished as the flap rotates through larger angles. However, in smaller sea states this effect is more prominent as the angle of rotation of the flap is smaller. For the 18 and 24 meter flaps two clutch brakes are required to provide the desired damping with the total damping torque being the sum of both. Figure 3 (a), (b) shows a typical torque trace using two clutch brakes and the total torque experienced.

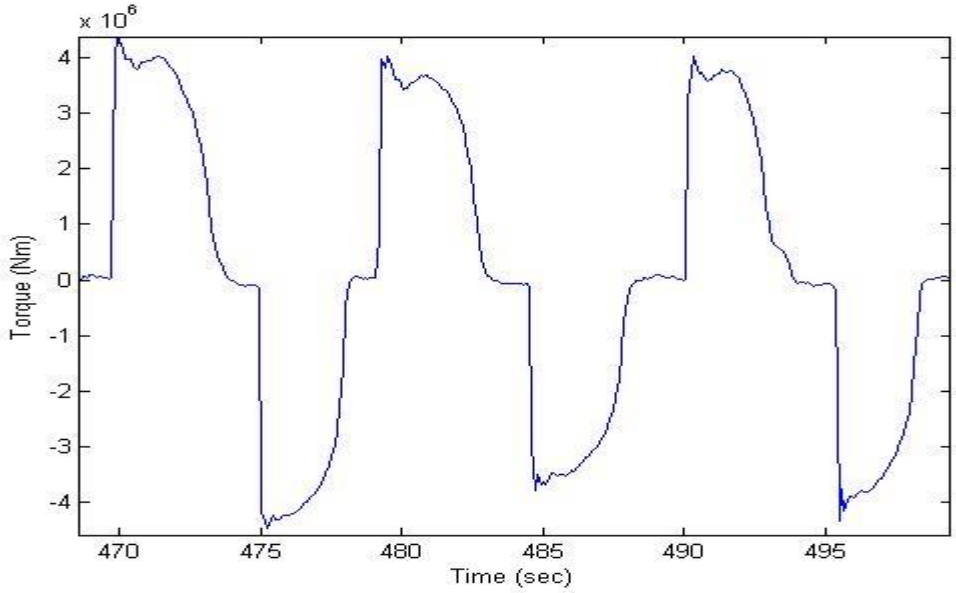

Figure 2. Torque signal from the 40th scale model showing the effect of backlash.

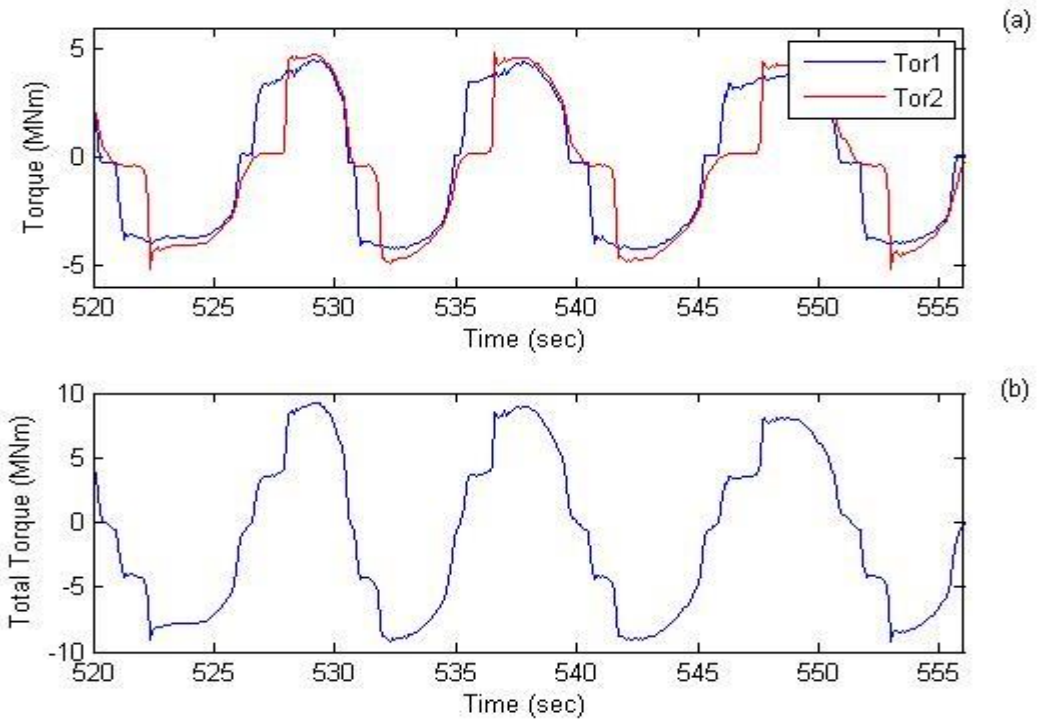

Figure 3. (a) Individual torque signals. (b) Total torque equal to the sum on the individual signals.

With these issues highlighted, the average power capture and capture factor are now reported for each flap width and are shown in Figures 4 & 5. The percentage power losses from using global damping instead of optimal damping are 6.7%, 5.9%, 12% and 10.5% for flap widths of 9, 12, 18 and 24 meters respectively. Indicating that imposing a single global damping has a considerable effect.

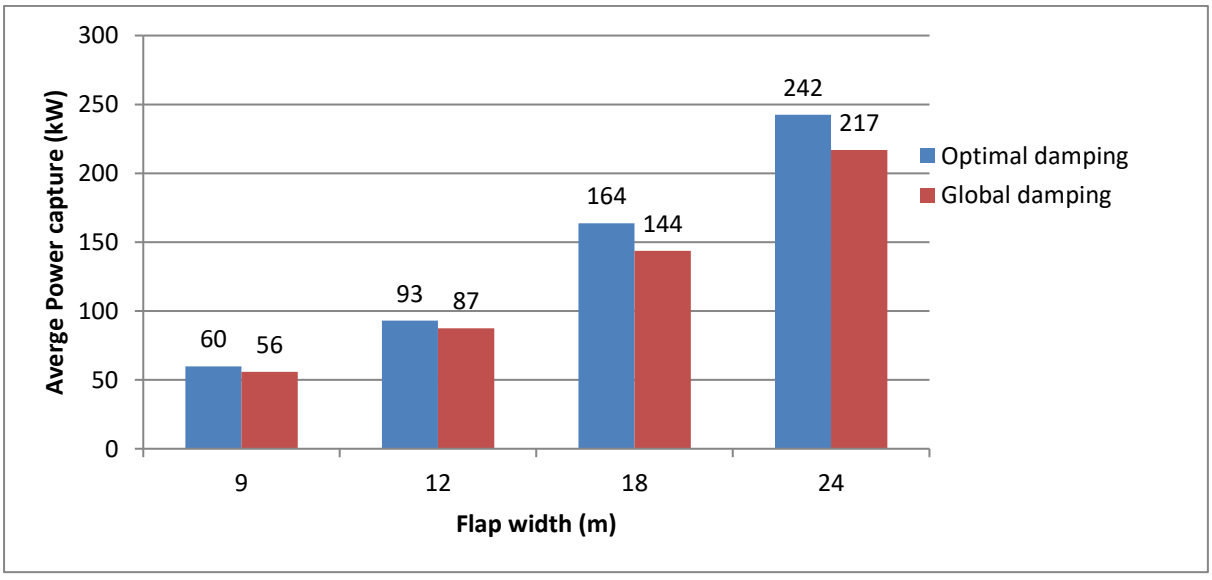

Figure 4. Average power capture set at optimal and global RMS damping values.

The capture factor $CF\ is$ determined from the equation

$$CF = \frac{P_C}{w\, P_i}$$

where P_i and P_C are the incident wave power and average power captured respectively and w is the width of the flap.

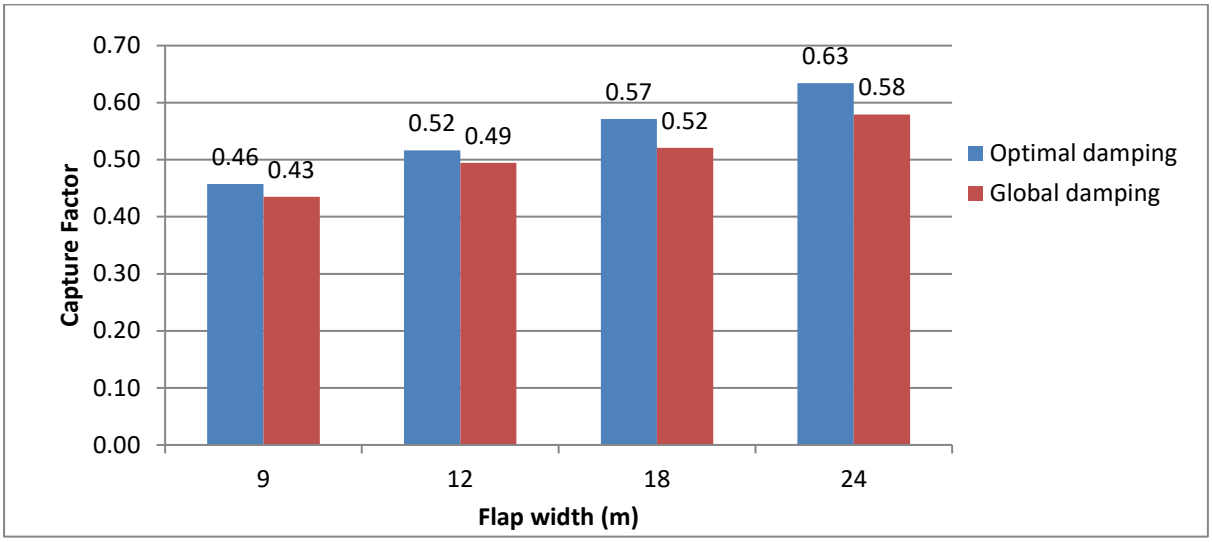

Figure 5. Capture factor for four flap widths using both optimal and global RMS damping values.

3. Foundation Loads

Foundation loads on the device in extreme seas are determined using a six degree of freedom elbow rig. A description of the operation, calibration and accuracy of this load rig is given in (1). The results of these tests report the loads at the hinge/pivot point for each flap width which is both damped (using the global RMS damping value for that width) and undamped. From (1) the error estimate on the surge load is (maximum) 10%, a (maximum) 5% error in heave with the error on the other loads typically less than 3%. It should be noted that the static load of the device in still water has been subtracted from all the foundation results. So essentially the load values reported are those generated purely by the wave motion. The sign convention of the foundation loads is shown in the diagram below where the moments follow a right hand rule about their complimentary positive force axis.

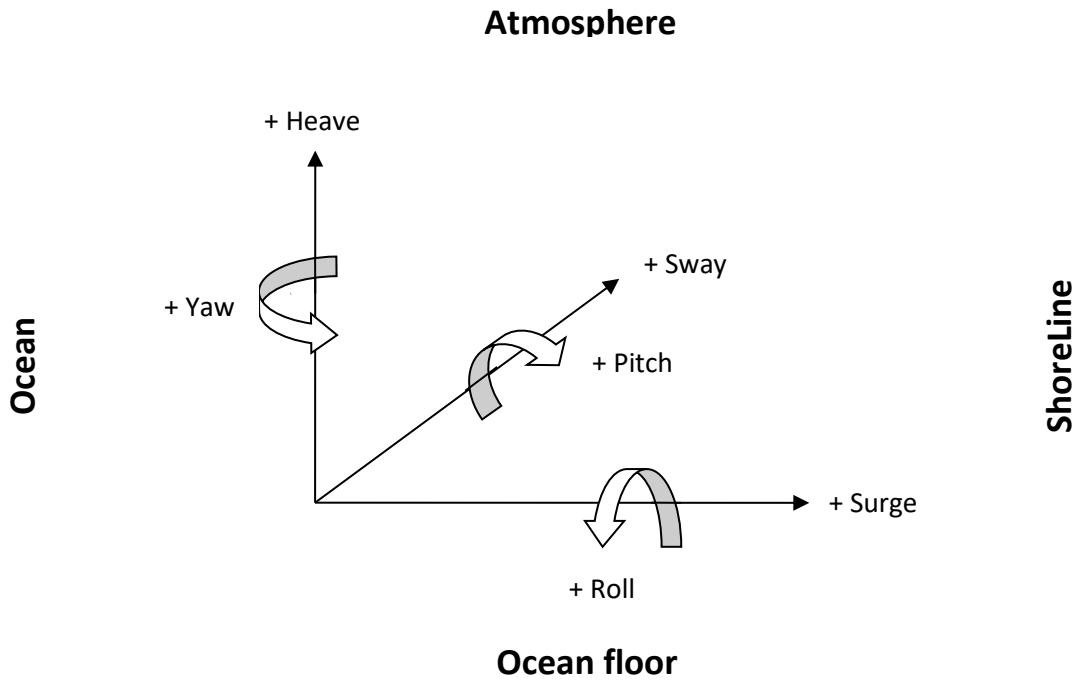

A different set of six long-crested Bretschneider extreme seas are used for the foundation load tests, these are

	Sea State	Energy Period T(s)	Wave Height H_s (m)
Extreme	1	9	10
	2	11	10
	3	13	8
	4	13	10
	5	15	8
	6	15	10

Table 3. **Extreme sea states used for the foundation load tests.**

A discussion on the selection of this set of seas is discussed in (6). The FS significant wave heights reported in Table 3 are the demand wave heights which are slightly above what is achievable in the

experimental tank. The calibration of these waves was done in deep water, so that essentially at the model location (13m water depth) these wave break due to shoaling effects. Wave breaking onto the device is predicted to cause the largest foundation loads and so this set of sea states should capture a large range of extreme foundation load events. Each sea state test is run for a FS time of approximately 3.6 hours (2048 seconds MS). Thus the total test length of one flap width is approximately 21.6 hours FS. The wave climate data given in (4) shows that the average number of hours of extreme sea conditions (waves with significant wave height above 6 meters) per year is approximately 27, with more than half of these hours coming from wave with a height less than 7 meters. Thus the experimental testing of 21 hours at larger sea conditions could be used as a rough estimate of the storm conditions the device may encounter on average in a year. It should also be noted that each extreme sea state used is given the same weighting factor, whereas in reality the smaller seas states are more common.

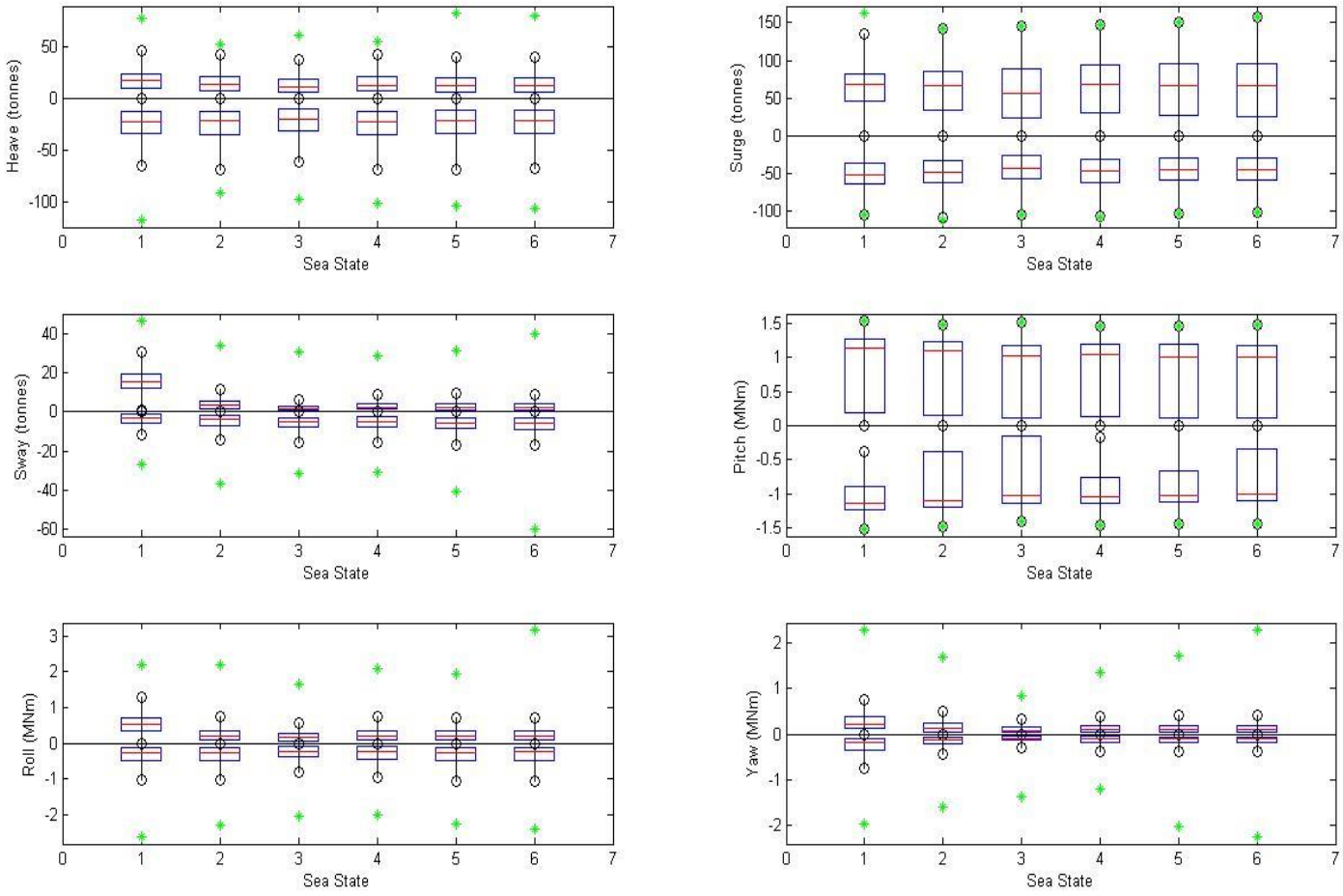

Figure 6. **Foundation loads of the 9 meter damped flap in each extreme sea state.**

Appendices A-D show the scatter plots of the foundation loads for each flap width in each of the 6 extreme sea states. The red data points correspond to an undamped flap and the blue points are for a damping torque approximately set to global damping value. (Note that the actual global damping

calculated each time varies slightly from sea to sea even though the clutch brake settings are the same). The average global damping values achieved for each flap are given in Table 44.

Global Damping (MNm)	9 m	12 m	18 m	24 m
Required	1.09	1.62	2.76	3.92
Achieved	0.77	1.13	2.07	3.32

Table 4. Required global damping values and those achieved during extreme sea testing.

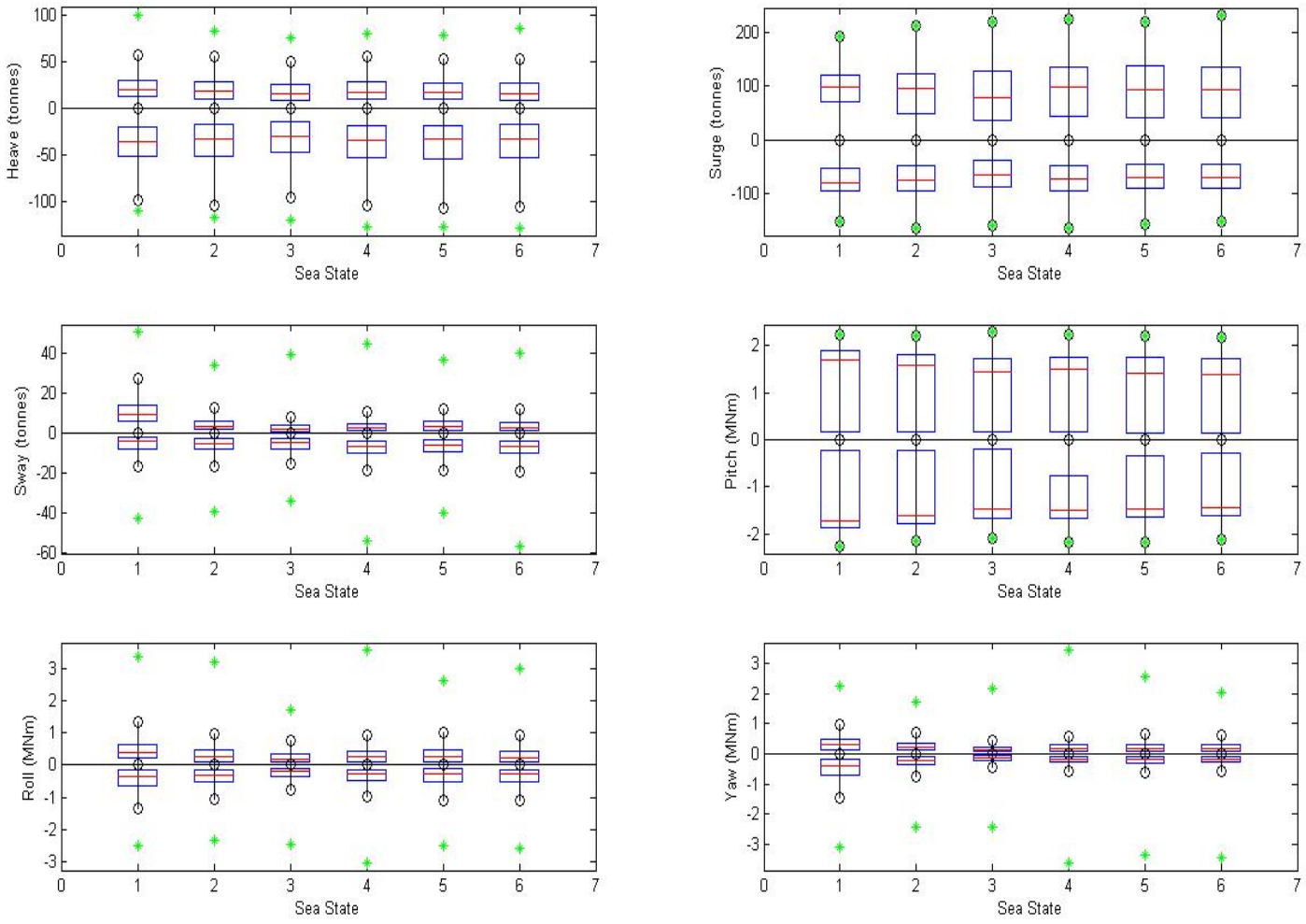

Figure 7. **Foundation loads of the 12 meter damped flap in each extreme sea state.**

Table 55 below gives the maximum angle of rotation (from the vertical) for each flap width recorded during the tests. Positive rotation is towards the beach which is consistent with the sign convention used for the pitching moment.

Max rotation	9 m	12 m	18 m	24 m
Damped	+70° to -70°	+64° to -70°	+61° to -73°	+65° to -72°

Undamped	+67° to -74°	+70° to -75°	+64° to -78°	+66° to -80°

Table 5. Amplitude of rotation from the vertical.

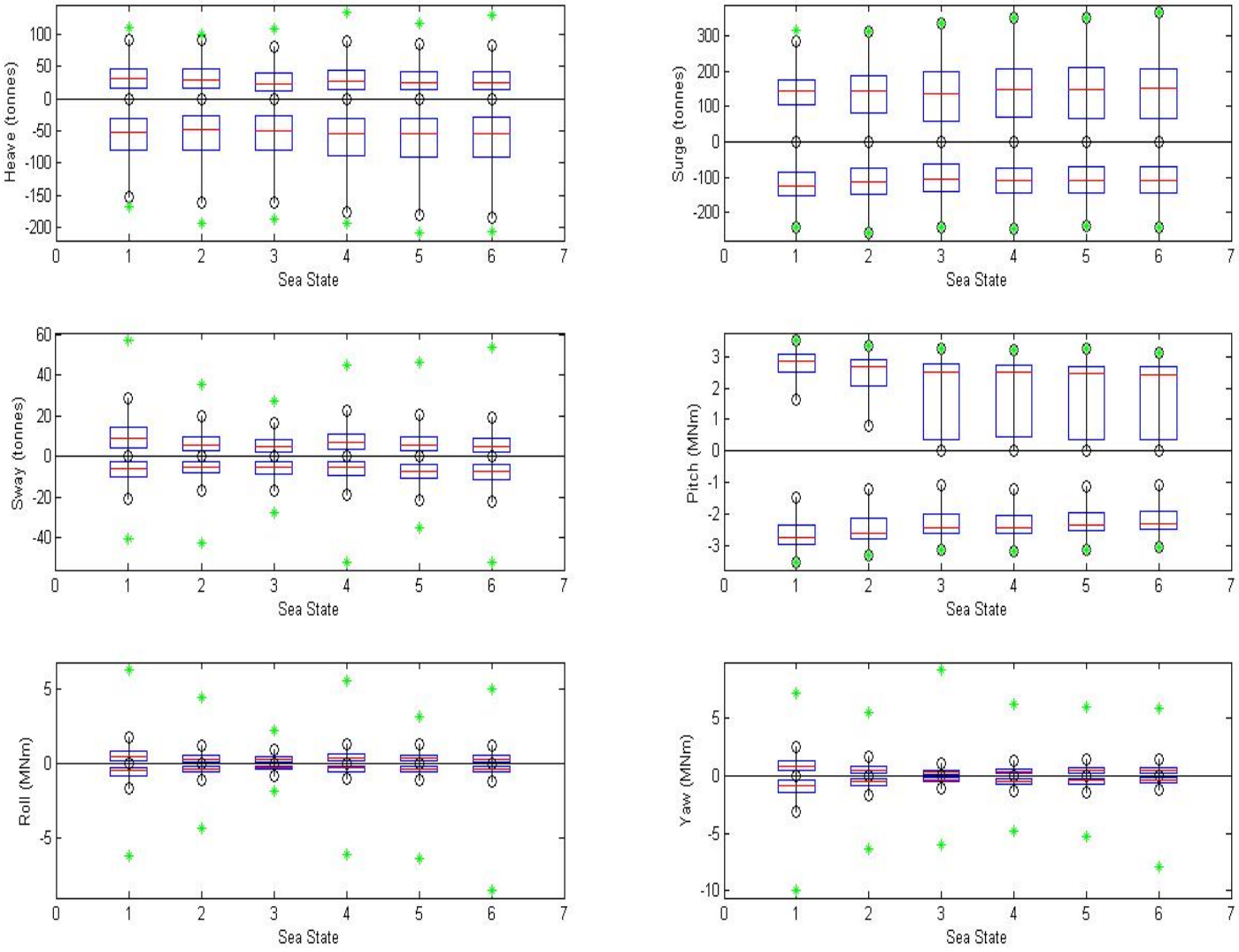

Figure 8. Foundation loads of the 18 meter damped flap in each extreme sea state.

The box plots shown in Figures 6-9 are an additional way of displaying the foundation load results and they are constructed as follows: For each sea state the foundation loads are split up into positive and negative sets. Only peak load events are selected and arranged in ascending order of magnitude. The horizontal red line is the median of the set and the lower and upper ends of the blue boxes are the first (Q_1) and third (Q_3) quartiles, indicating the 25 and 75 percentile levels respectively. The vertical black lines which terminate with an 'o' symbol, define the range outside of which the data points are considered outliers. This range extends from $Q_1 - 1.5(IQR)$ to $Q_3 + 1.5(IQR)$ where IQR is the Inter-Quartile Range defined as the 'distance' between the first and third quartiles, i.e $IQR = |Q_3 - Q_1|$.

The maximum positive and minimum negative outliers for each foundation load in each sea state is denoted with a green asterex (∗). The box plots give an indication of the distribution of the peak foundation loads and also show the scatter of extreme loading events represented by the asterex. The extreme load events are of paramount importance to the foundation analysis as they are an indication of the loads that a device must be able to withstand in the most extreme sea conditions.

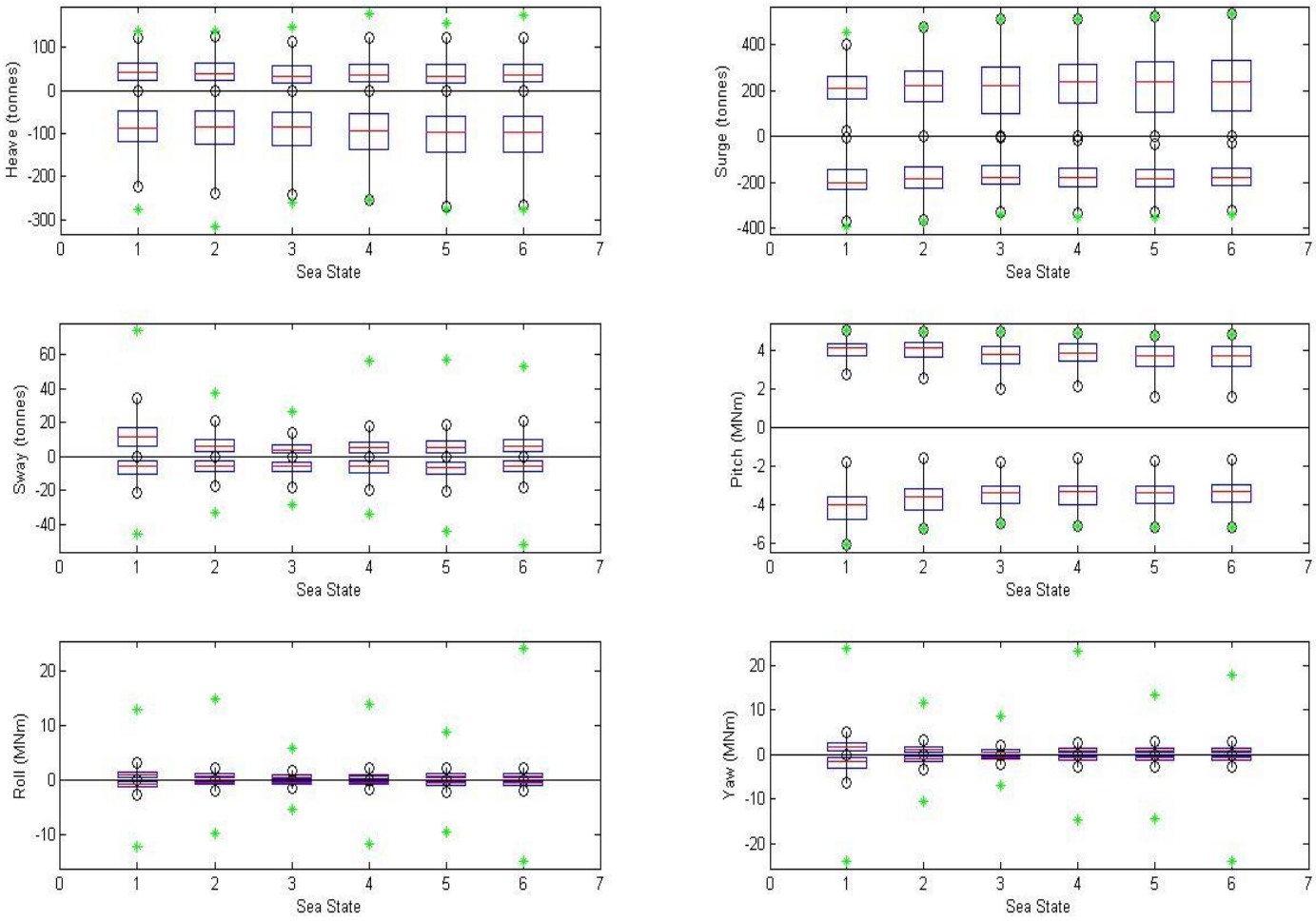

Figure 9. **Foundation loads of the 24 meter damped flap in each extreme sea state.**

Selecting the largest extreme event (outlier) out of all the sea states gives an estimate of the typical load that the device must withstand. However, the data recorded represents only a finite period of storm conditions and there is no guarantee that during this period the combination of conditions that result in maximum loads have occurred. An alternative method of predicting the maximum loads that may occur is discussed in Section 4: Extreme Value Analysis. Although the testing period is finite we can still gain some insight by examining the largest extreme loading event which occurred during the test. Coincidence load tables for each flap width are given in the Excel spread sheet (7). These tables display, for each sea state, the magnitude of the remaining five foundation loads when one reaches its maximum.

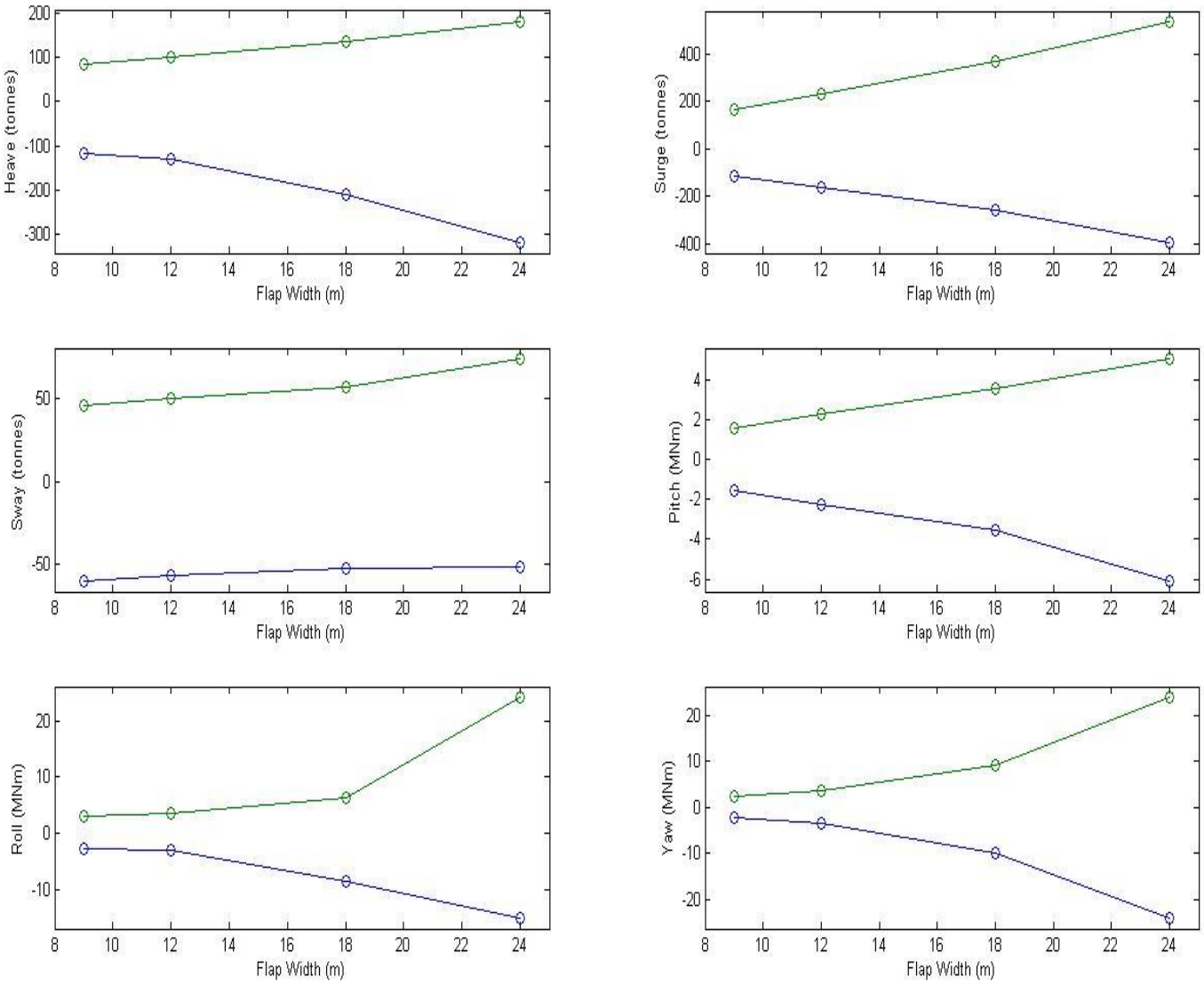

Figure 10. **Variation of the largest extreme loads with flap width.**

An understanding of how the largest extreme load varies with flap width is also important. Figure 10 shows the variation of the largest extreme load events recorded with flap width. In each case the maximum positive and minimum negative loads out of all the 6 sea states is selected and displayed. The results clearly show that the foundation loads increase in magnitude as the flap width increases. A more informative way of displaying these results is to scale the foundation loads with the flap width, giving a measure of the load per meter flap width. These are displayed in Figure 11 and shows that there is still some variation as the flap width increases.

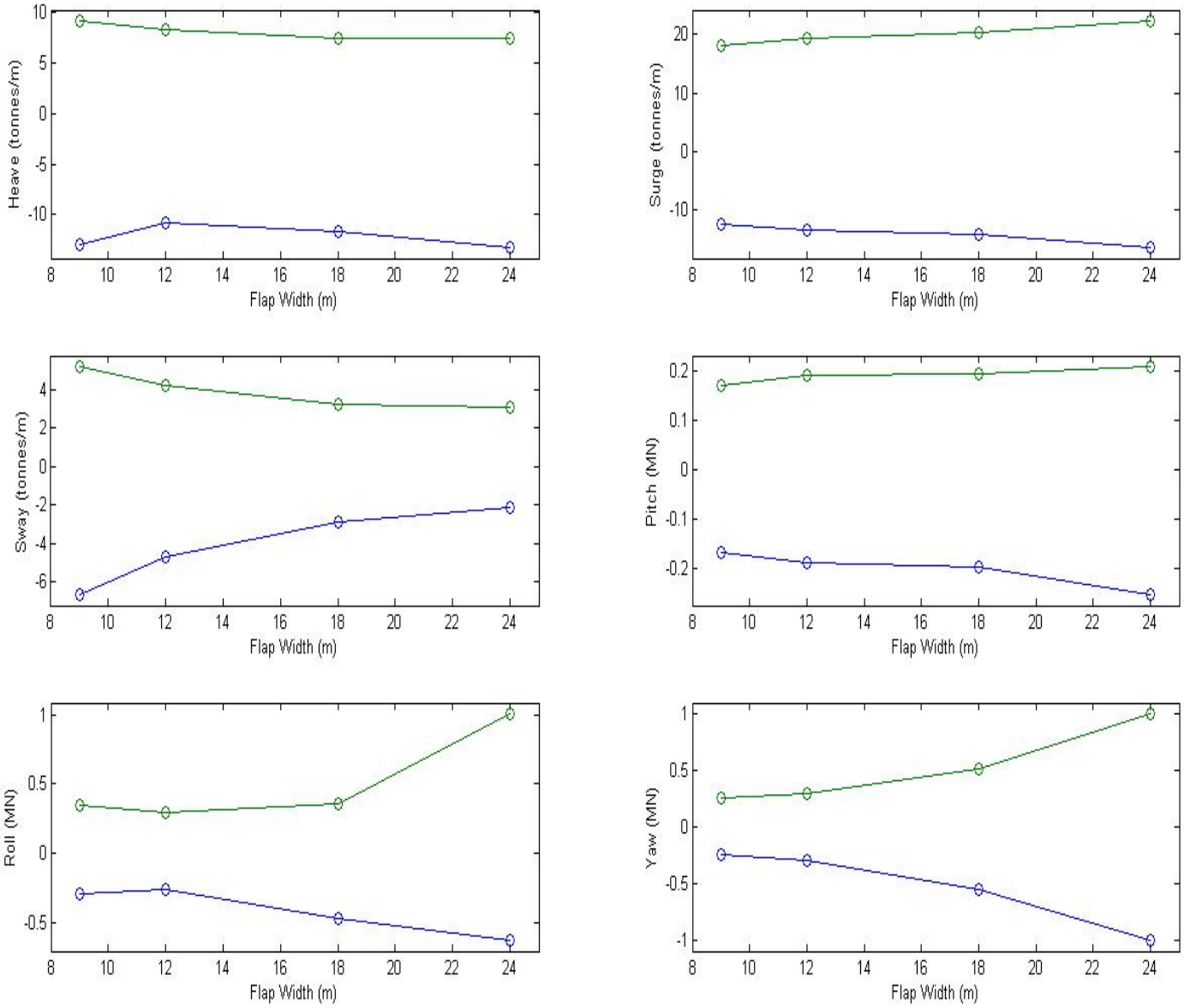

Figure 11. **Largest extreme loads per meter flap width.**

The variation of foundation loads with flap width should be considered in parallel with the performance of each flap, as a small improvement in power capture may be overshadowed by a large increase in the foundation loads. Figure 12 below displays the power captured per foundation load for each flap width. The negative values simply mean that it is associated with the negative foundation load (an artefact of the sign convention used), thus it is the magnitude of these values which should be considered. Ideally a more useful metric would be an overall kilowatt per load measurement combining all 6 foundation loads. However, the combination of forces and moments makes it difficult to combine these into a single practical measurement. Another restriction is that the maximum of

each foundation load do not occur simultaneously, for example, a maximum in Surge may correspond to a minimum in Sway.

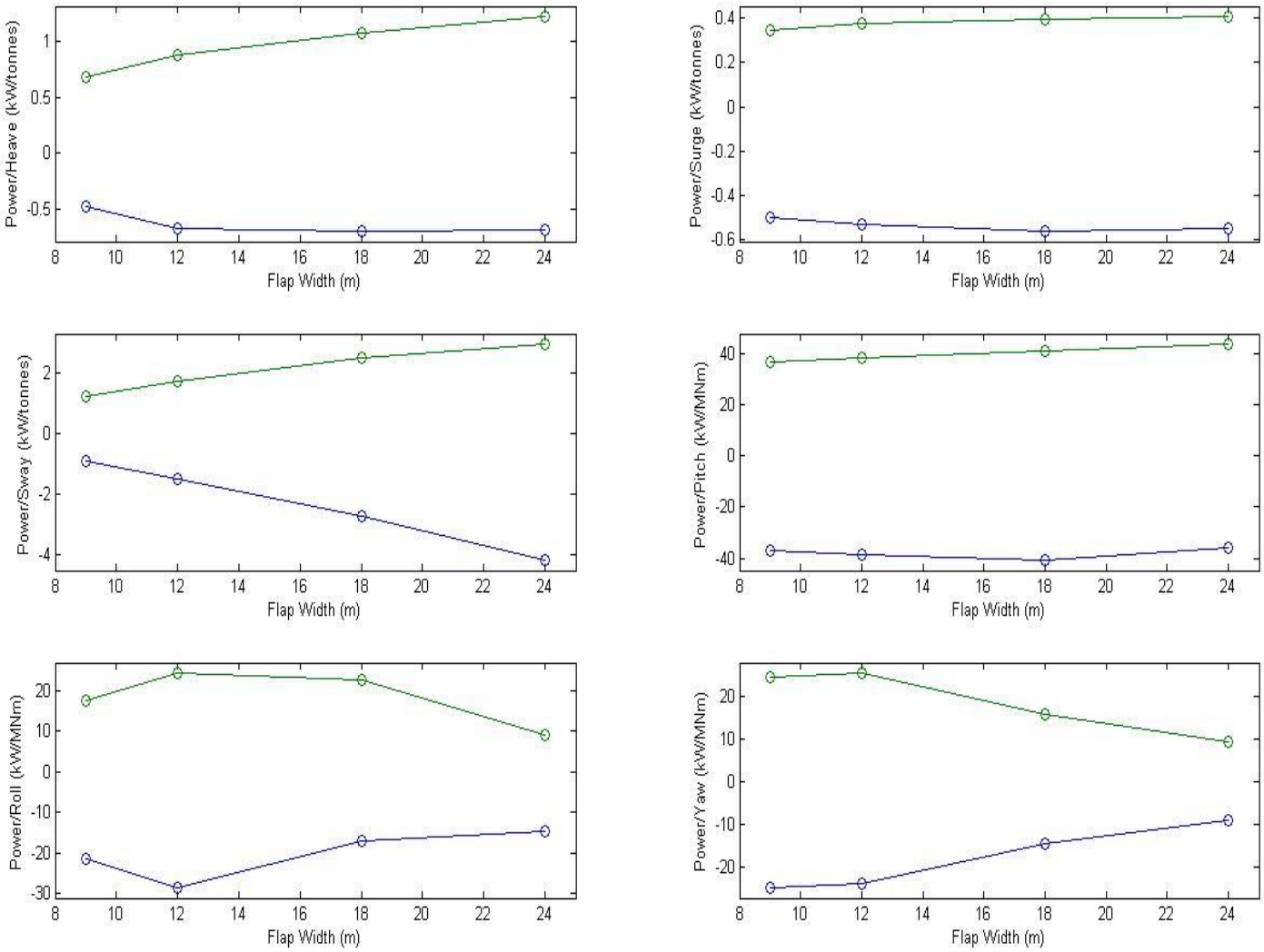

Figure 12. Power capture per foundation load for each of the 4 flap widths.

4. Extreme Value Analysis

Determining the maximum loads that a device may encounter throughout its lifetime is vital to the design of the device. Although the actual extreme foundation load events recorded during the experimental tests are a good indication of the maximum loads that a device my encounter, (they asymptotically approach the maximum loads due to depth limited wave height). A more robust methodology of extreme value analysis (EVA) is required to determine the maximum loads on the device. This establishes the return periods of the measured experimental events and permits a possible extrapolation of a cumulative distribution function to predict the occurrence more severe events which were not recorded during the experimental tests. A discussion of the EVA used for the extreme foundation load events is given in (6) but will be outlines here again for clarity.

The theory is based on constructing a cumulative distribution function (CDF) of the extreme load events. This requires identifying the probability P that an extreme event of a certain magnitude will not be exceeded in one time step, (the time step used in this analysis is an hour). A variety of techniques have been employed by different authors to determine this probability, however there seems to be a fundamental misunderstanding of the logic behind the process. The most common mistake is that the data is manipulated (for easy extrapolation and interpolation) in such a way that probability is actually fitted to a theoretical CDF, rather than the reverse procedure. This implicitly assumes that the CDF of the data is known before it is even recorded or displayed! Many of these issues along with a proof of the correct probability formula are presented in (8). From (8) it is shown that if the data of N events is arranged in ascending order of magnitude with each event assigned a rank $m, (1 \leq m \leq N)$, the probability of non-exceedance P is given by

$$P = \frac{m}{N+1} \tag{2}$$

(Note: This corrects a typo which appears in (6)). This formula follows from the definition of statistically probability and actually corresponds to the mean of the CDF without assuming a unique CDF. From this we can construct the return period R, this is the time during which an event is exceeded on average once

$$R = \frac{1}{1-P}$$

If in a data set there are k events sampled per hour, then the return period is given by

$$R = \frac{1}{k(1-P)} \tag{3}$$

The return period is a statistical quantity determined from experimental data. Despite its name 'return period' it does not mean that a 100 hour event will happen regularly every 100 hours. In fact, if in any given hour/hours the event is not exceeded the return period still remains 100 hours. Equally, when dealing with the probability of exceedance $(1-P)$, this does not mean that an event happens with a 1% probability, only that it has been observed exactly once in 100 hours. Thus it is not a probability of occurrence. The probability Q_r^n of an event occurring exactly r times in n hours can be found using the binominal distribution

$$Q_r^n = \binom{n}{r}(1-P)^r(P)^{n-r}$$

where the binomial coefficient is given by

$$\binom{n}{r} = \frac{n!}{r!\,(n-r)!}$$

Thus the probability of an event occurring at all in n hours is given by $(1 - Q_0^n)$.

The EVA is applied to the foundation load results as follows: Like before the foundation load data is split up into positive and negative sets. Then the peak load events are selected, arranged in ascending order of magnitude and given a rank number m ranging from 1 to N, where N is the total number of peak events. For this analysis all 6 sea states are considered in one data set, thus the total test time is approximately 21.6 hours FS (3.42 hours MS). From this the number of events per hour k can be determined and the return period of each event can be found using Equations 1 & 2. The graphs in Appendices 1-4 plot the return period verses peak load on a semi-log axis for all four flap widths. For each foundation load the positive and negative components are separated and both damped and undamped flap results are displayed, with the colour convention matching the scatter plots in Appendix A to D. From these graphs it may be a possible to extrapolate the data curve to predict the loads associated with larger return period events. However, extreme care must be taken when extrapolating as it is the data at the tail of the distribution which are of most significance. Not only are there are few data points in the tail but in some cases they also deviate away from the general curve introducing many uncertainties into the extrapolation process. Implicit to the practice of extrapolation is the assumption that the underlying physics remain the same. Thus any future predictions achieved by extrapolation should be verified by some external procedure where possible.

5. Summary

The results from the performance tests reported in Section 2 shows that both the power captured and the capture factor increases with flap width, reaching a maximum of 0.58 for a 24 meter flap which is globally damped. Imposing a single global damping value on each flap is shown to reduce the power capture by up to 12% relative to a more optimal damping mechanism. This indicates that significant improvement in performance could be achieved with the use of a more sophisticated damping mechanism.

The foundation loads measured during the tests show that the load per meter flap width in almost all degrees of freedom increase in magnitude as the flap gets wider. An exception to this is positive heave and sway, which actually seem to decrease. The data used corresponds to the largest extreme event (for each degree of freedom) which was recorded during the total test time of 21.6 hours FS. The power captured per unit load increases slightly (except in yaw and roll) with flap width. However, it is difficult to extract constructive information by examining the power captured from each degree of freedom in isolation. Again it should be noted from (1) that measured error on the loads are 10% (max) in surge, 5% (max) in heave and typically less than 3% in the rest of the loads.

During the tests it was observed that for each flap width, both damped and undamped, the maximum rotation angle achieved was consistently larger in the negative direction (pitching away from shore) by approximately 6^{o}-10^{o}. A possible explanation for this is that when a wave crest approaches the device, the flap pitches in the positive direction (towards the shoreline) and is eventually completely submerged and the wave overtops the device. The fact that it is fully submerged means that the full natural buoyancy of the flap is opposing the motion along with the inertia of the water in front of the flap. There is also the possibility of a so called water squeezing effect between the flap and the sea-bed which may restrict very large amplitudes of rotation. As the crest of the wave passes, the device springs backwards due to the water particle motion and buoyancy forces. However, in this case the flap is now situated in the trough of the wave and so it is not subjected to the same magnitude of opposing forces. Thus larger rotation angles are achieved in the negative direction.

The return period plots from the extreme value analysis give an indication of the distribution of extreme load events and provide the possible frame work for predictions of larger events which were not recorded during the tests. However, extrapolating data at the end of a distribution where there are few data points introduces a large uncertainty into the validity of the predictions. (6) argues that provided the data and analysis are reasonably well conditioned then an extrapolation to between 10 and 50 times the expected return period may be possible. If the tail of the distribution is not well conditioned (i.e it deviates off the main curve) then a possible range of maximum to minimum events could be found, where obviously the smaller the extrapolation the better the estimate. However, any extrapolation should be verified by some external argument/procedure. A greater understanding into the cause of these extreme foundation loads is required to resolve this issue and so no future predictions are made in this report.

Bibliography

1. **Doherty, Kenneth.** AMPL-OY02-H5004-RPT-R01 *Calibration and Analysis of a Six Degree of Freedom Elbow Rig Load Transducer.* 2008.

2. —. *AMPL-OY02-H5005-DOC-R01 Pitch Stiffness of the 40th Scale Model.* 2008.

3. —. AMPL-OY02-H5002-RPT-R01 *Formulation of Performance and Fatigue Sea States.* 2008.

4. **RPS.** *Wave Resource Study at EMEC.* IBE0024.00.R03rev2 Report / AKB.

5. **Henry, Alan.** *global damping.* 2008. QUB AH 081119.

6. **Folley, Matt.** *Modification of the method used to estimate maximum foundation loads.* 2007. QUB-MF 070719-03a .

7. **Howard, Damien.** *Coincident loads summary all flaps.* 2008. QUB DH081126-01a.

8. *Problems in the extreme value analysis.* **Makkonen, Lasse.** 2008, Structural Safety, Vol. 30, pp. 405-419.

APPENDIX A: Scatter plots-9 meter wide flap

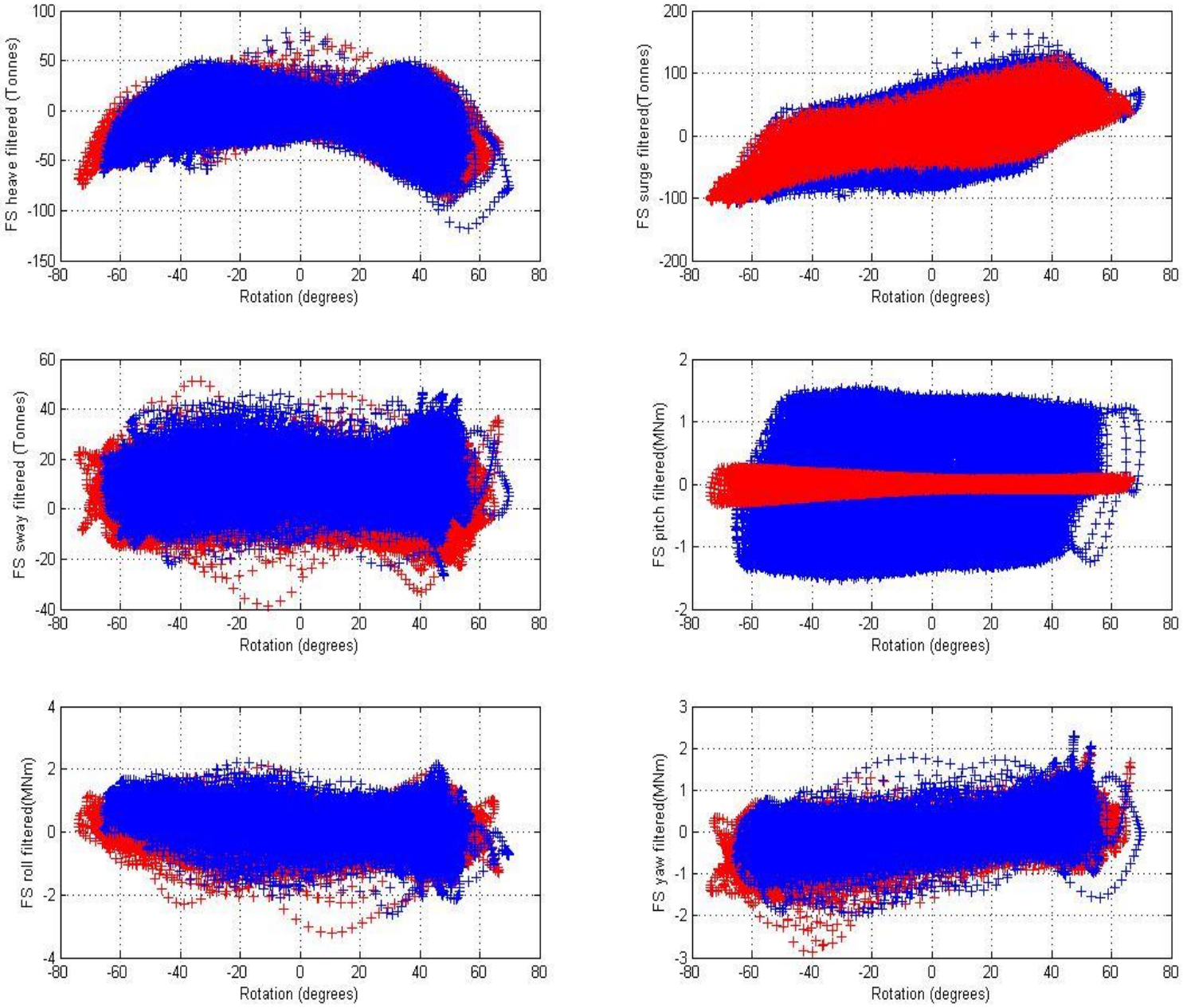

Figure A1

Foundation loads at the pivot point in extreme sea state 1 with energy period and significant wave height of Te=9s and Hs=10m respectively. The red data points correspond to an undamped flap and blue data points are for a global **RMS** damping torque of approximately 0.95 MNm. The required global damping torque is 1.09 MNm.

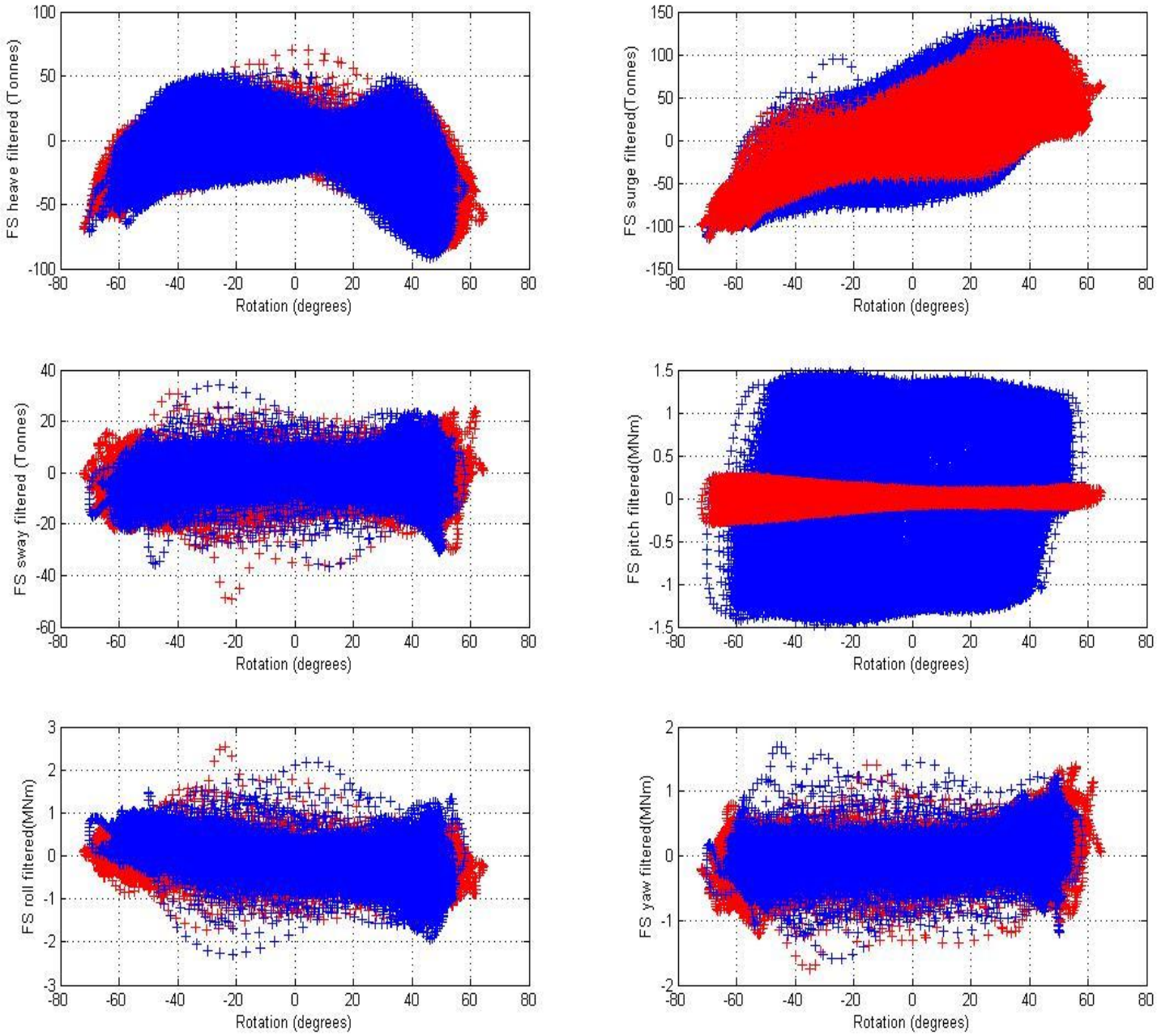

Figure A2

Foundation loads at the pivot point in extreme sea state 2 with energy period and significant wave height of Te=11s and Hs=10m respectively. The red data points correspond to an undamped flap and blue data points are for a global **RMS** damping torque of approximately 0.91 MNm. The required global damping torque is 1.09 MNm.

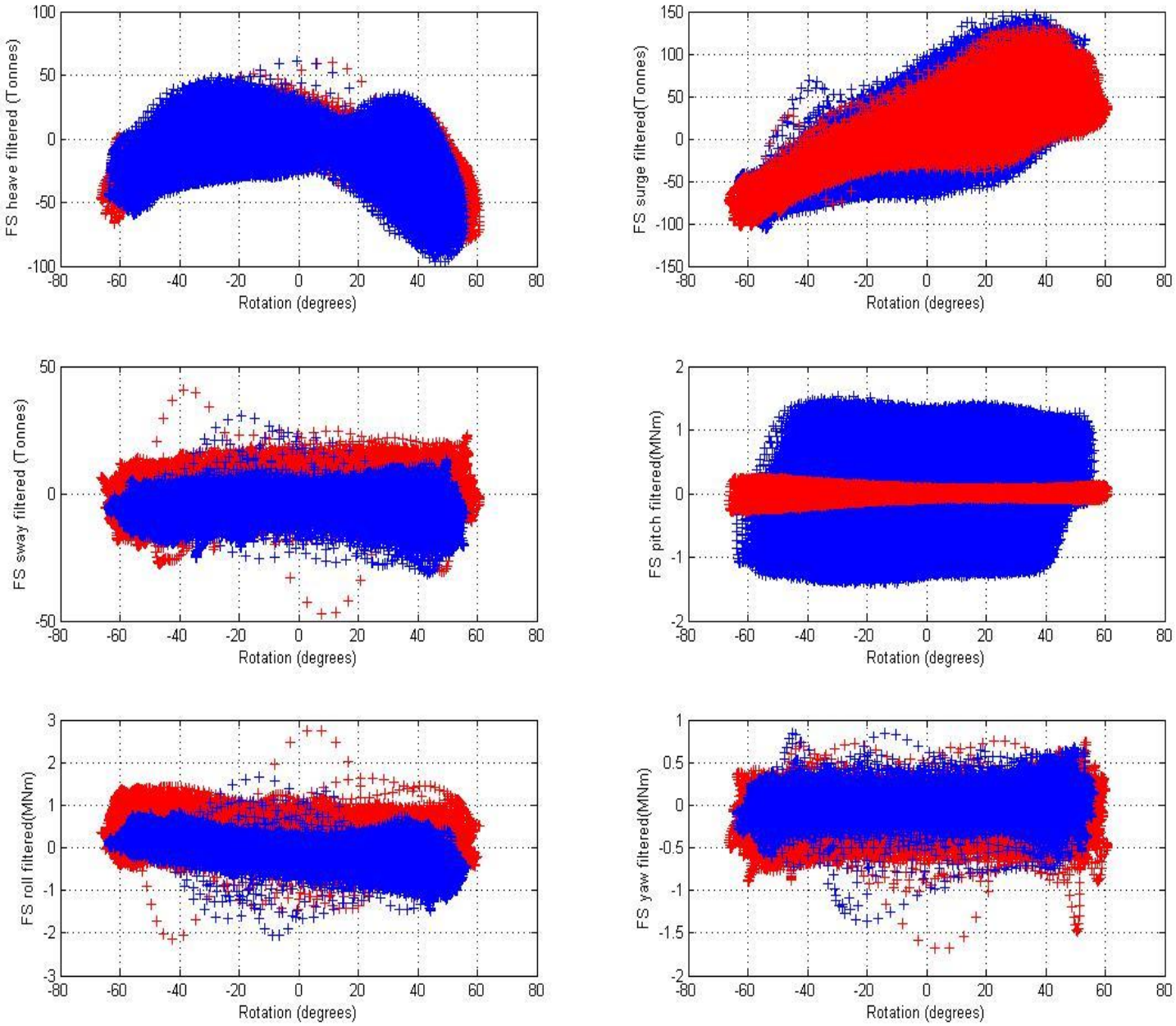

Figure A3

Foundation loads at the pivot point in extreme sea state 3 with energy period and significant wave height of Te=13s and Hs=8m respectively. The red data points correspond to an undamped flap and blue data points are for a global **RMS** damping torque of approximately 0.87 MNm. The required global damping torque is 1.09 MNm.

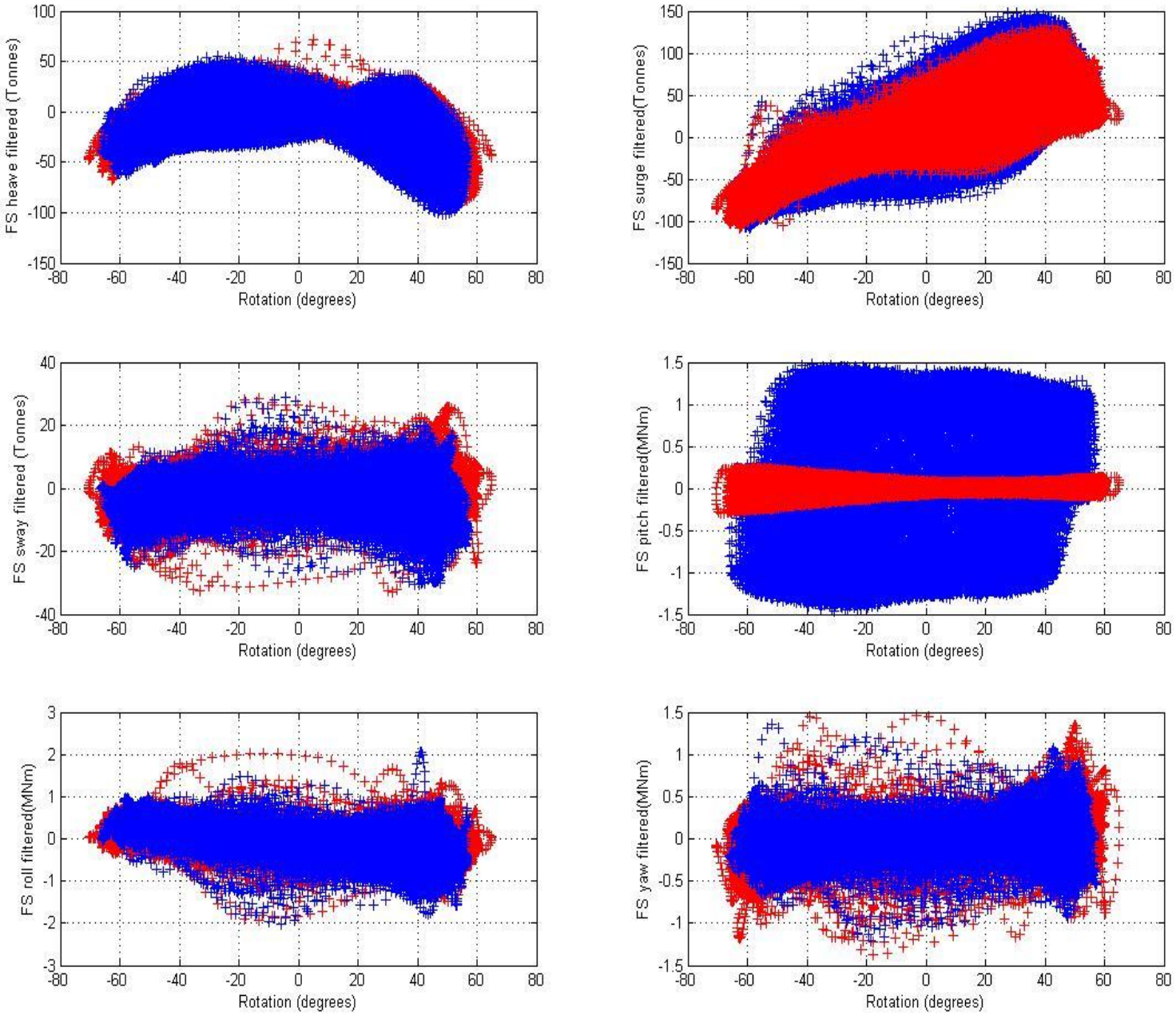

Figure A4

Foundation loads at the pivot point in extreme sea state 4 with energy period and significant wave height of Te=13s and Hs=10m respectively. The red data points correspond to an undamped flap and blue data points are for a global **RMS** damping torque of approximately 0.88 MNm. The required global damping torque is 1.09 MNm.

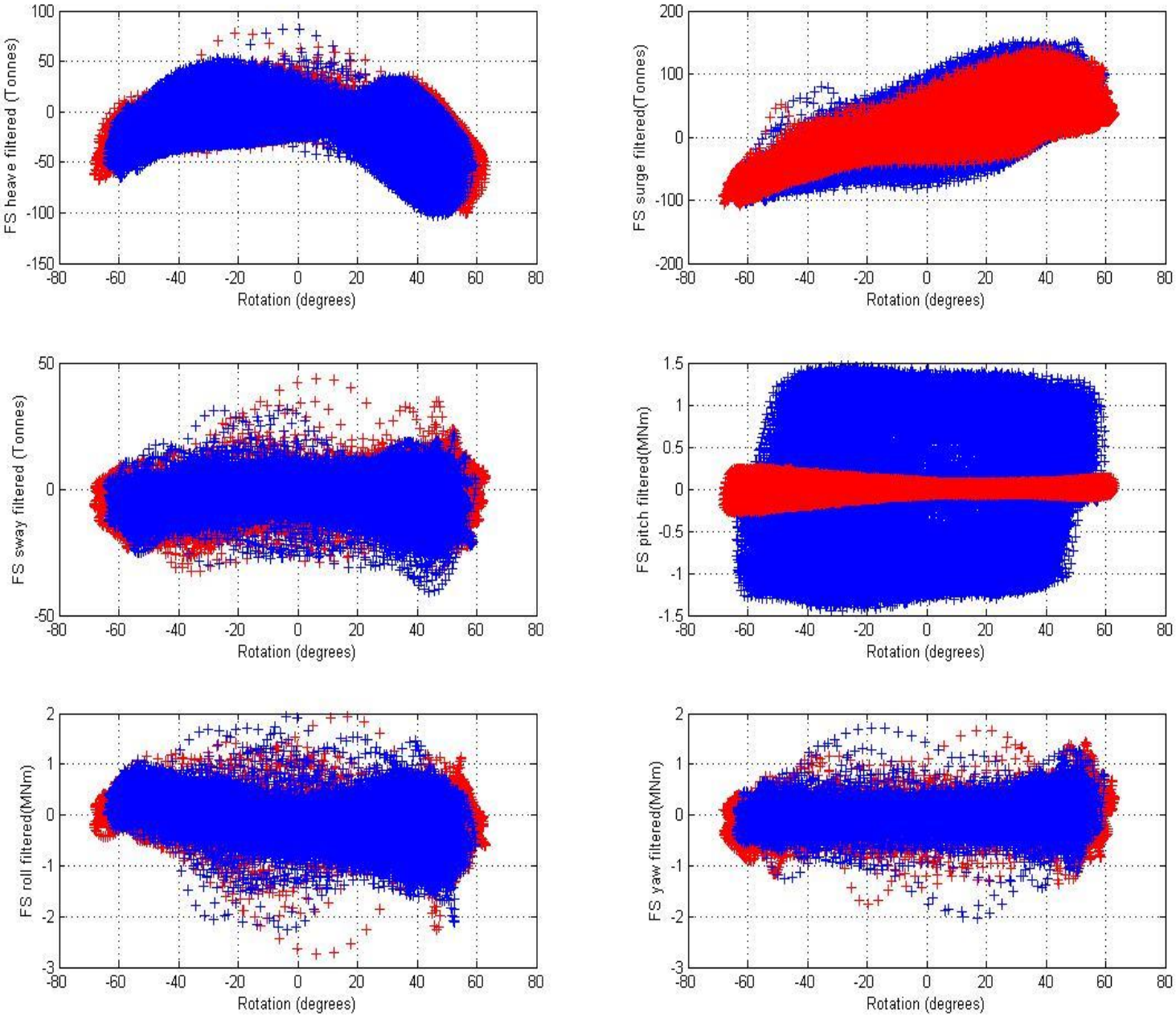

Figure A5

Foundation loads at the pivot point in extreme sea state 5 with energy period and significant wave height of Te=15s and Hs=8m respectively. The red data points correspond to an undamped flap and blue data points are for a global **RMS** damping torque of approximately 0.86 MNm. The required global damping torque is 1.09 MNm.

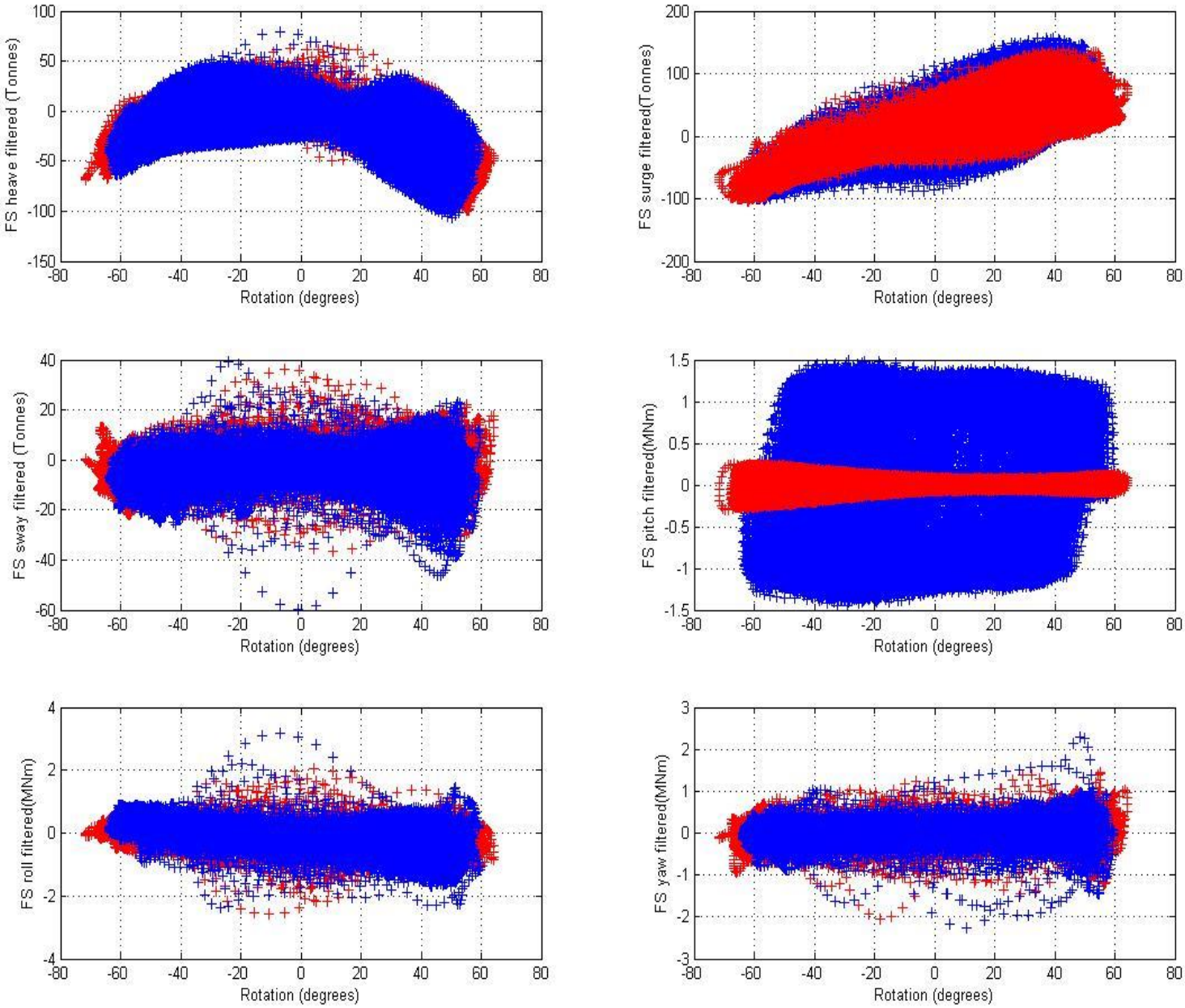

Figure A6

Foundation loads at the pivot point in extreme sea state 6 with energy period and significant wave height of Te=15s and Hs=10m respectively. The red data points correspond to an undamped flap and blue data points are for a global **RMS** damping torque of approximately 0.86 MNm. The required global damping torque is 1.09 MNm.

APPENDIX B: Scatter plots-12 meter wide flap

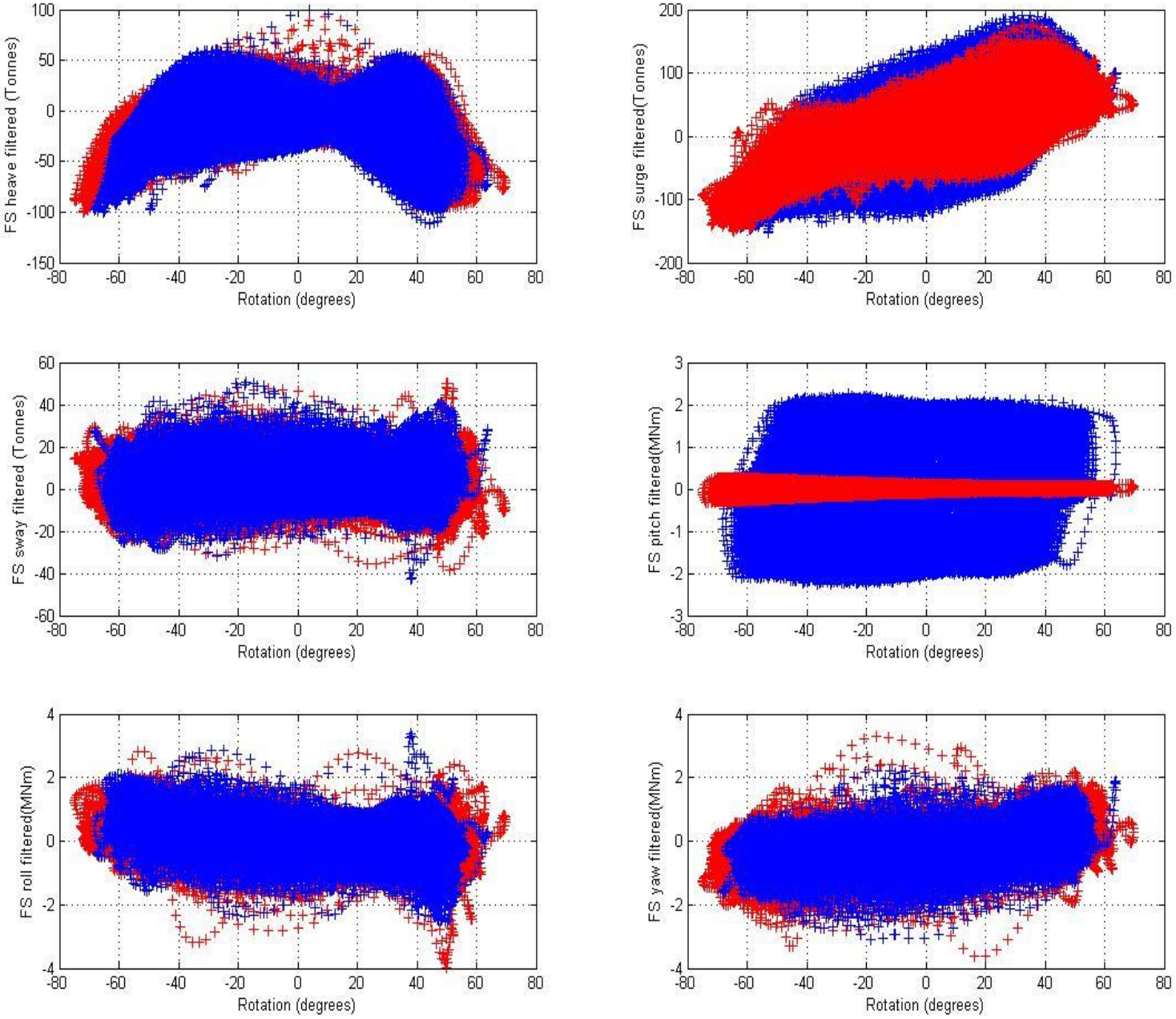

Figure B1

Foundation loads at the pivot point in extreme sea state 1 with energy period and significant wave height of Te=9s and Hs=10m respectively. The red data points correspond to an undamped flap and blue data points are for a global **RMS** damping torque of approximately 1.41 MNm. The required global damping torque is 1.62 MNm.

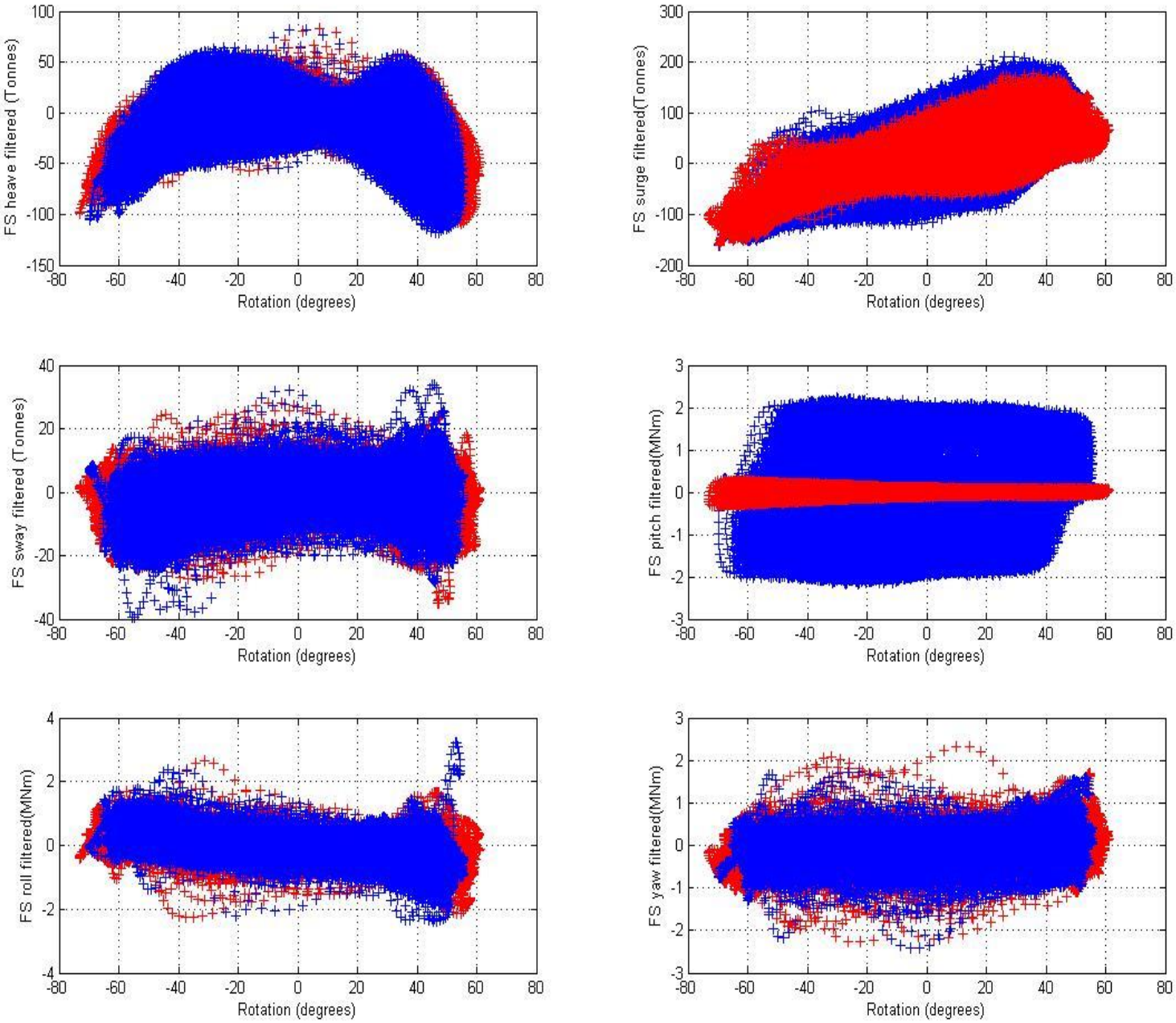

Figure B2

Foundation loads at the pivot point in extreme sea state 2 with energy period and significant wave height of Te=11s and Hs=10m respectively. The red data points correspond to an undamped flap and blue data points are for a global **RMS** damping torque of approximately 1.35 MNm. The required global damping torque is 1.62 MNm.

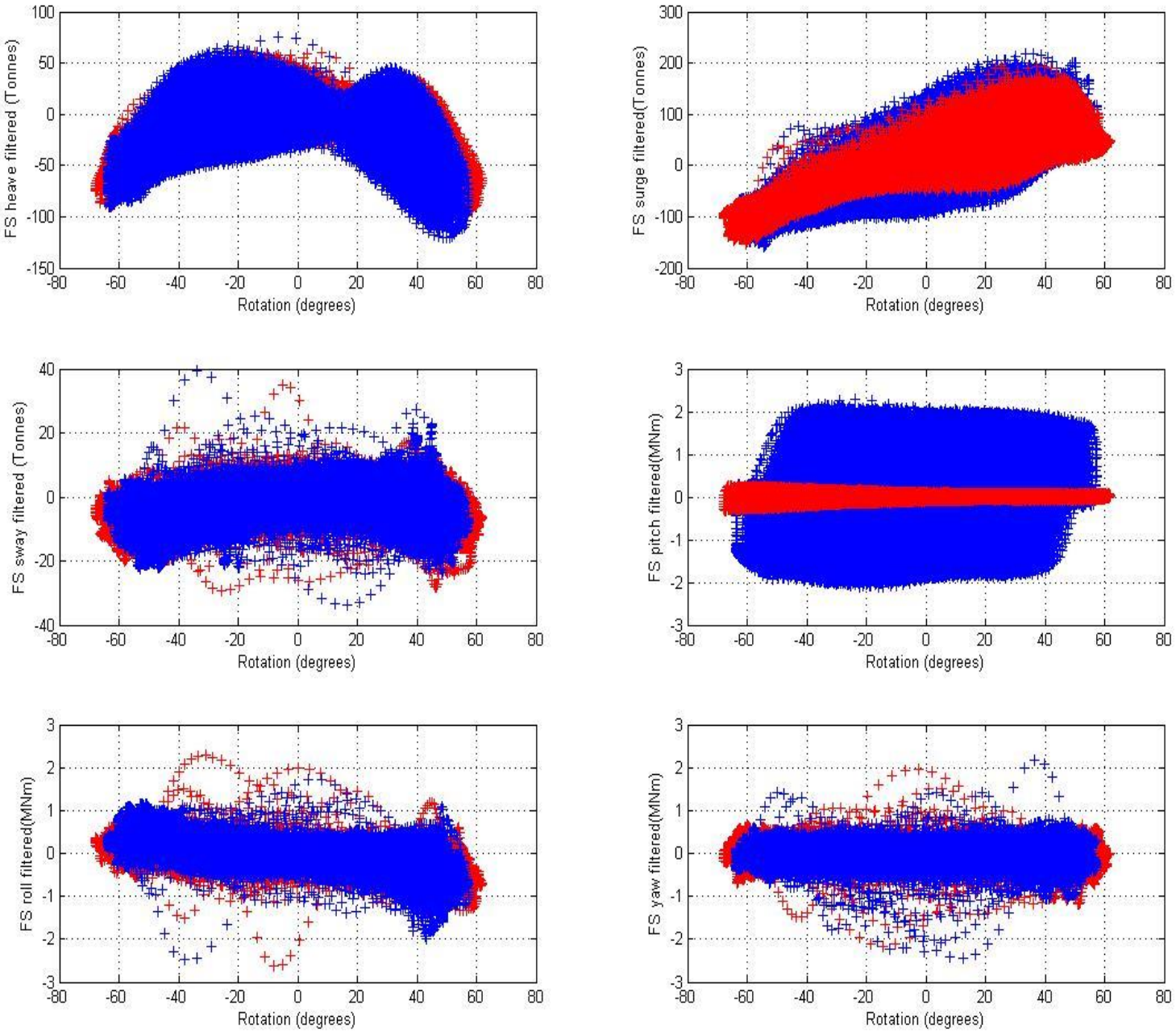

Figure B3

Foundation loads at the pivot point in extreme sea state 3 with energy period and significant wave height of Te=13s and Hs=8m respectively. The red data points correspond to an undamped flap and blue data points are for a global **RMS** damping torque of approximately 1.26 MNm. The required global damping torque is 1.62 MNm.

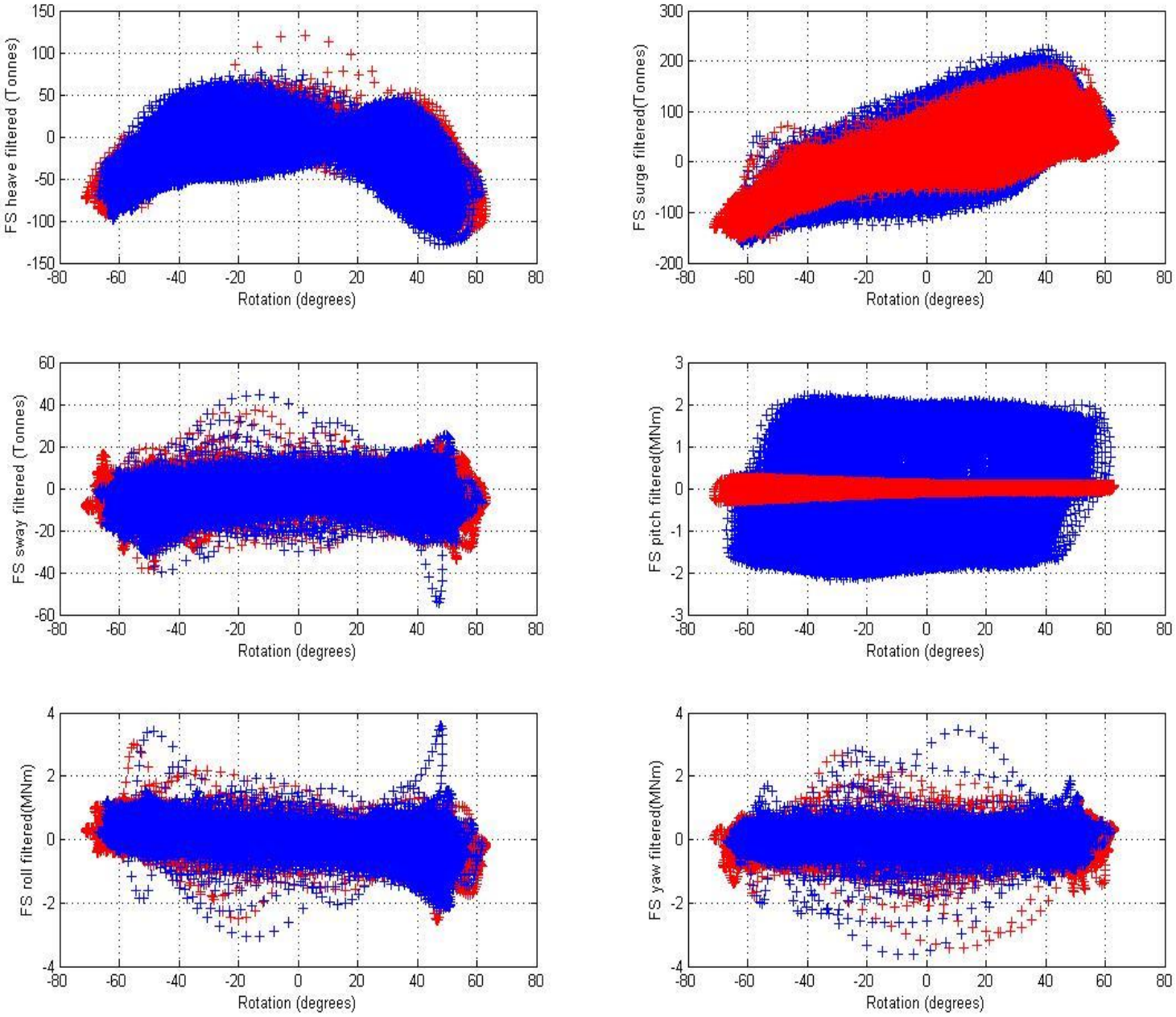

Figure B4

Foundation loads at the pivot point in extreme sea state 4 with energy period and significant wave height of Te=13s and Hs=10m respectively. The red data points correspond to an undamped flap and blue data points are for a global **RMS** damping torque of approximately 1.28 MNm. The required global damping torque is 1.62 MNm.

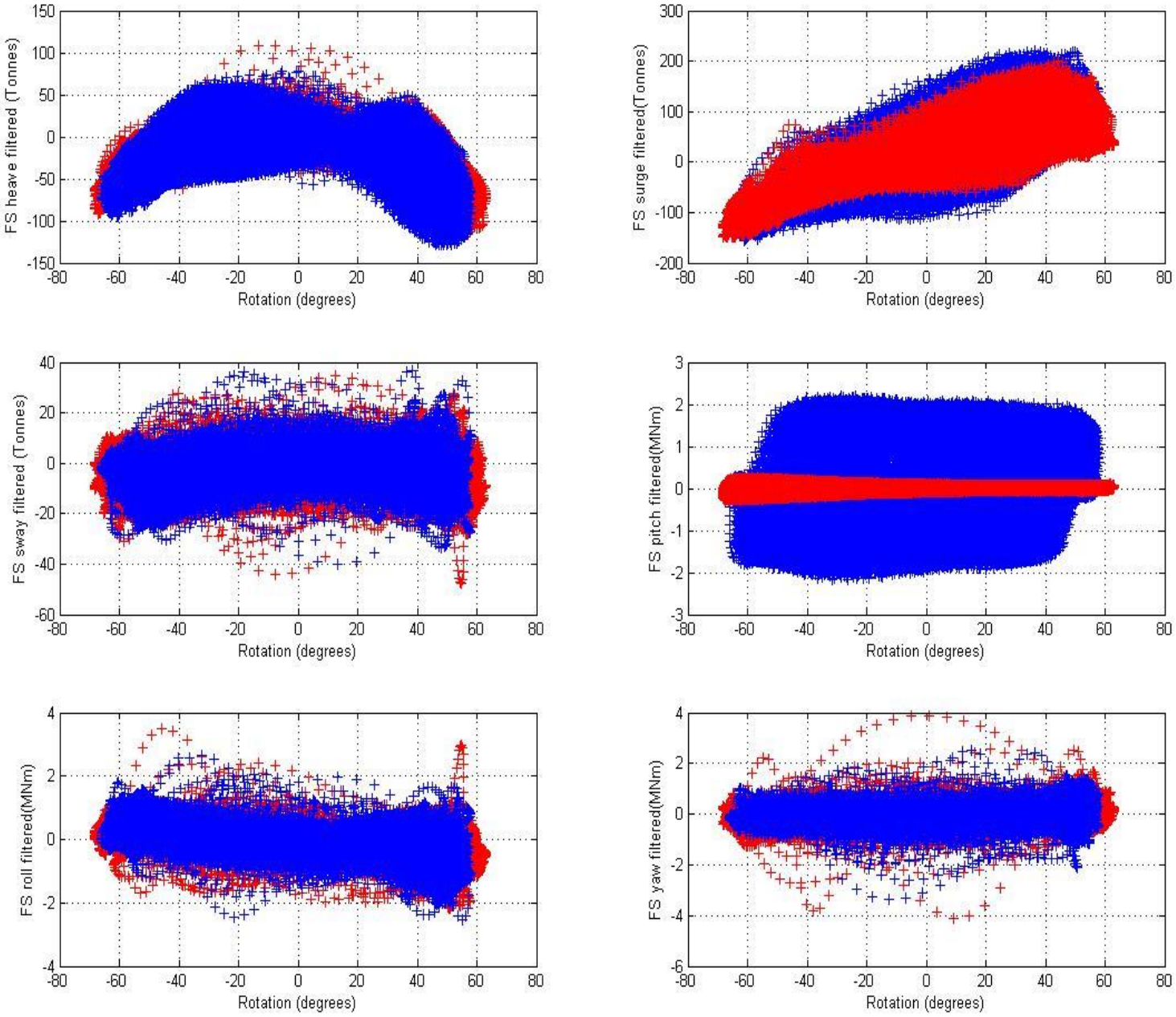

Figure B5

Foundation loads at the pivot point in extreme sea state 5 with energy period and significant wave height of Te=15s and Hs=8m respectively. The red data points correspond to an undamped flap and blue data points are for a global **RMS** damping torque of approximately 1.26 MNm. The required global damping torque is 1.62 MNm.

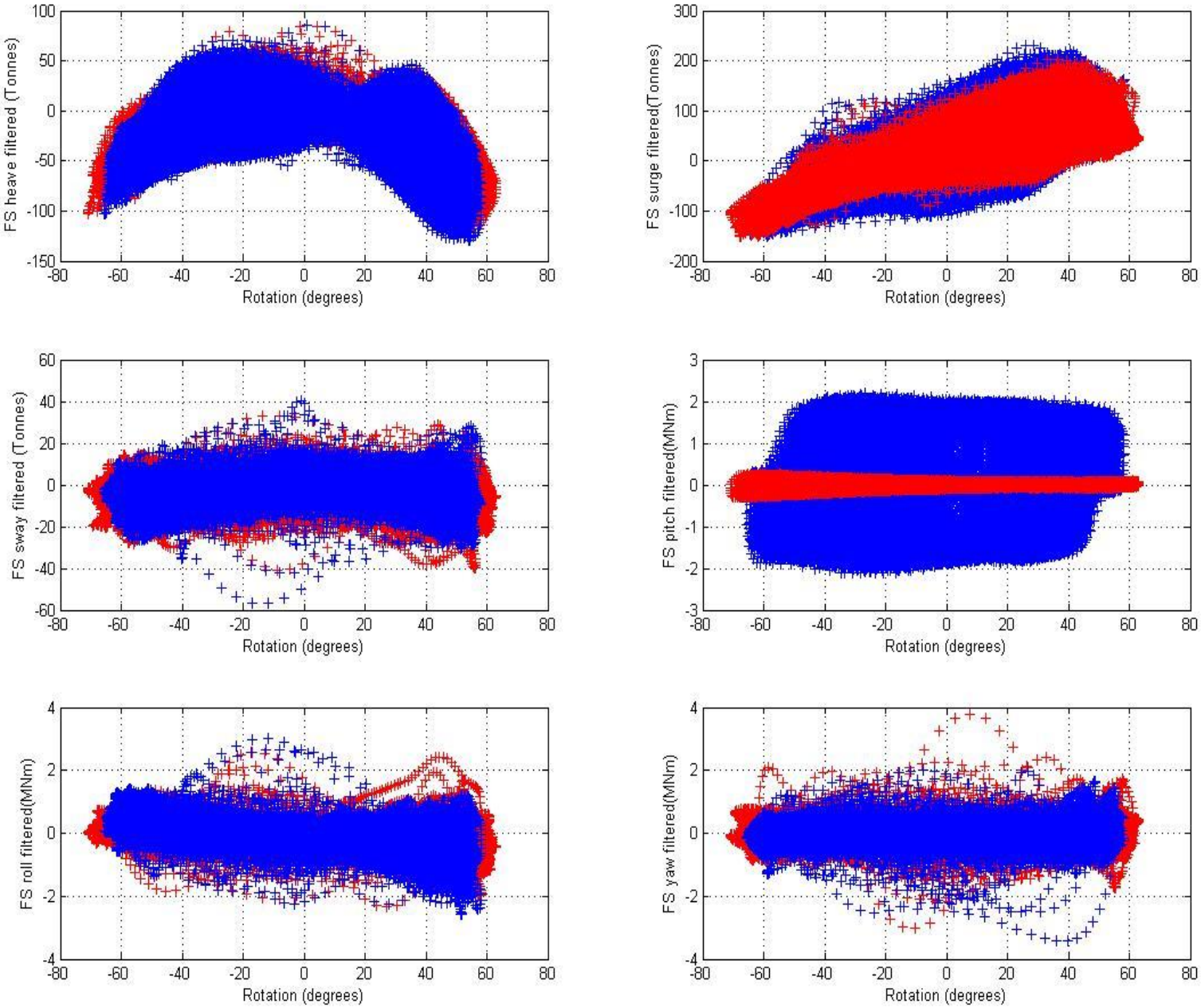

Figure B6

Foundation loads at the pivot point in extreme sea state 6 with energy period and significant wave height of Te=15s and Hs=10m respectively. The red data points correspond to an undamped flap and blue data points are for a global **RMS** damping torque of approximately 1.24 MNm. The required global damping torque is 1.62 MNm.

APPENDIX C: Scatter plots-18 meter wide flap

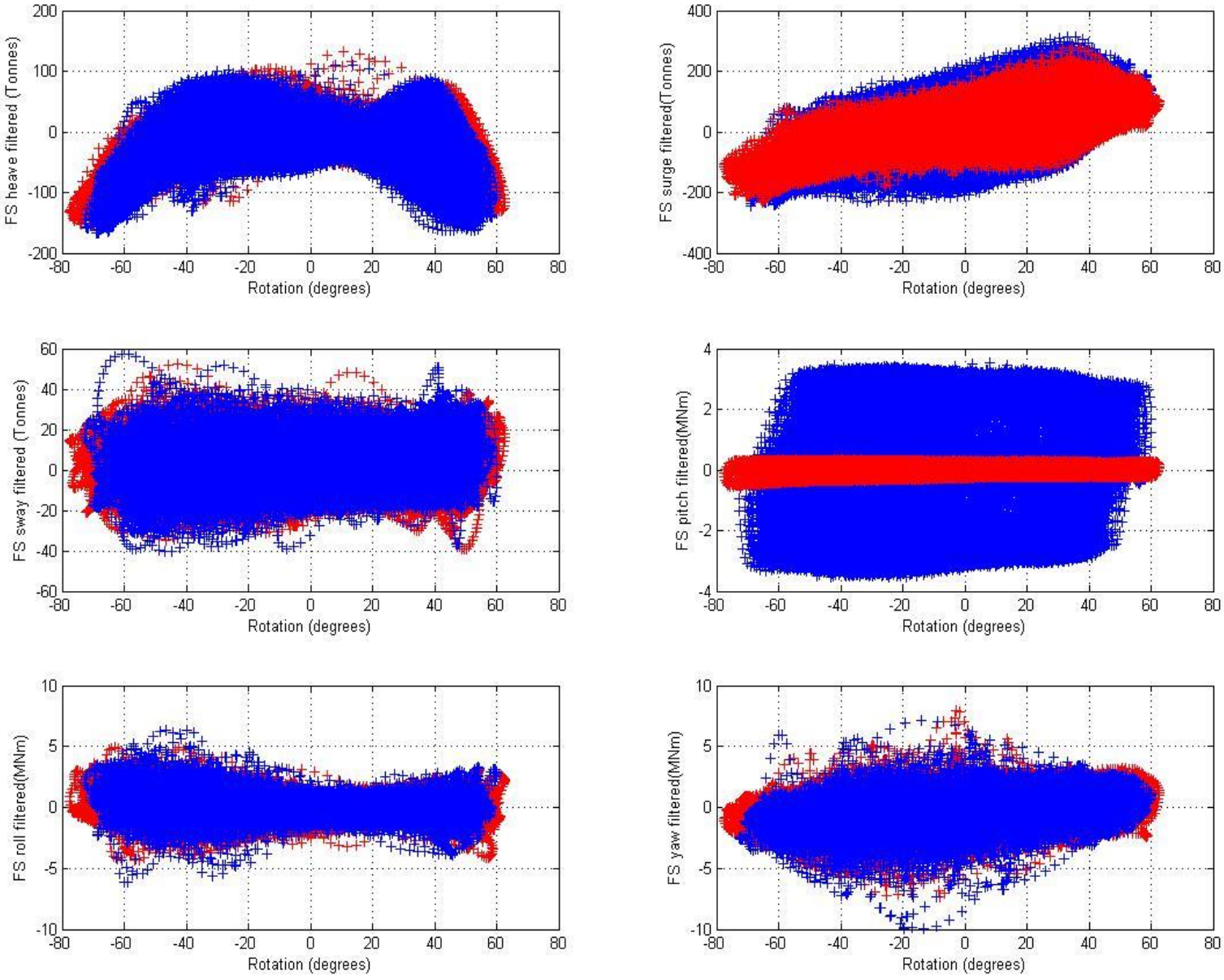

Figure C1

Foundation loads at the pivot point in extreme sea state 1 with energy period and significant wave height of Te=9s and Hs=10m respectively. The red data points correspond to an undamped flap and blue data points are for a global **RMS** damping torque of approximately 2.28 MNm. The required global damping torque is 2.78 MNm.

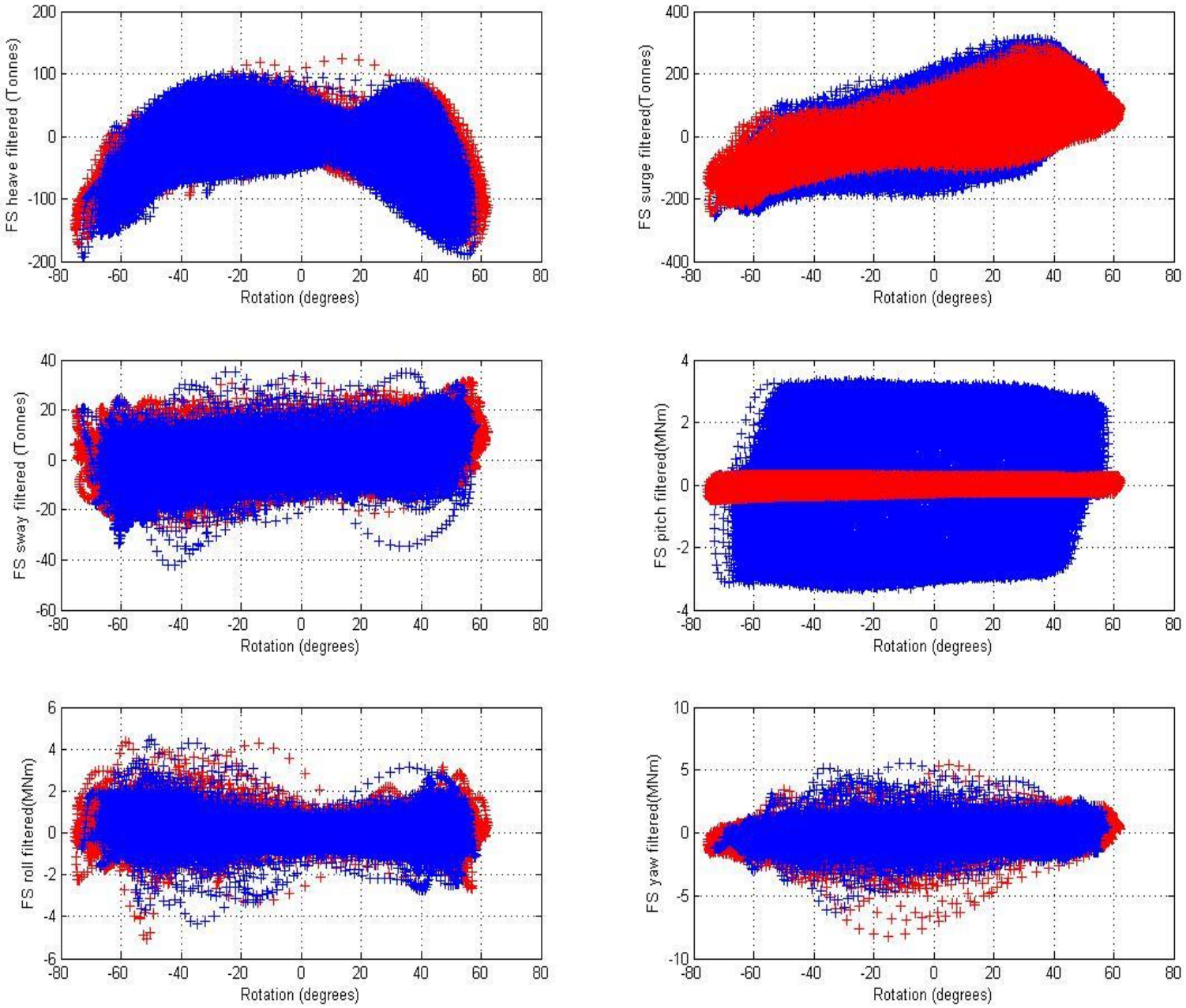

Figure C2

Foundation loads at the pivot point in extreme sea state 2 with energy period and significant wave height of Te=11s and Hs=10m respectively. The red data points correspond to an undamped flap and blue data points are for a global **RMS** damping torque of approximately 2.16 MNm. The required global damping torque is 2.78 MNm.

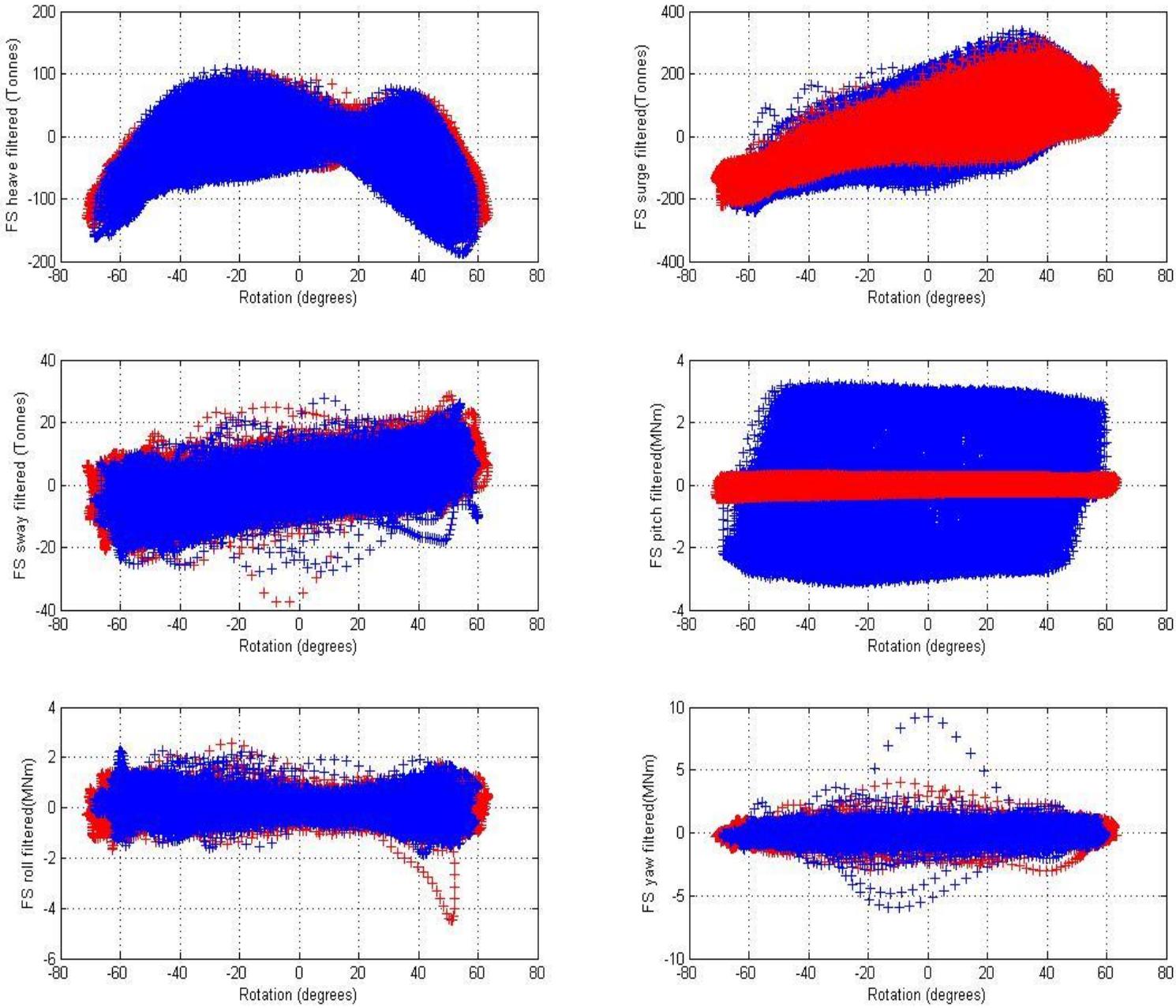

Figure C3

Foundation loads at the pivot point in extreme sea state 3 with energy period and significant wave height of Te=13s and Hs=8m respectively. The red data points correspond to an undamped flap and blue data points are for a global **RMS** damping torque of approximately 2.05 MNm. The required global damping torque is 2.78 MNm.

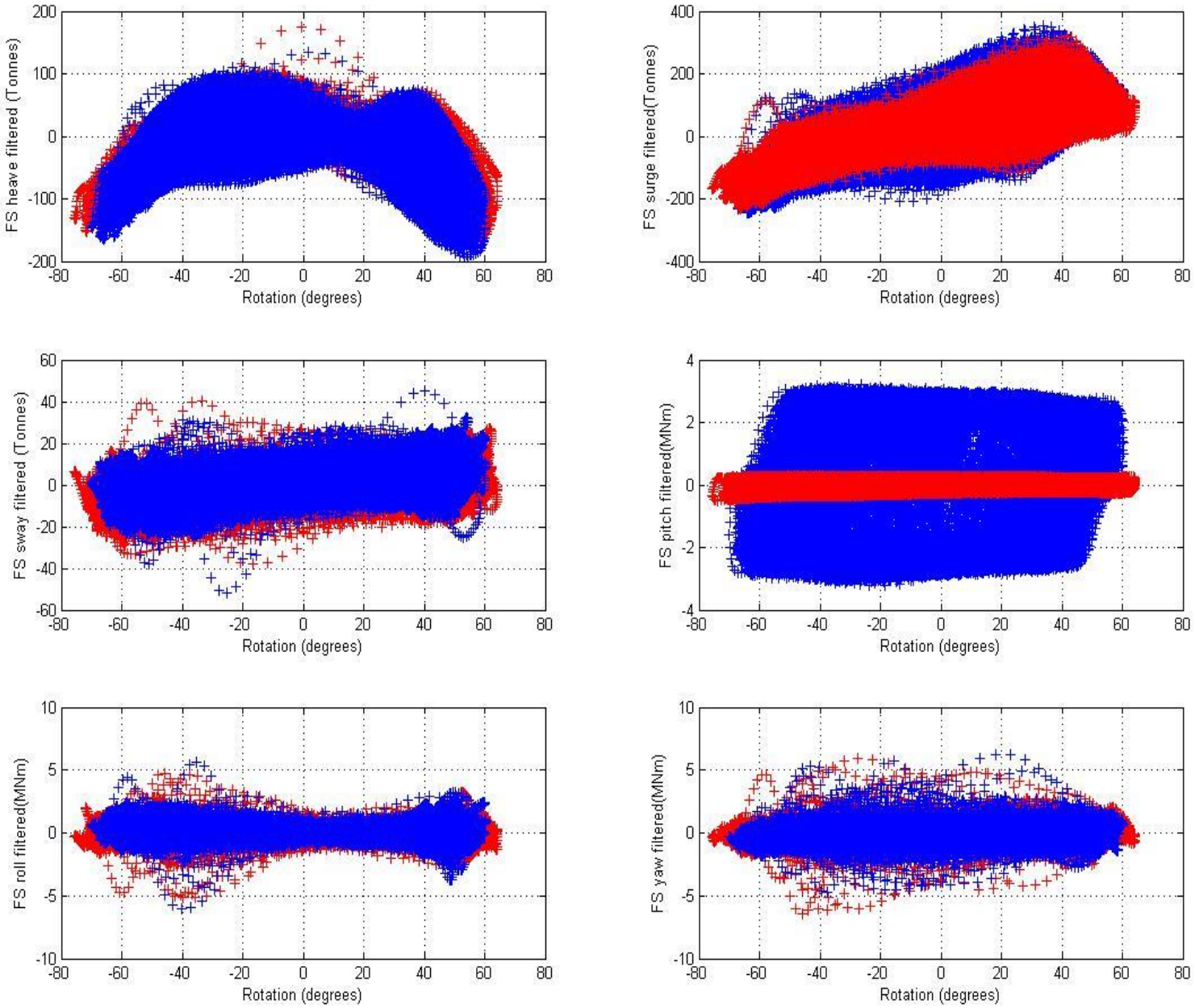

Figure C4

Foundation loads at the pivot point in extreme sea state 4 with energy period and significant wave height of Te=13s and Hs=10m respectively. The red data points correspond to an undamped flap and blue data points are for a global **RMS** damping torque of approximately 2.05 MNm. The required global damping torque is 2.78 MNm.

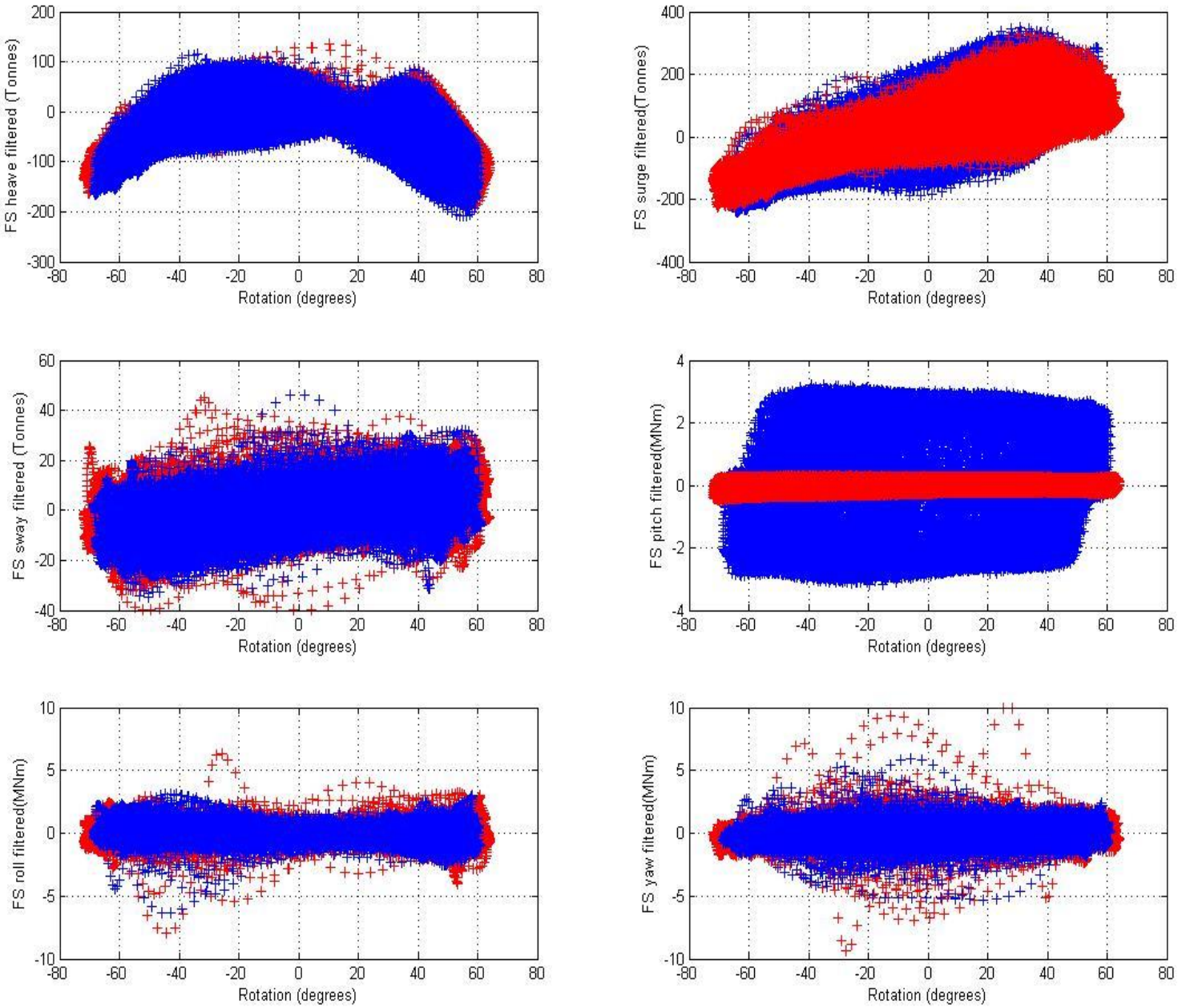

Figure C5

Foundation loads at the pivot point in extreme sea state 5 with energy period and significant wave height of Te=15s and Hs=8m respectively. The red data points correspond to an undamped flap and blue data points are for a global **RMS** damping torque of approximately 1.98 MNm. The required global damping torque is 2.78 MNm.

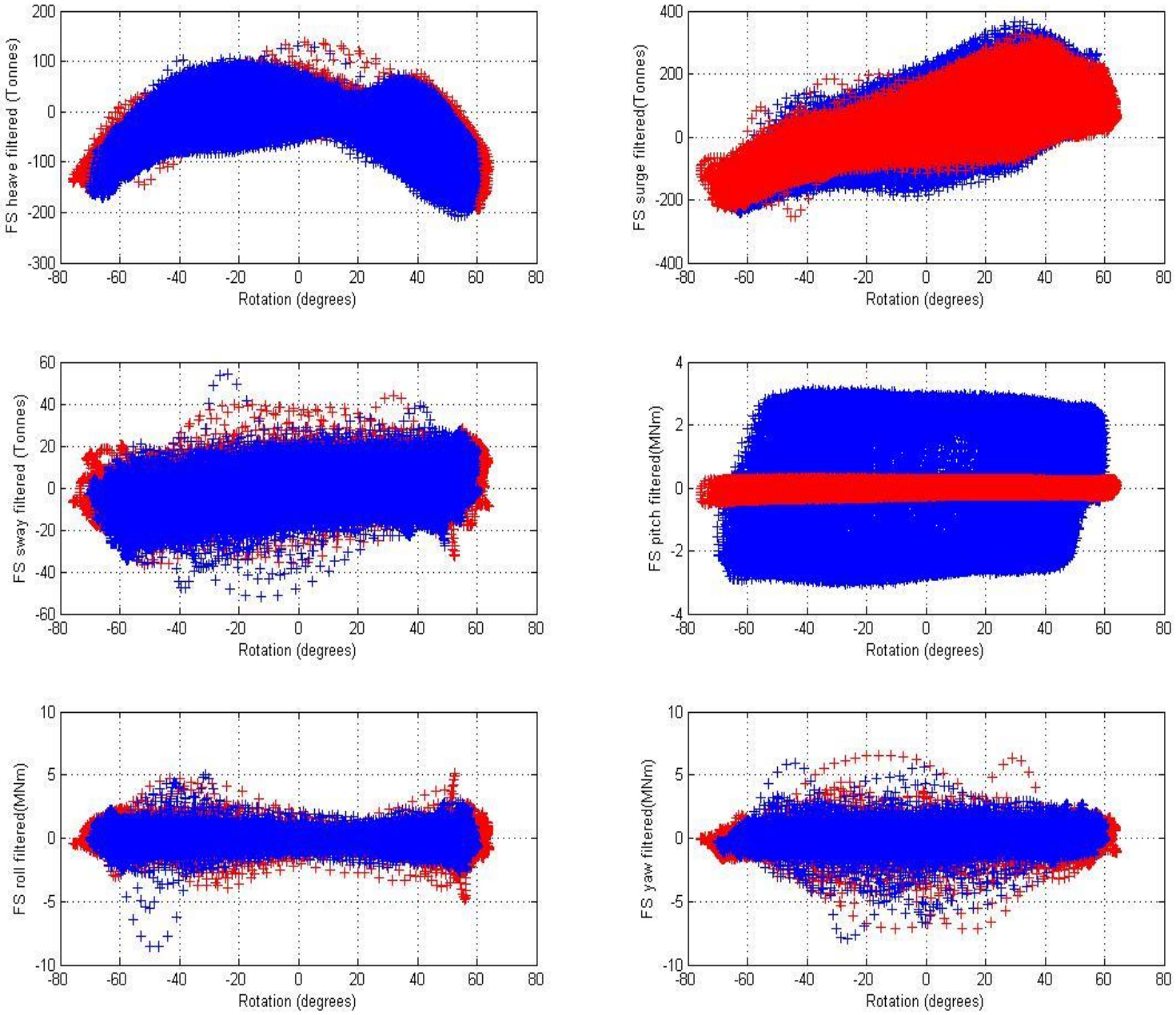

Figure C6

Foundation loads at the pivot point in extreme sea state 6 with energy period and significant wave height of Te=15s and Hs=10m respectively. The red data points correspond to an undamped flap and blue data points are for a global **RMS** damping torque of approximately 1.96 MNm. The required global damping torque is 2.78 MNm.

APPENDIX D: Scatter plots-24 meter wide flap

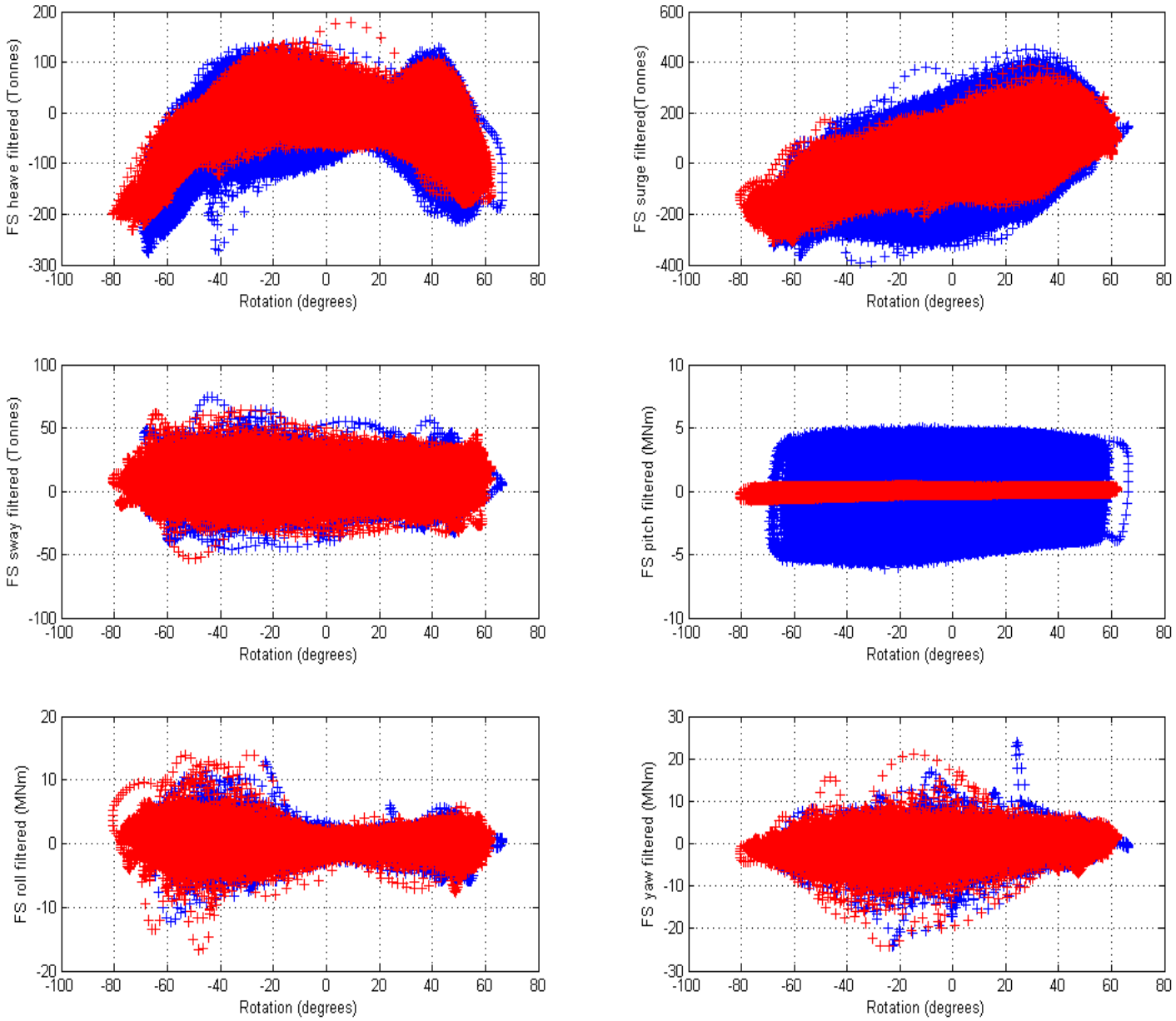

Figure D1

Foundation loads at the pivot point in extreme sea state 1 with energy period and significant wave height of Te=9s and Hs=10m respectively. The red data points correspond to an undamped flap and blue data points are for a global **RMS** damping torque of approximately 3.59 MNm. The required global damping torque is 3.92 MNm.

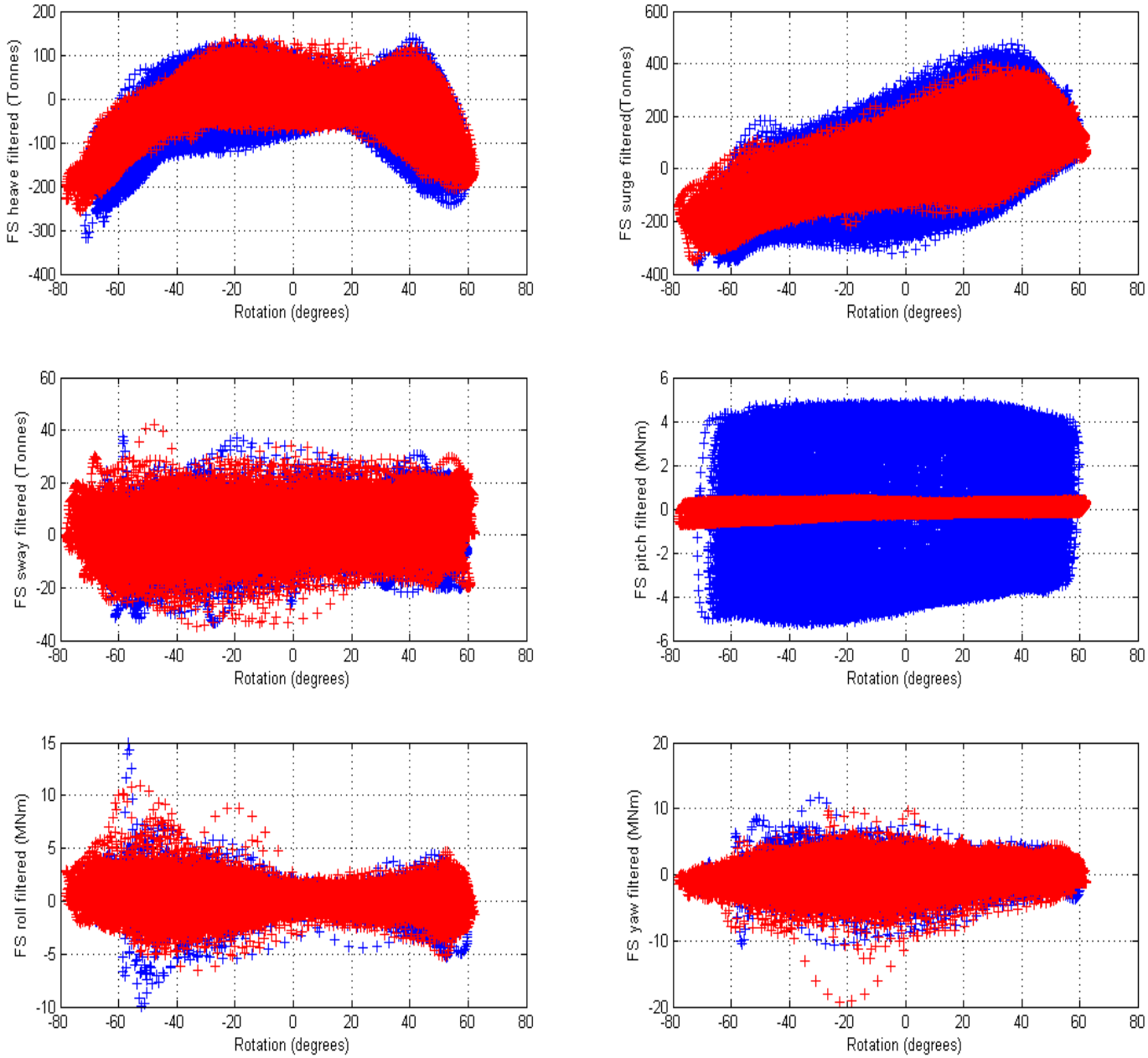

Figure D2

Foundation loads at the pivot point in extreme sea state 2 with energy period and significant wave height of Te=11s and Hs=10m respectively. The red data points correspond to an undamped flap and blue data points are for a global **RMS** damping torque of approximately 3.43 MNm. The required global damping torque is 3.92 MNm.

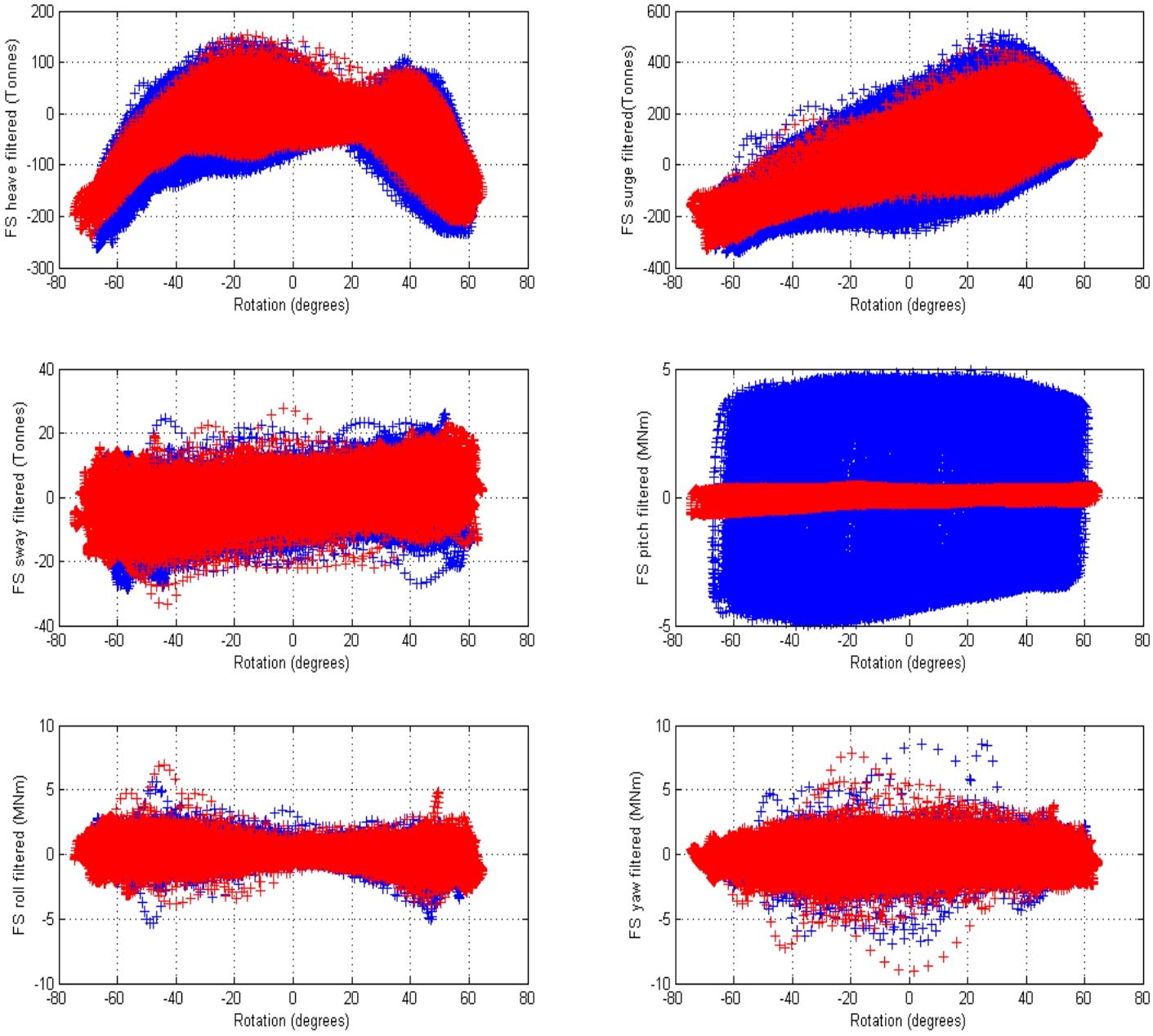

Figure D3

Foundation loads at the pivot point in extreme sea state 3 with energy period and significant wave height of Te=13s and Hs=8m respectively. The red data points correspond to an undamped flap and blue data points are for a global **RMS** damping torque of approximately 3.24 MNm. The required global damping torque is 3.92 MNm.

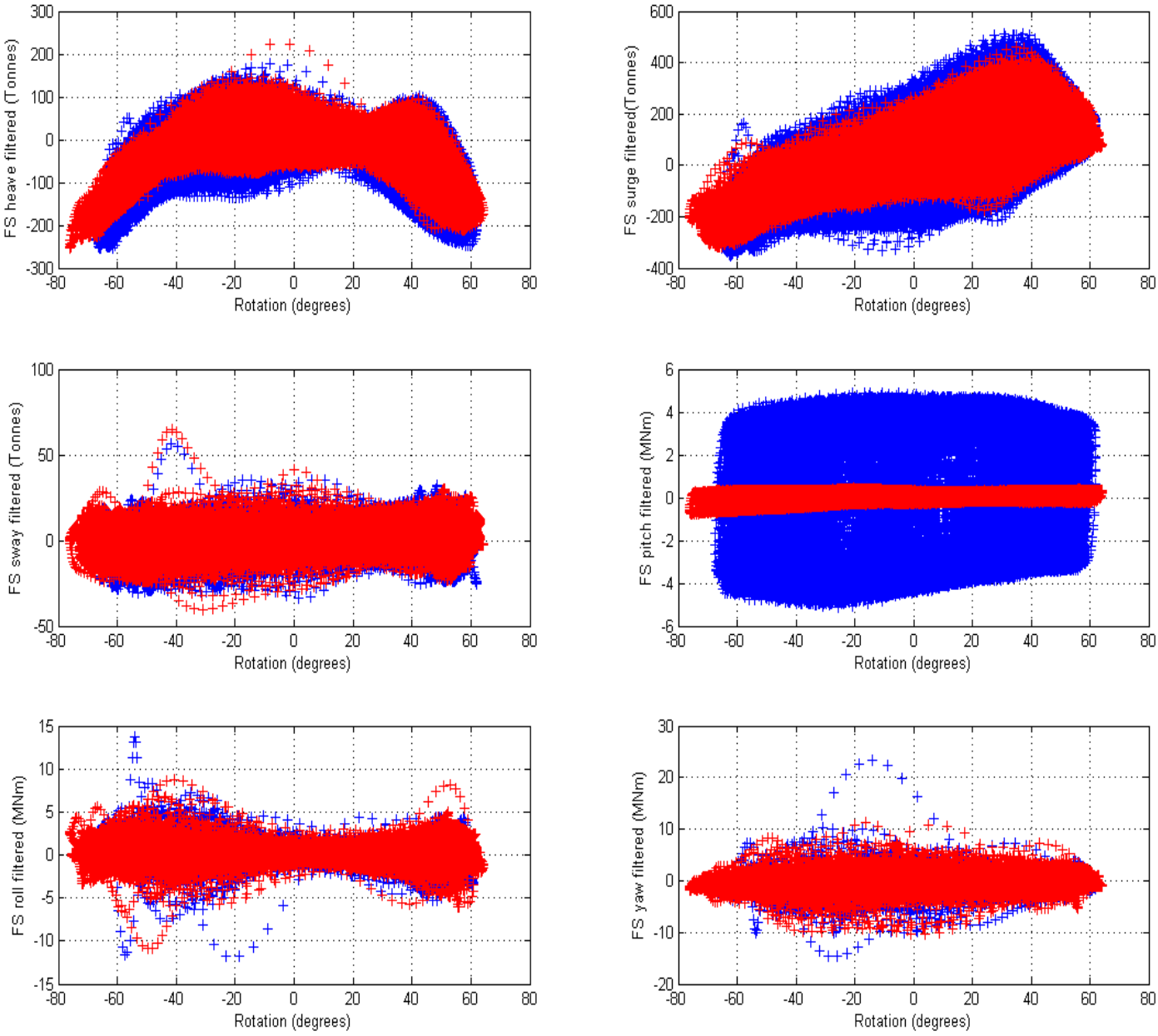

Figure D4

Foundation loads at the pivot point in extreme sea state 4 with energy period and significant wave height of Te=13s and Hs=10m respectively. The red data points correspond to an undamped flap and blue data points are for a global **RMS** damping torque of approximately 3.27MNm. The required global damping torque is 3.92 MNm.

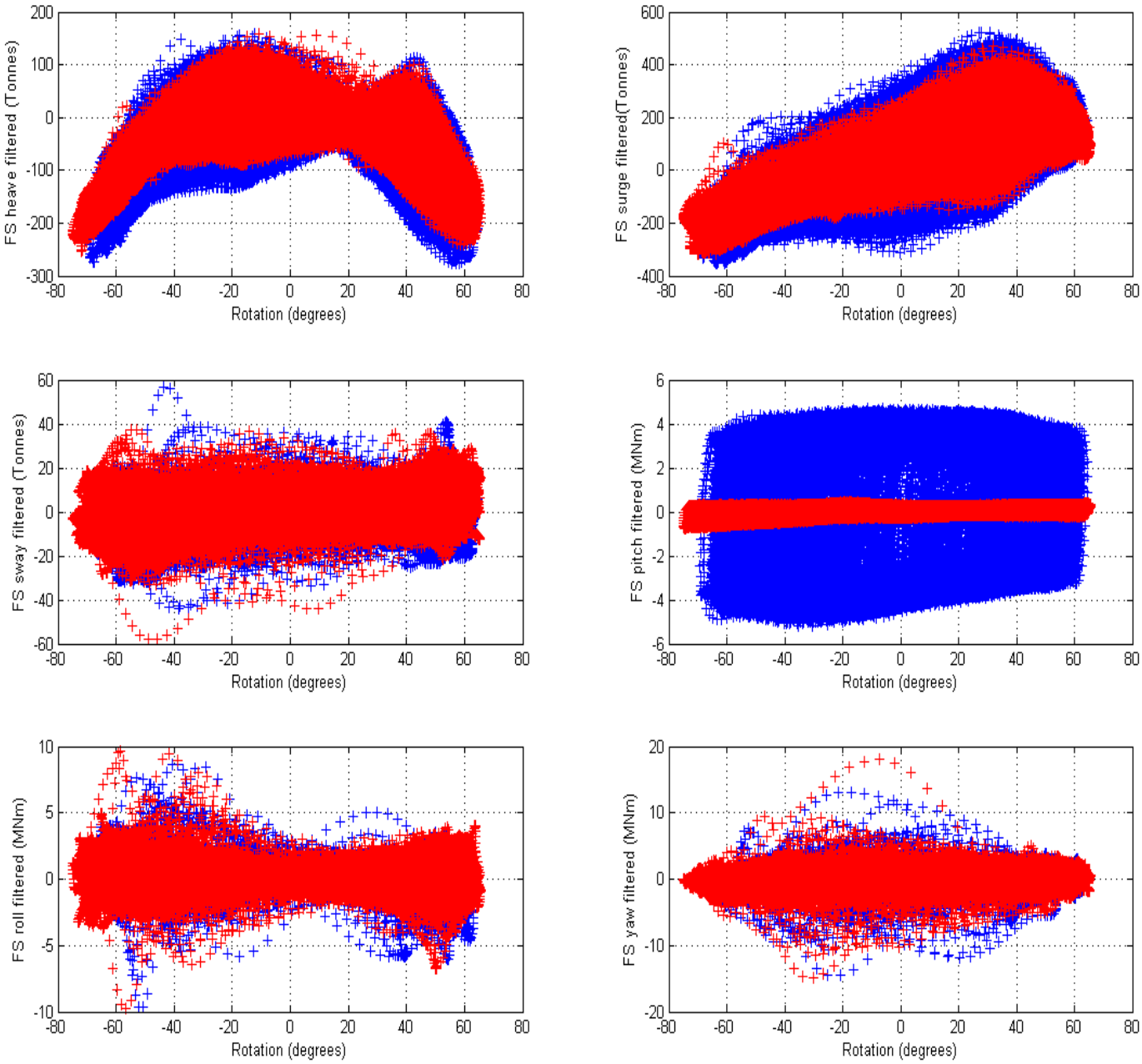

Figure D5

ndation loads at the pivot point in extreme sea state 5 with energy period and significant wave height of Te=15s and 8m respectively. The red data points correspond to an undamped flap and blue data points are for a global **RMS** ping torque of approximately 3.20 MNm. The required global damping torque is 3.92 MNm.

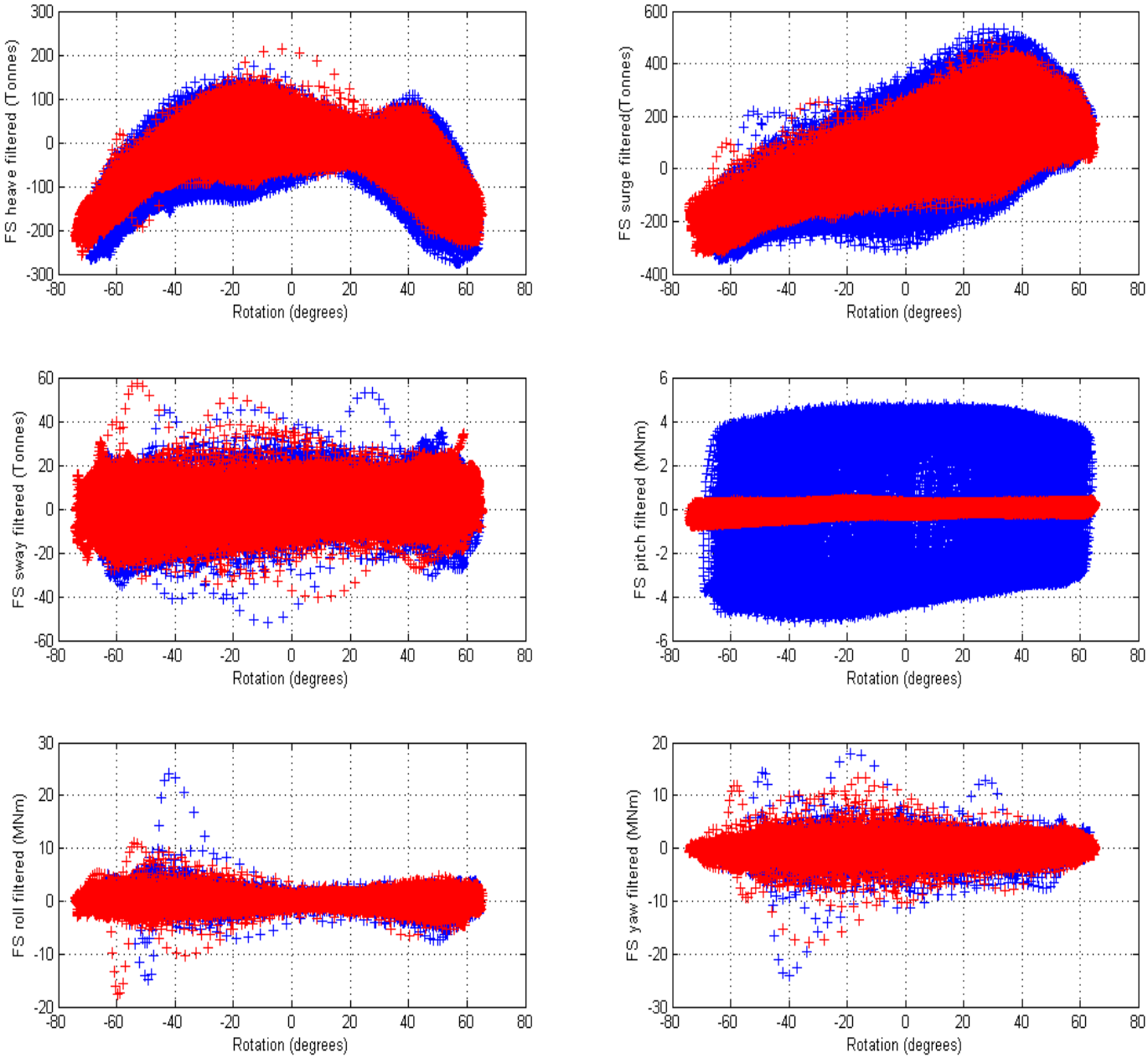

Figure D6

Foundation loads at the pivot point in extreme sea state 6 with energy period and significant wave height of Te=15s and Hs=10m respectively. The red data points correspond to an undamped flap and blue data points are for a global **RMS** damping torque of approximately 3.17 MNm. The required global damping torque is 3.92 MNm.

APPENDIX 1: Return Period-9 meter wide flap

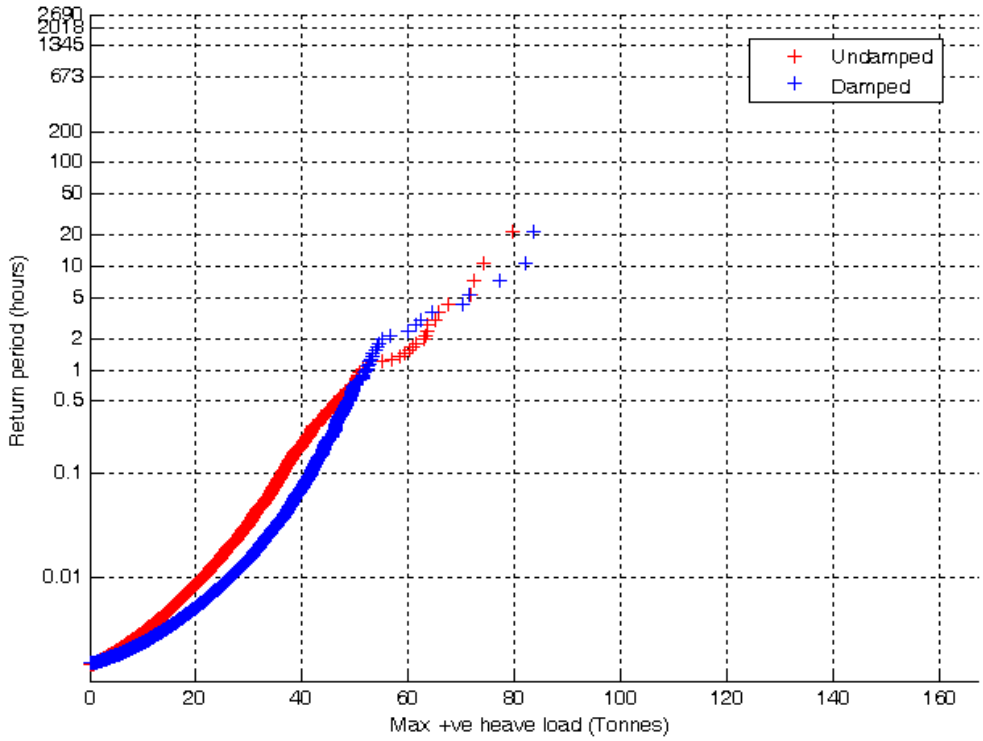

Figure 2a: Positive heave extreme value analysis plots for 9m damped and undamped flap

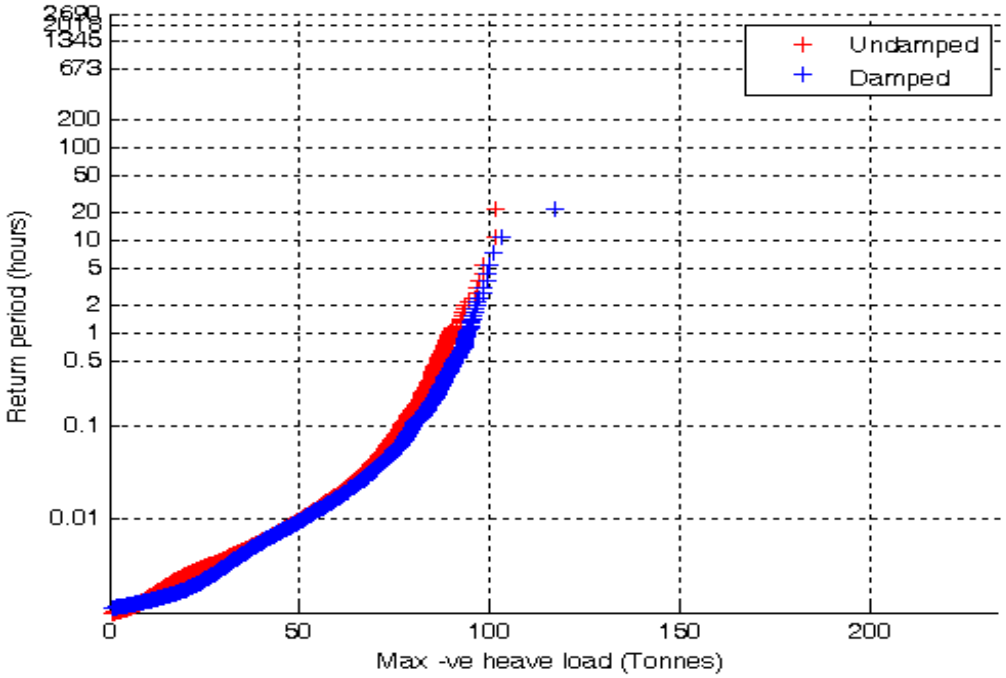

Figure 2b: Negative heave extreme value analysis plots for 9m damped and undamped flap

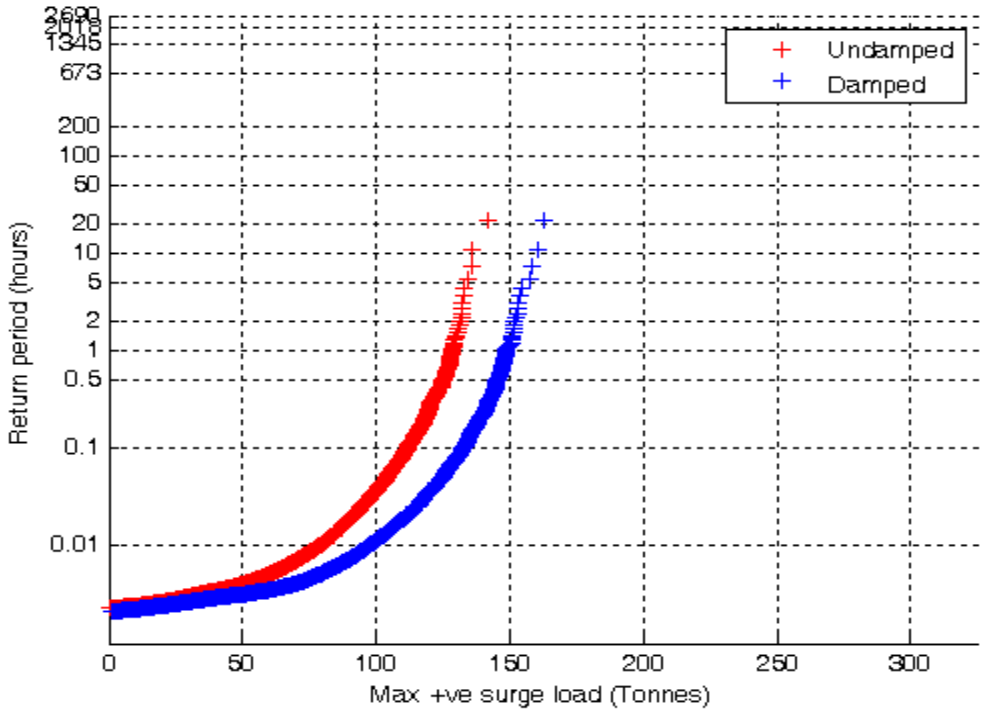

Figure 2c: Positive surge extreme value analysis plots for 9m damped and undamped flap

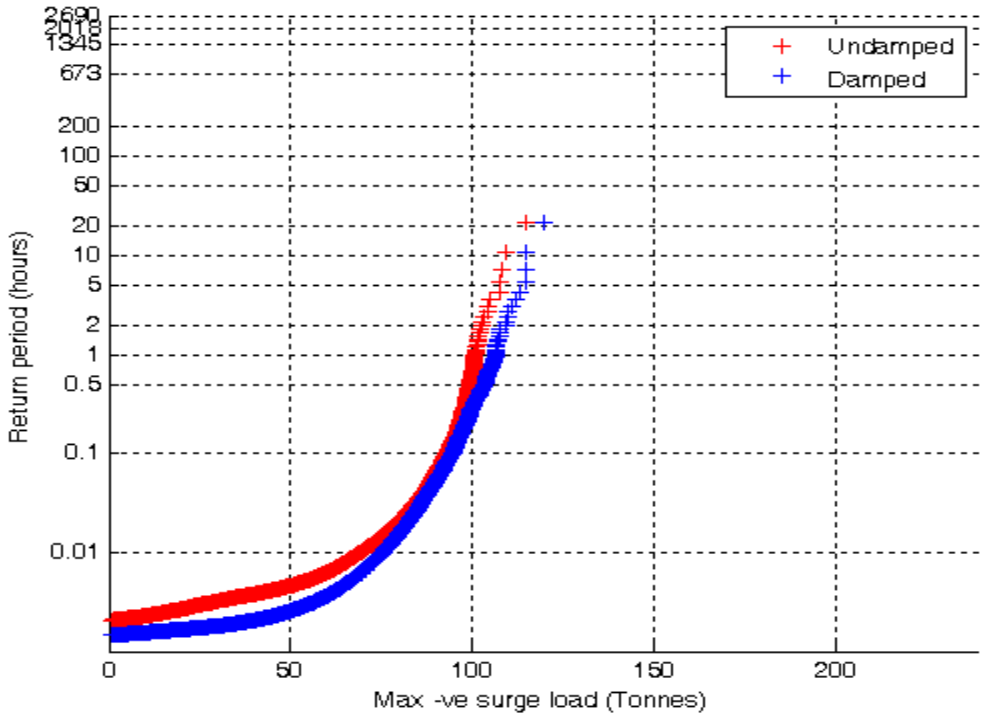

Figure 2d: Negative surge extreme value analysis plots for 9m damped and undamped flap

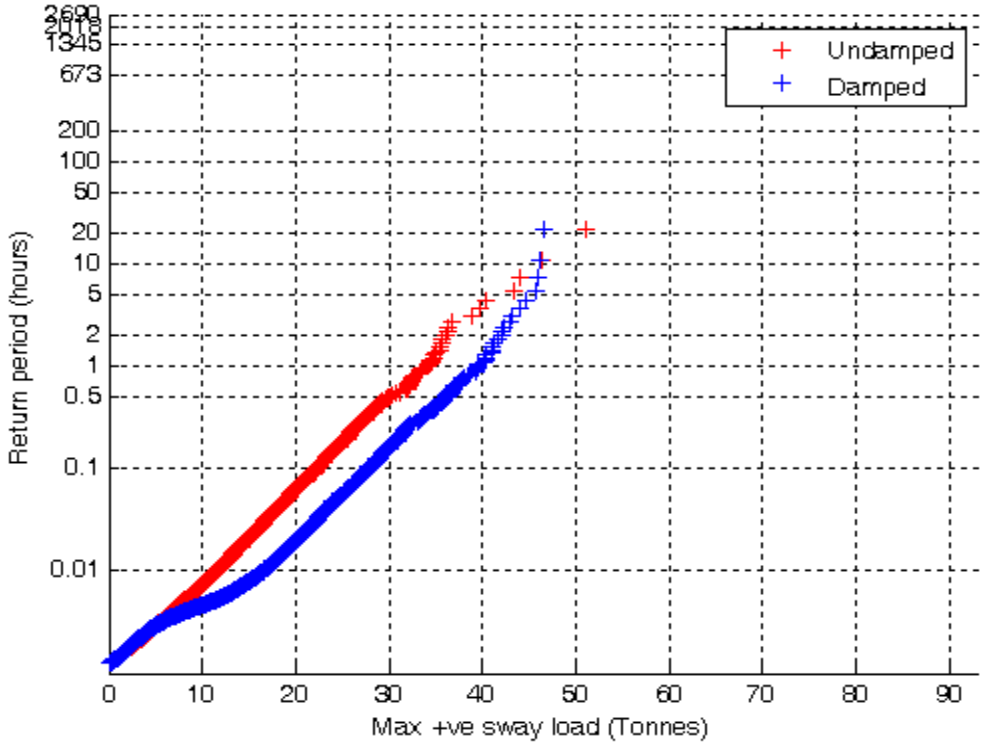

Figure 2e: Positive sway extreme value analysis plots for 9m damped and undamped flap

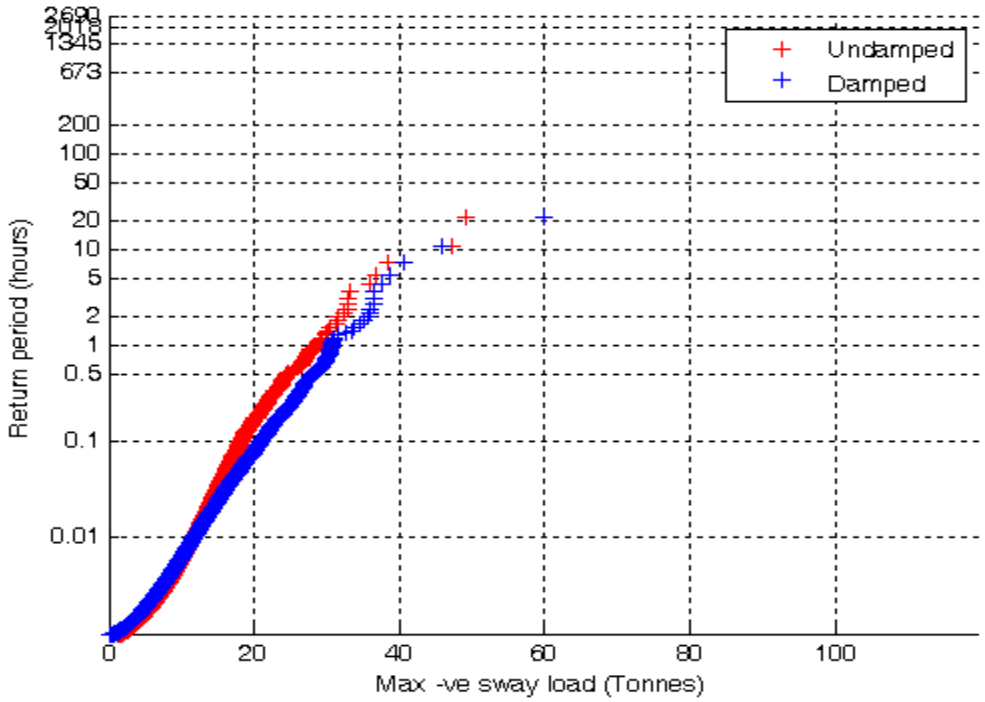

Figure 2f: Negative sway extreme value analysis plots for 9m damped and undamped flap

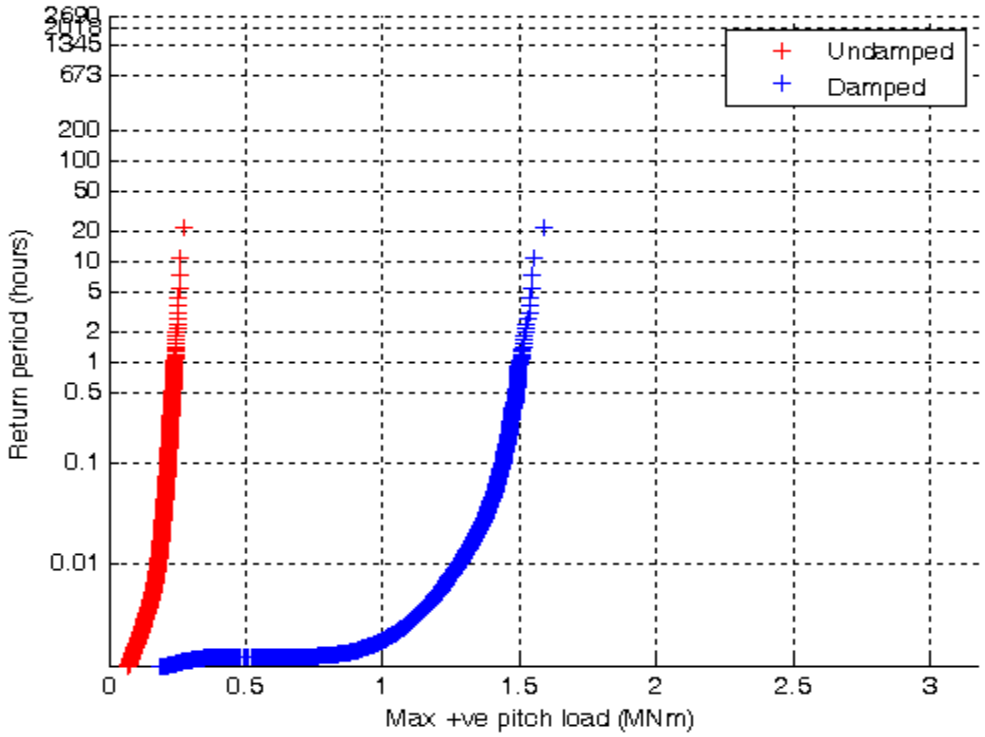

Figure 2g: Positive pitch extreme value analysis plots for 9m damped and undamped flap

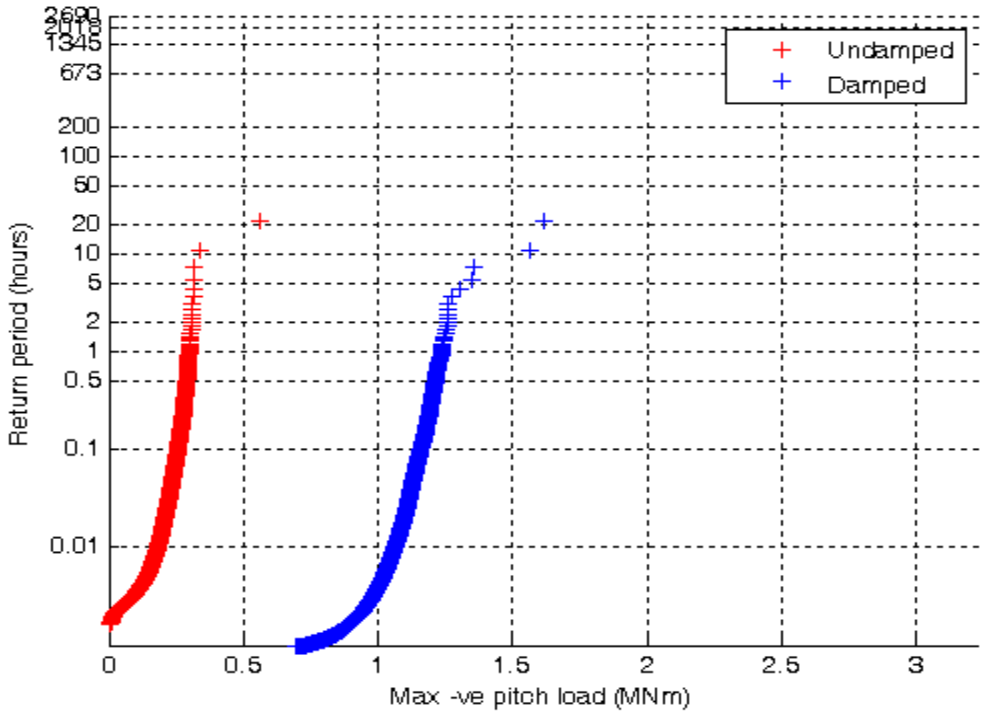

Figure 2h: Negative pitch extreme value analysis plots for 9m damped and undamped flap

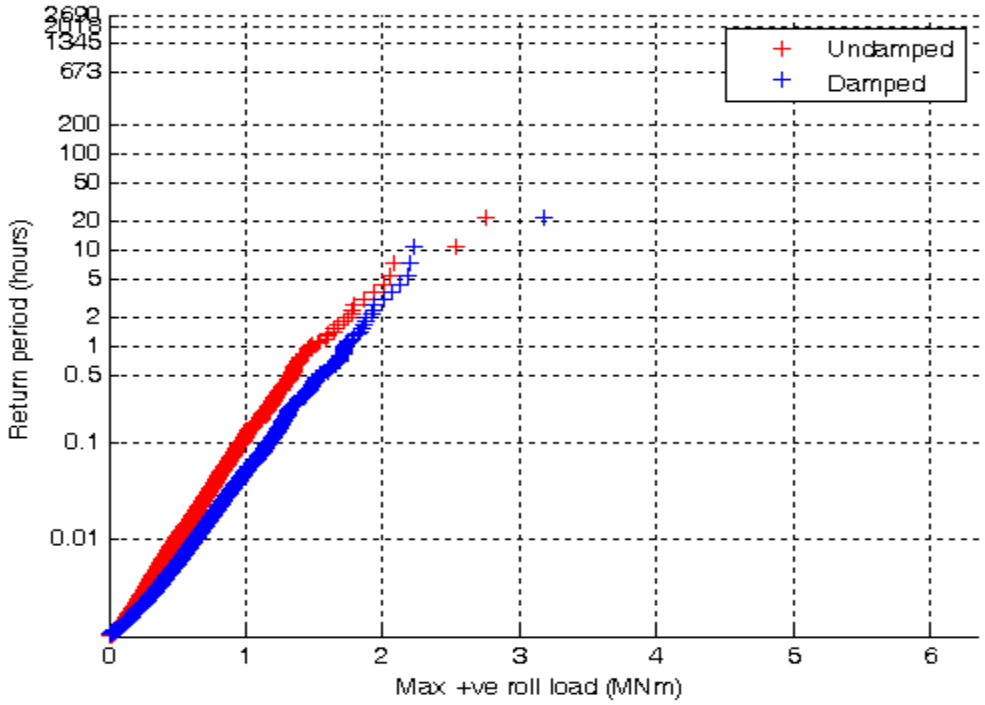

Figure 2i: Positive roll extreme value analysis plots for 9m damped and undamped flap

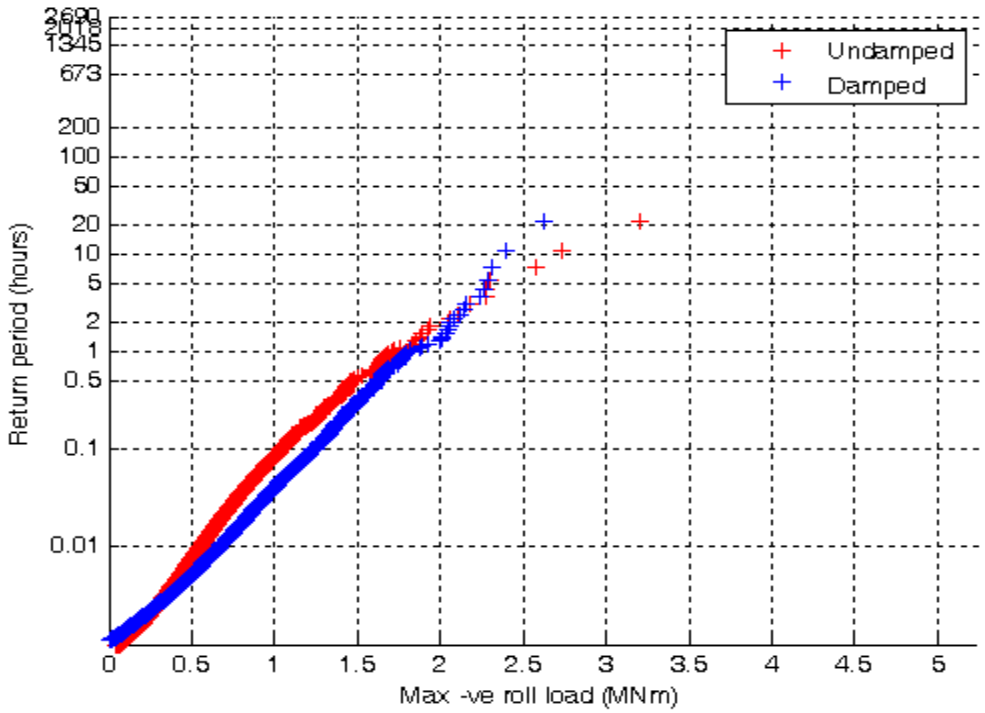

Figure 2j: Negative roll extreme value analysis plots for 9m damped and undamped flap

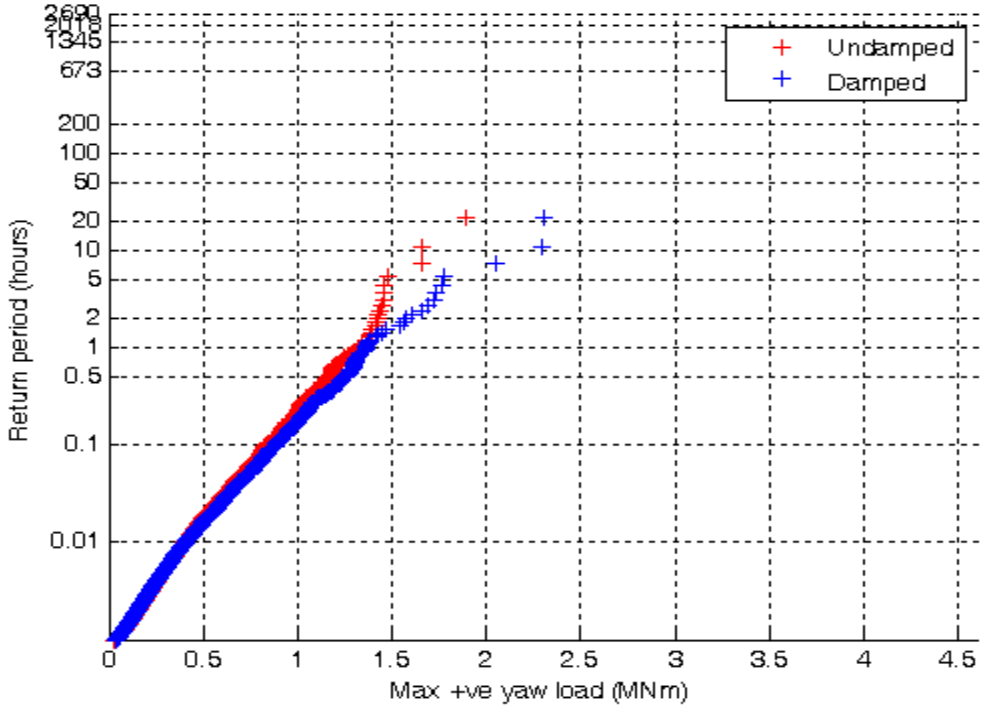

Figure 2k: Positive yaw extreme value analysis plots for 9m damped and undamped flap

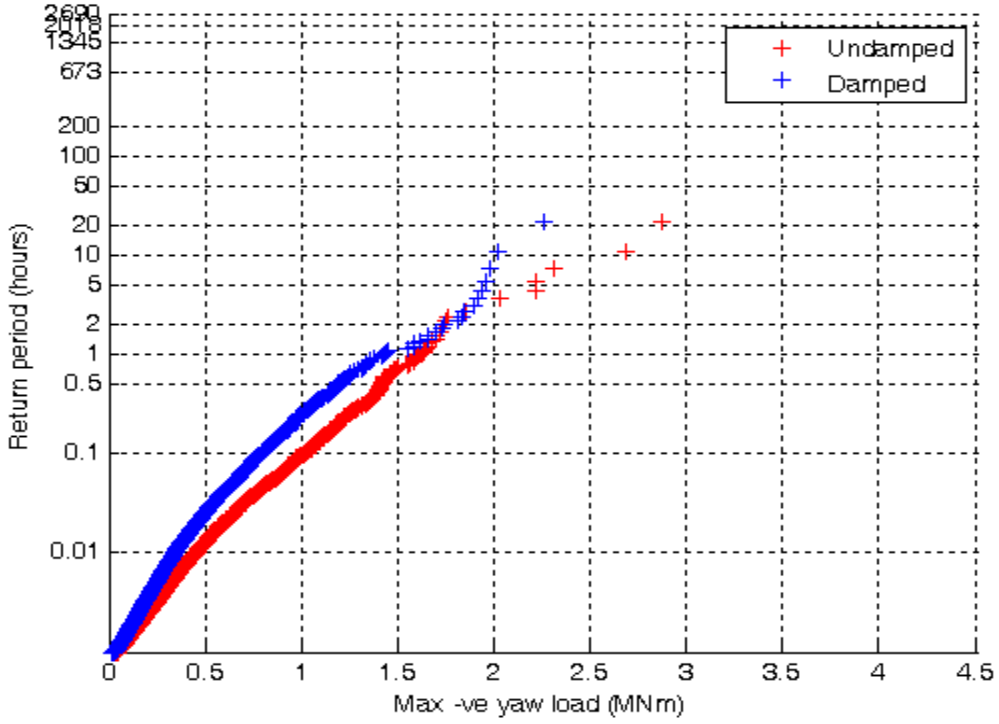

Figure 2l: Negative yaw extreme value analysis plots for 9m damped and undamped flap

APPENDIX 2: Return Period-12 meter wide flap

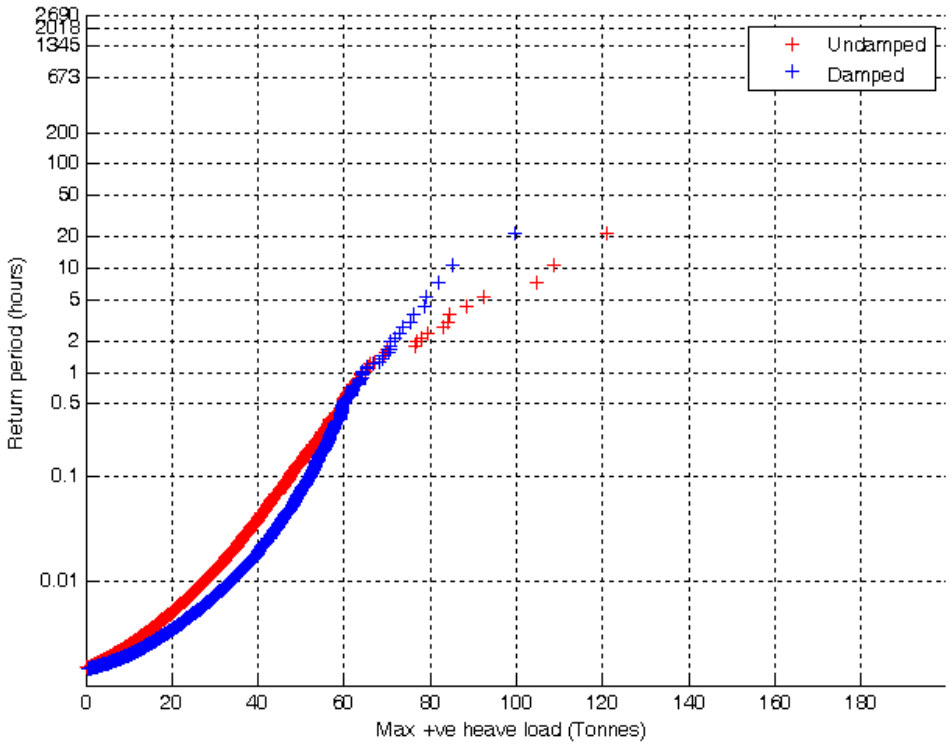

Figure 3a: Positive heave extreme value analysis plots for 12m damped and undamped flap

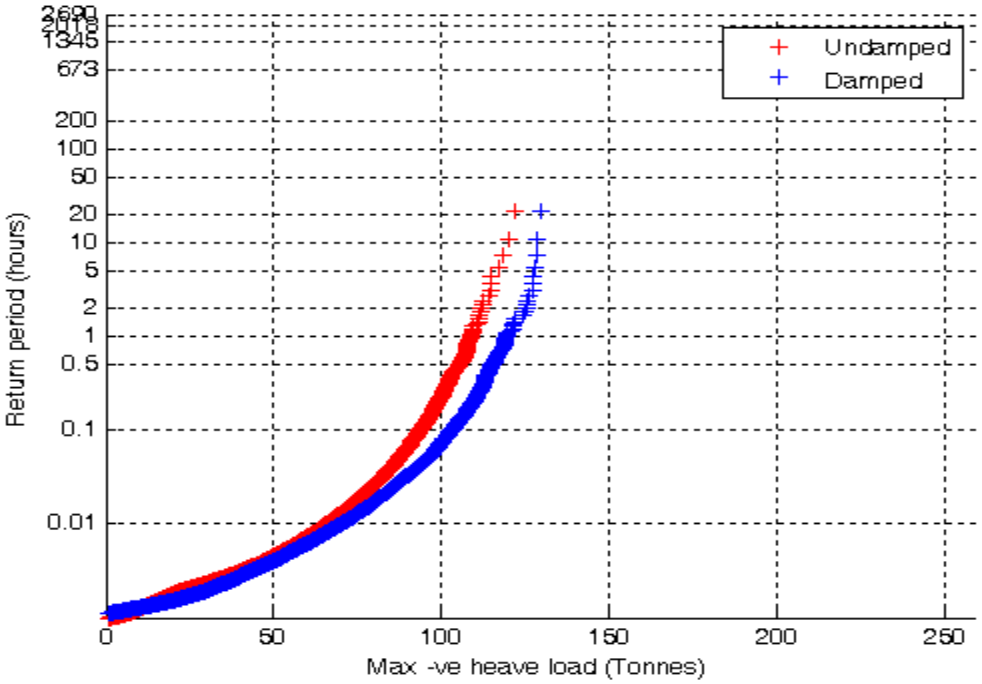

Figure 3b: Negative heave extreme value analysis plots for 12m damped and undamped flap

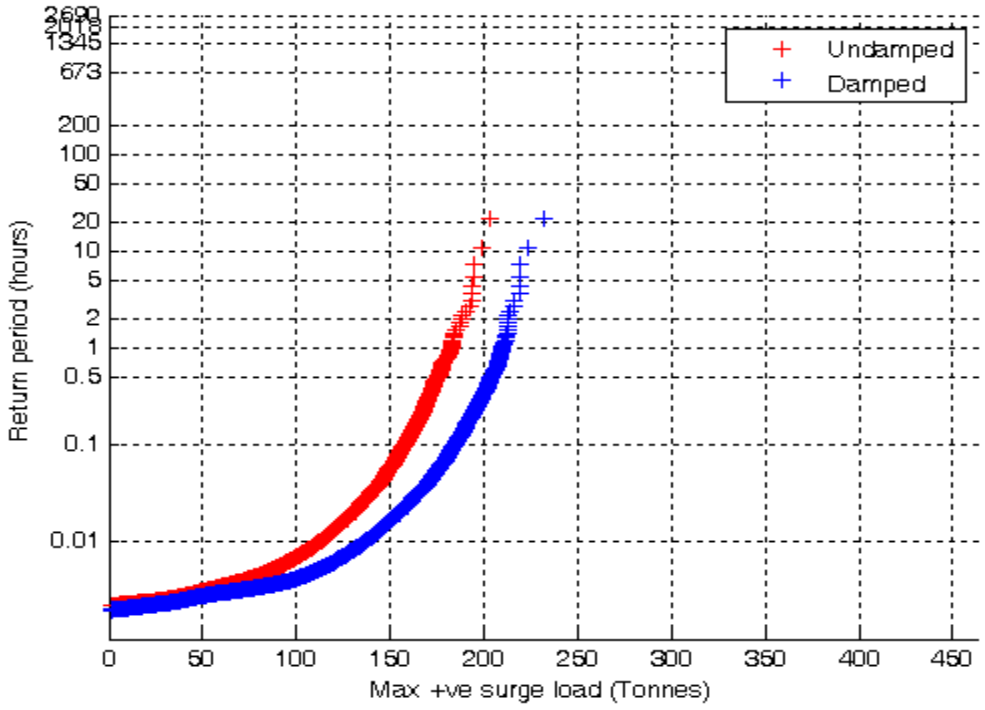

Figure 3c: Positive surge extreme value analysis plots for 12m damped and undamped flap

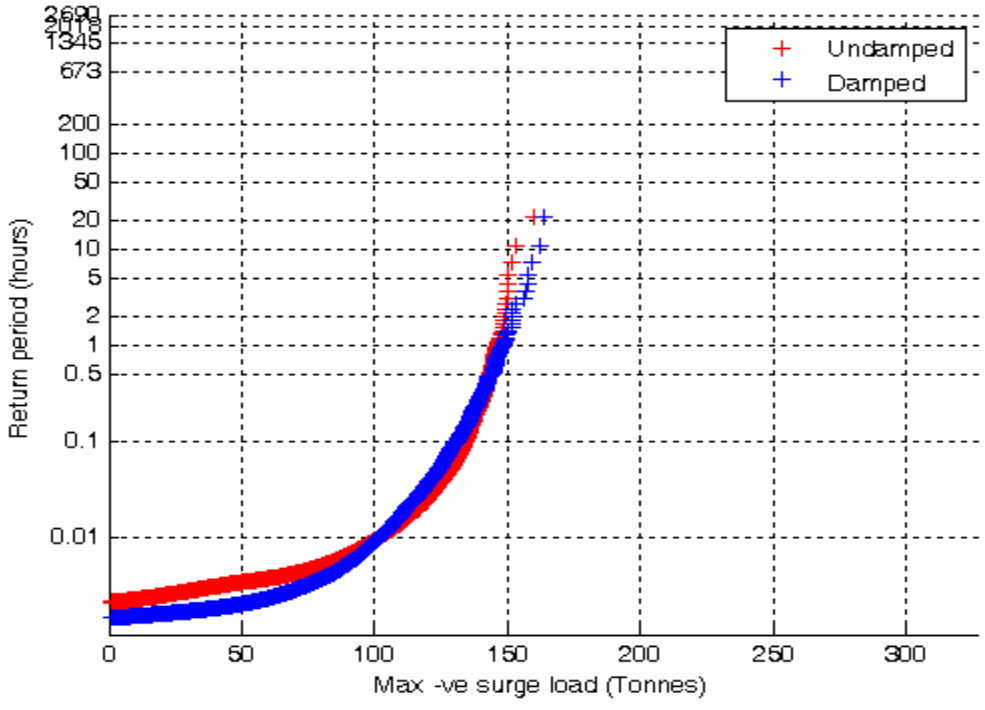

Figure 3d: Negative surge extreme value analysis plots for 12m damped and undamped flap

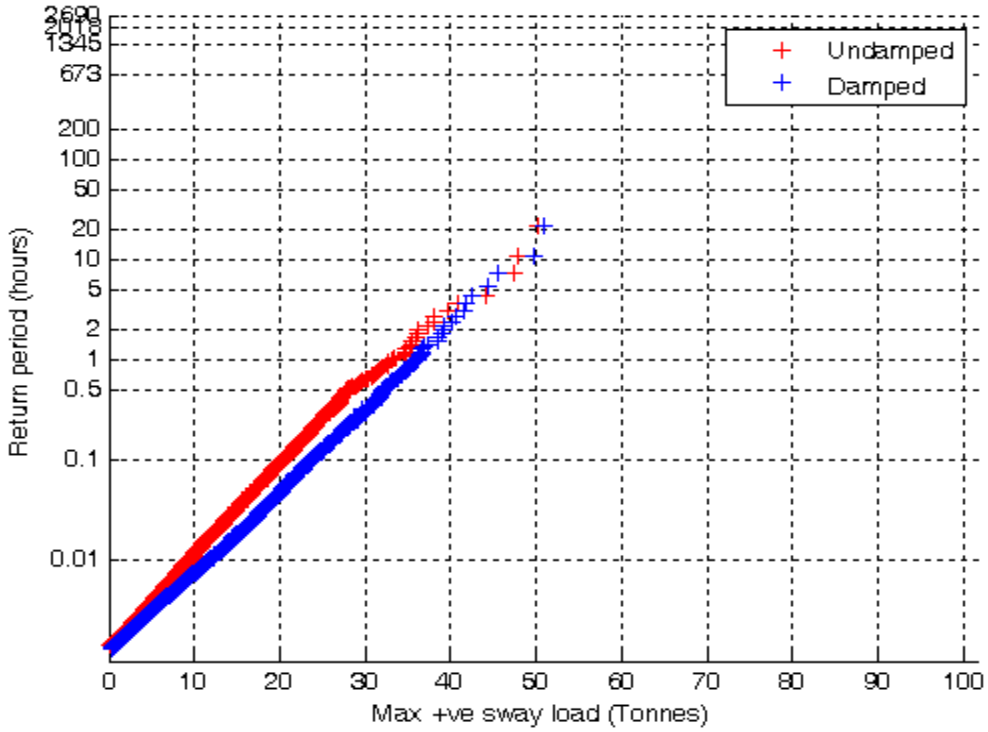

Figure 3e: Positive sway extreme value analysis plots for 12m damped and undamped flap

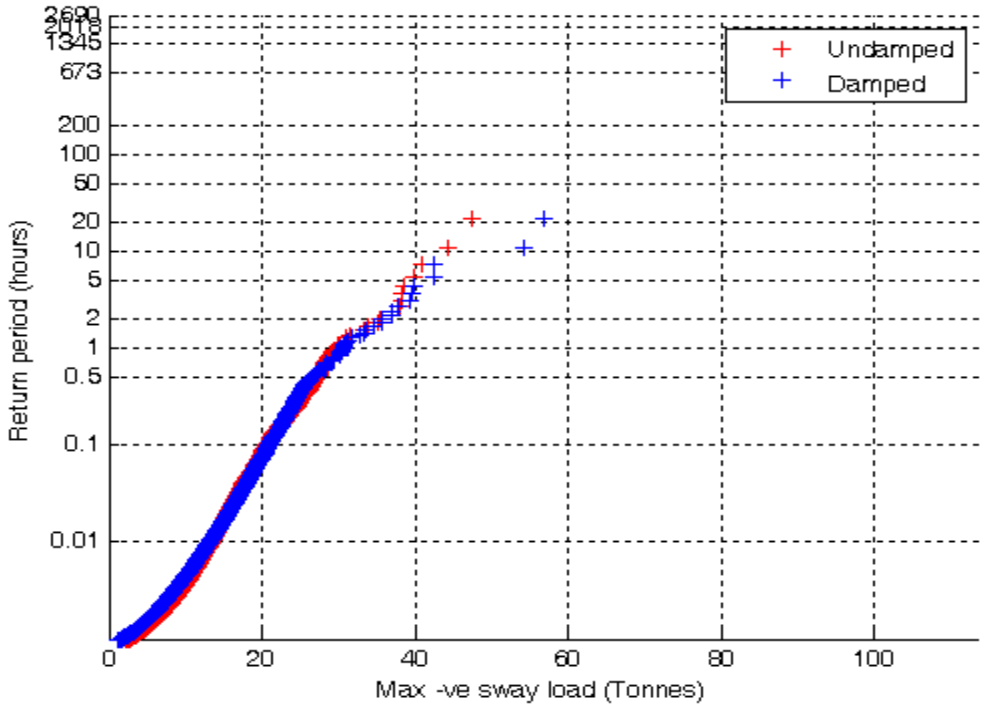

Figure 3f: Negative sway extreme value analysis plots for 12m damped and undamped flap

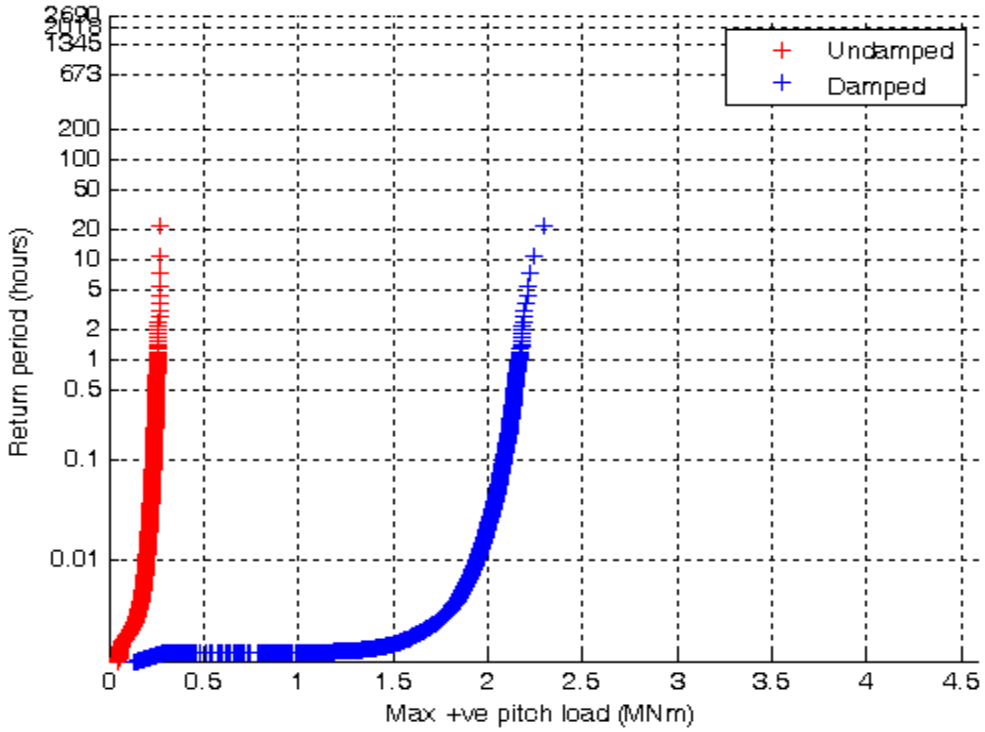

Figure 3g: Positive pitch extreme value analysis plots for 12m damped and undamped flap

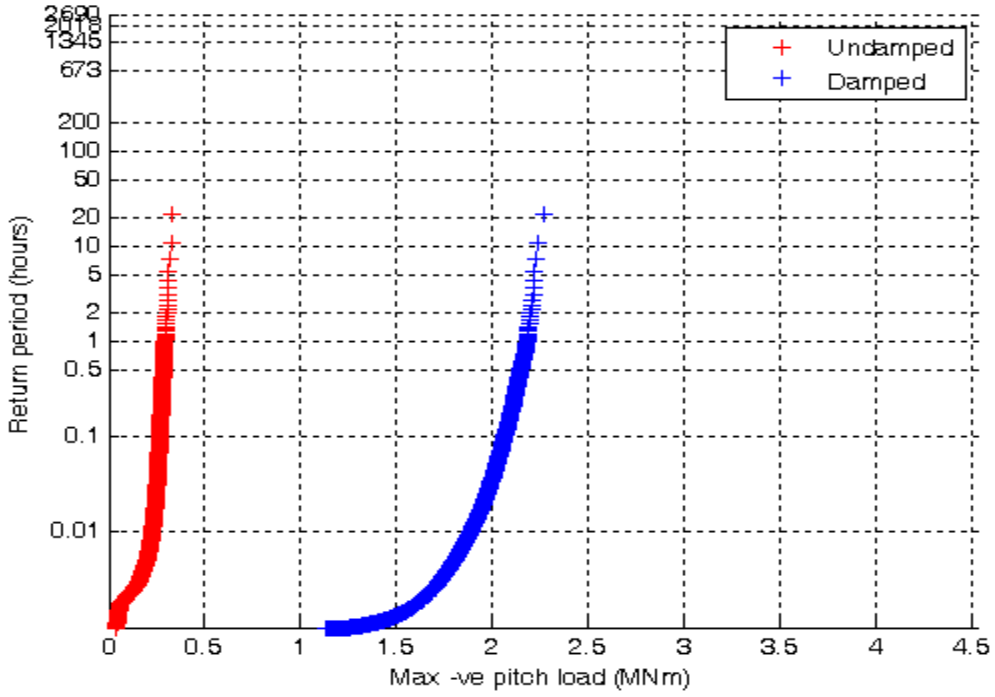

Figure 3h: Negative pitch extreme value analysis plots for 12m damped and undamped flap

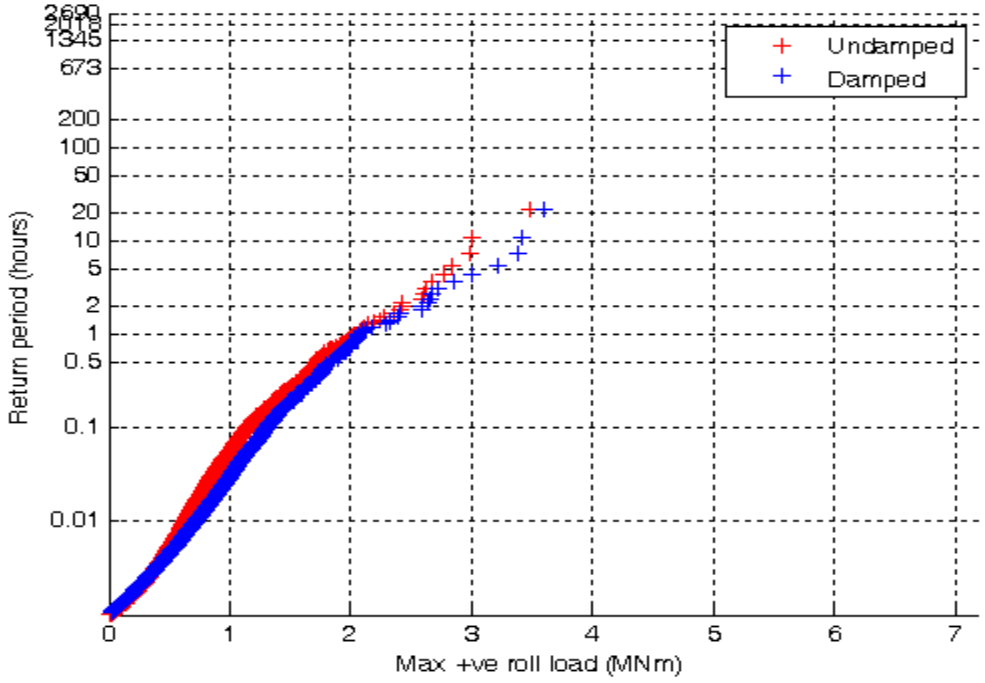

Figure 3i: Positive roll extreme value analysis plots for 12m damped and undamped flap

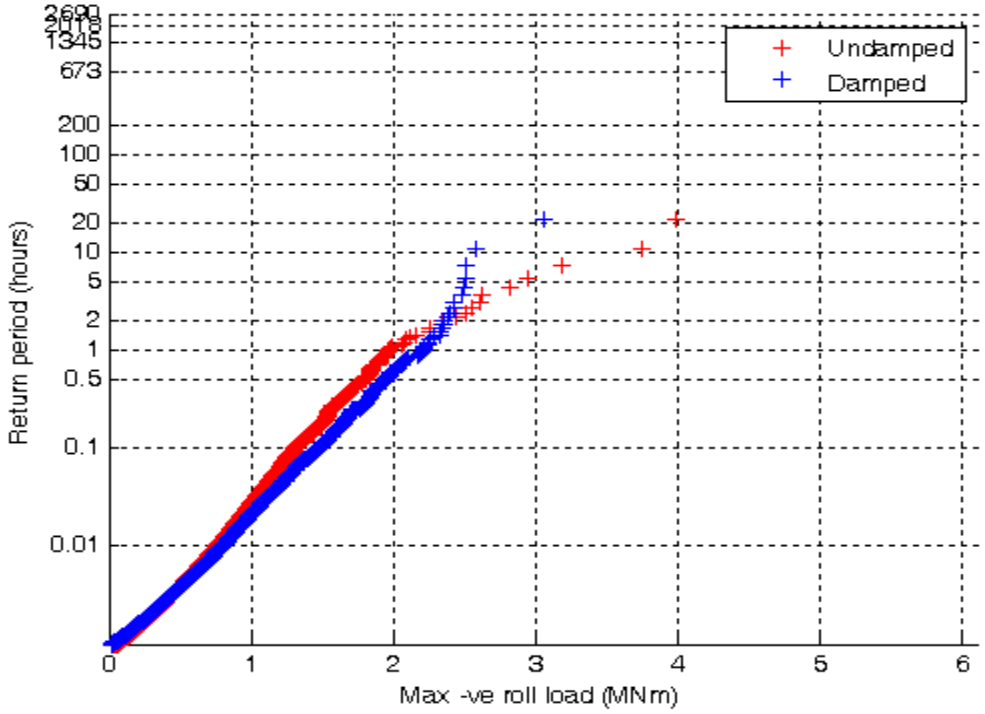

Figure 3j: Negative roll extreme value analysis plots for 12m damped and undamped flap

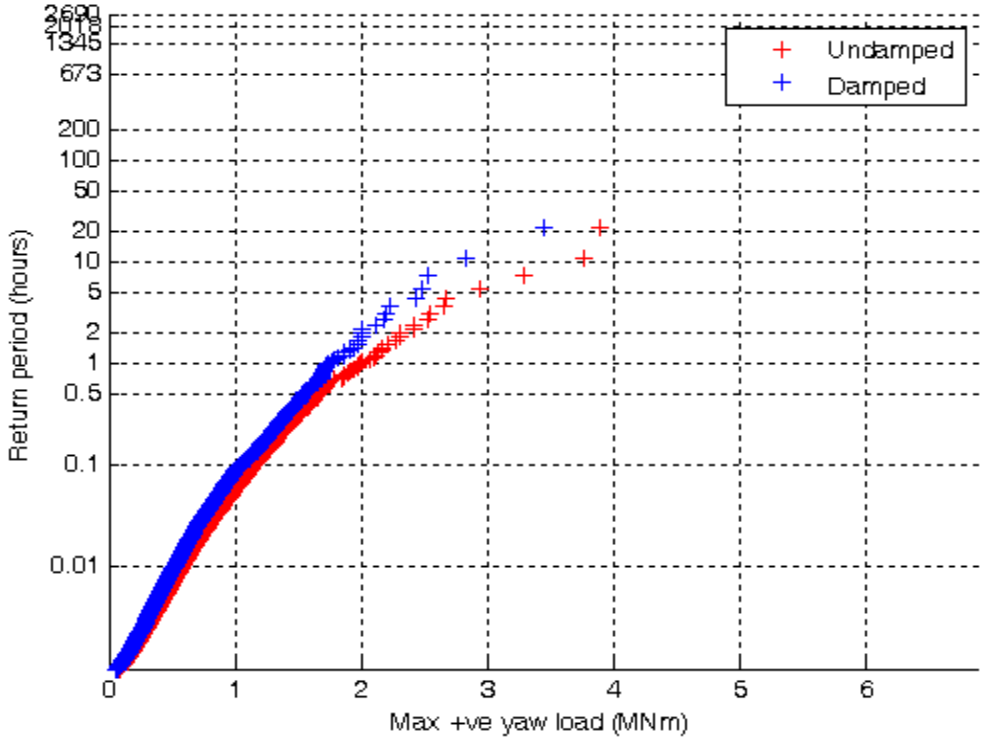

Figure 3k: Positive yaw extreme value analysis plots for 12m damped and undamped flap

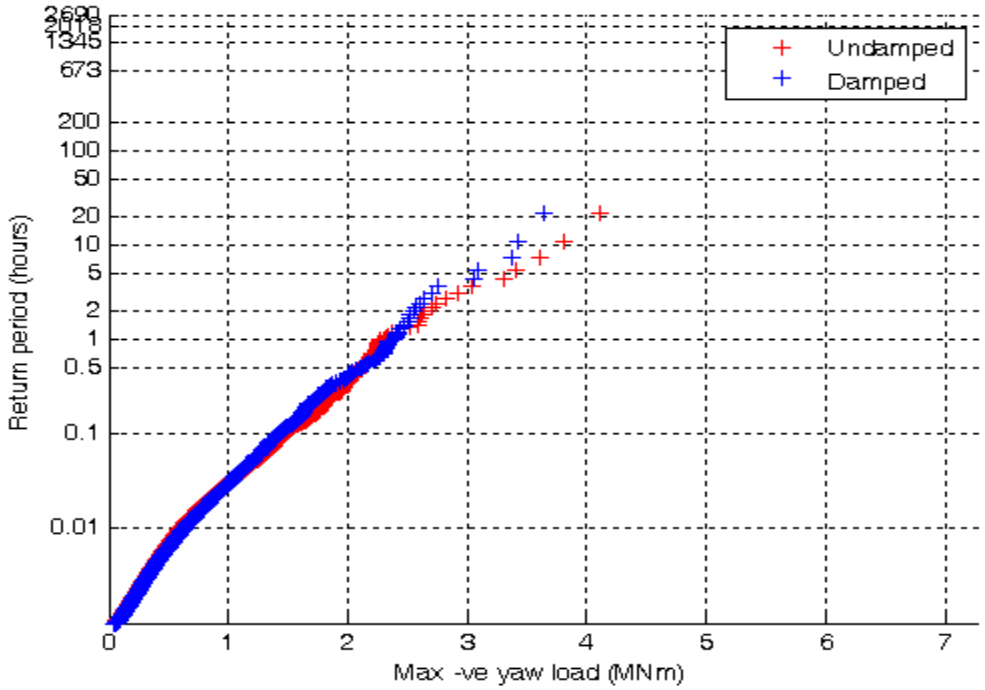

Figure 3l: Negative yaw extreme value analysis plots for 12m damped and undamped flap

APPENDIX 3: Return Period-18 meter wide flap

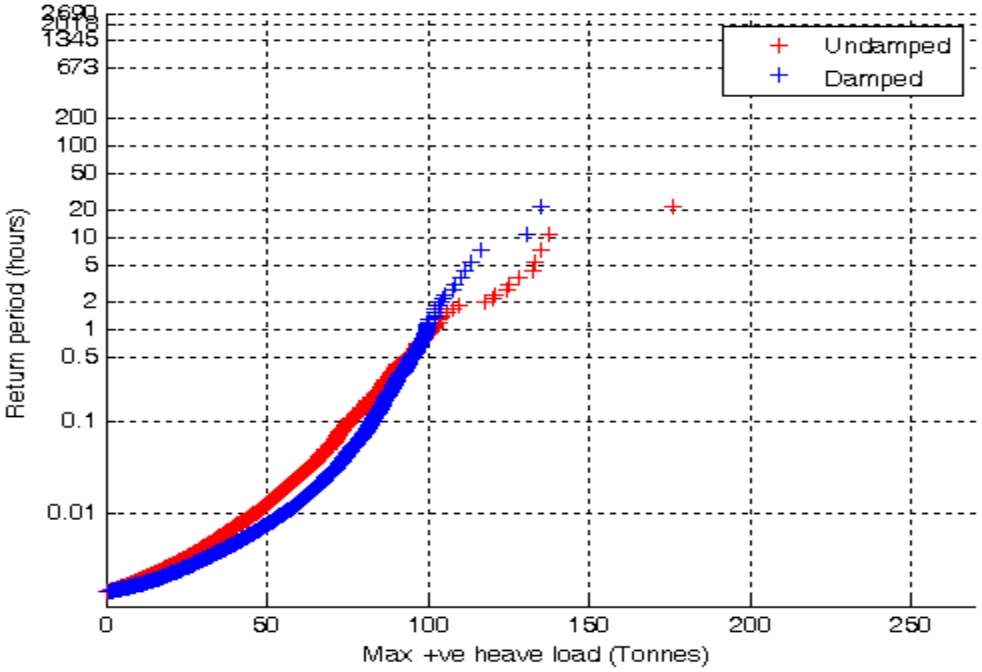

Figure 4a: Positive heave extreme value analysis plots for 18m damped and undamped flap

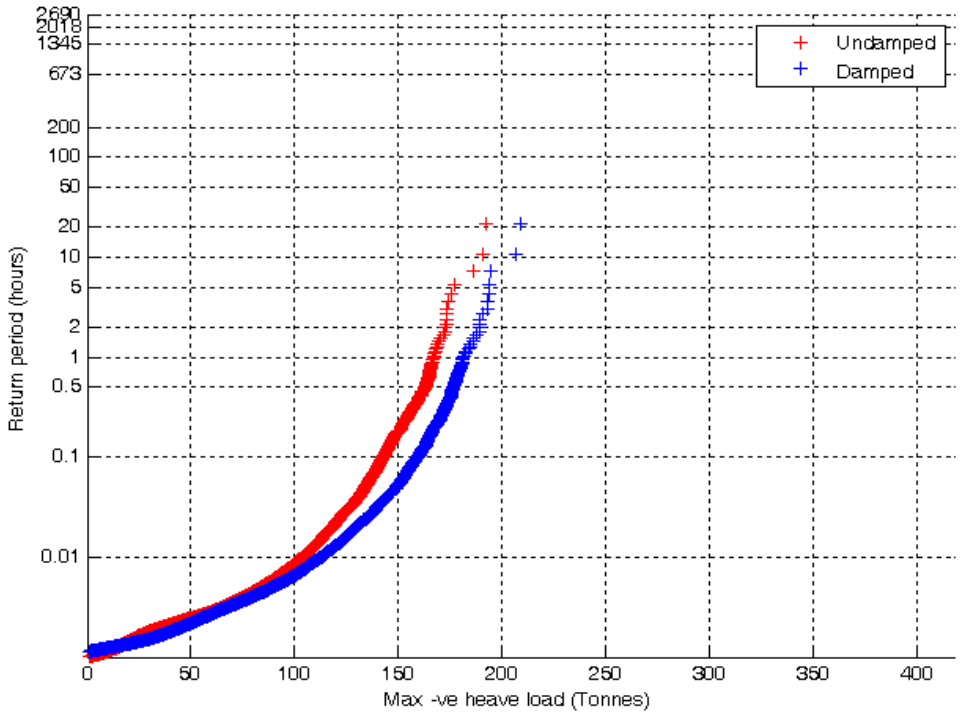

Figure 4b: Negative heave extreme value analysis plots for 18m damped and undamped flap

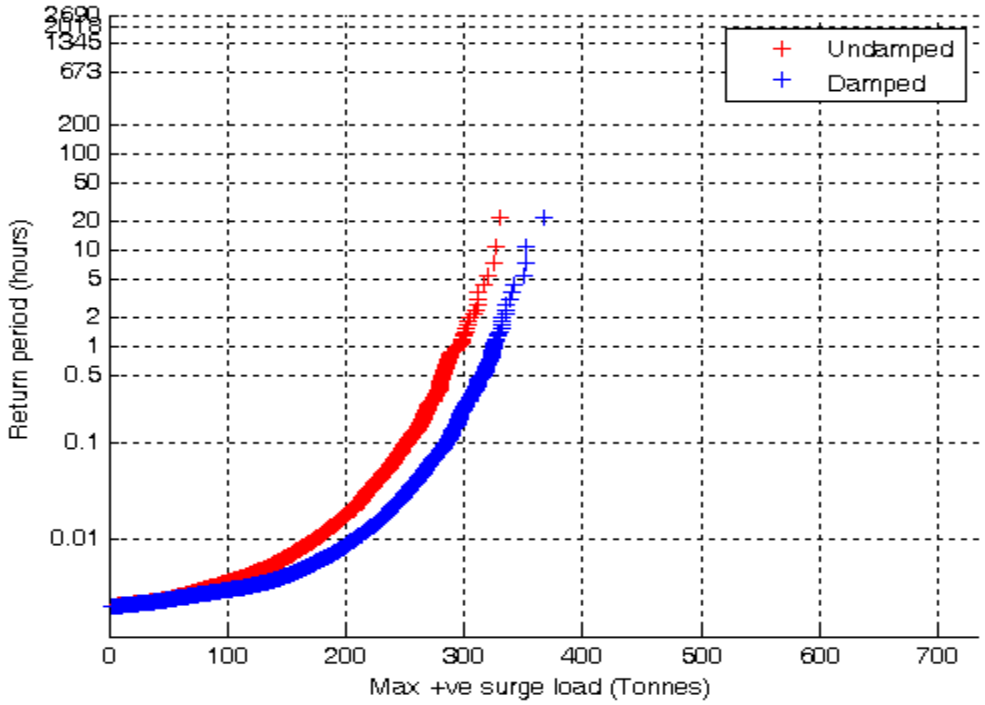

Figure 4c: Positive surge extreme value analysis plots for 18m damped and undamped flap

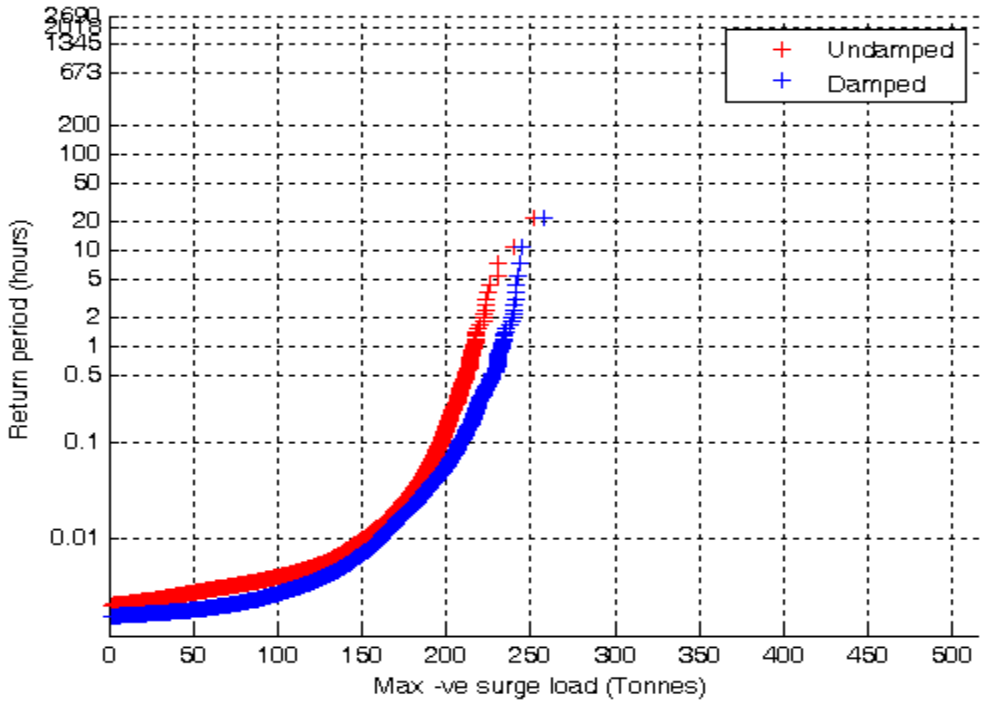

Figure 4d: Negative surge extreme value analysis plots for 18m damped and undamped flap

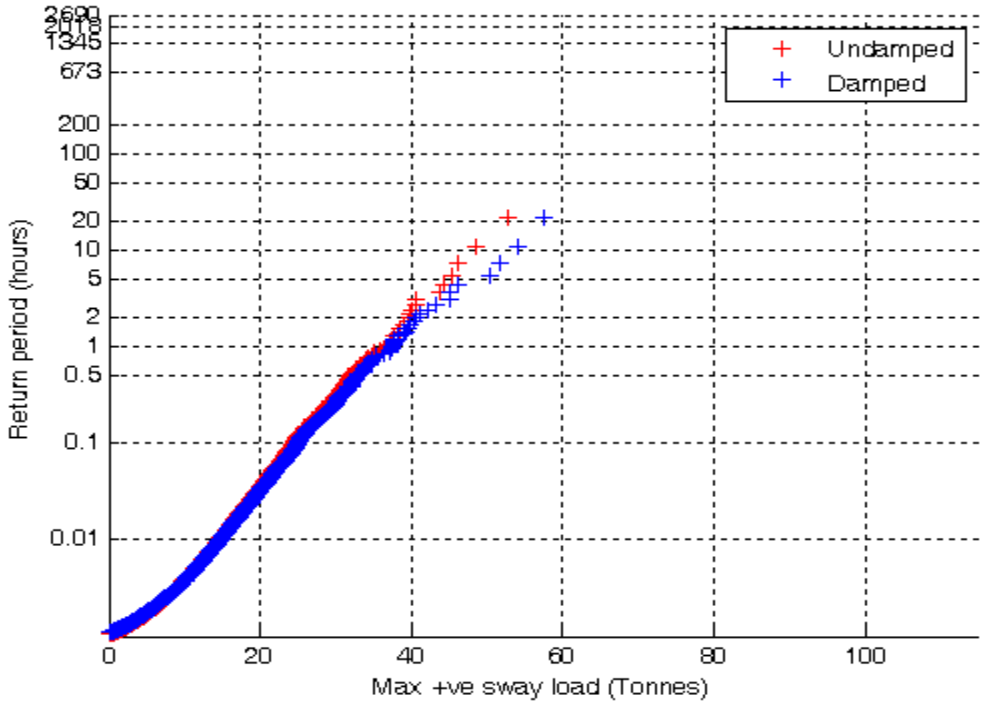

Figure 4e: Positive sway extreme value analysis plots for 18m damped and undamped flap

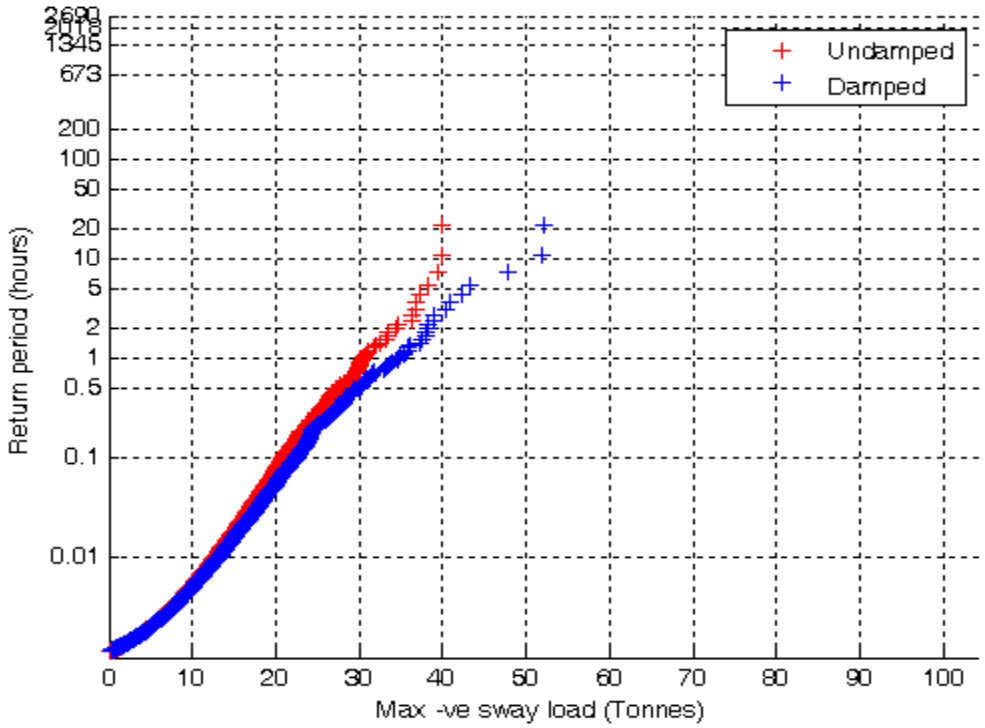

Figure 4f: Negative sway extreme value analysis plots for 18m damped and undamped flap

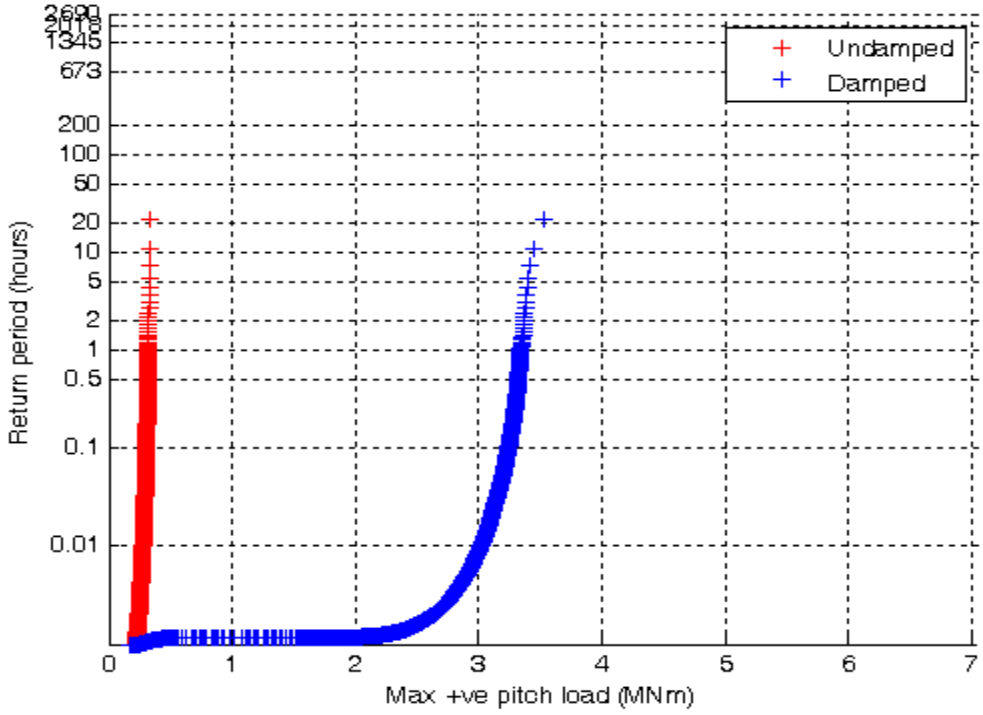

Figure 4g: Positive pitch extreme value analysis plots for 18m damped and undamped flap

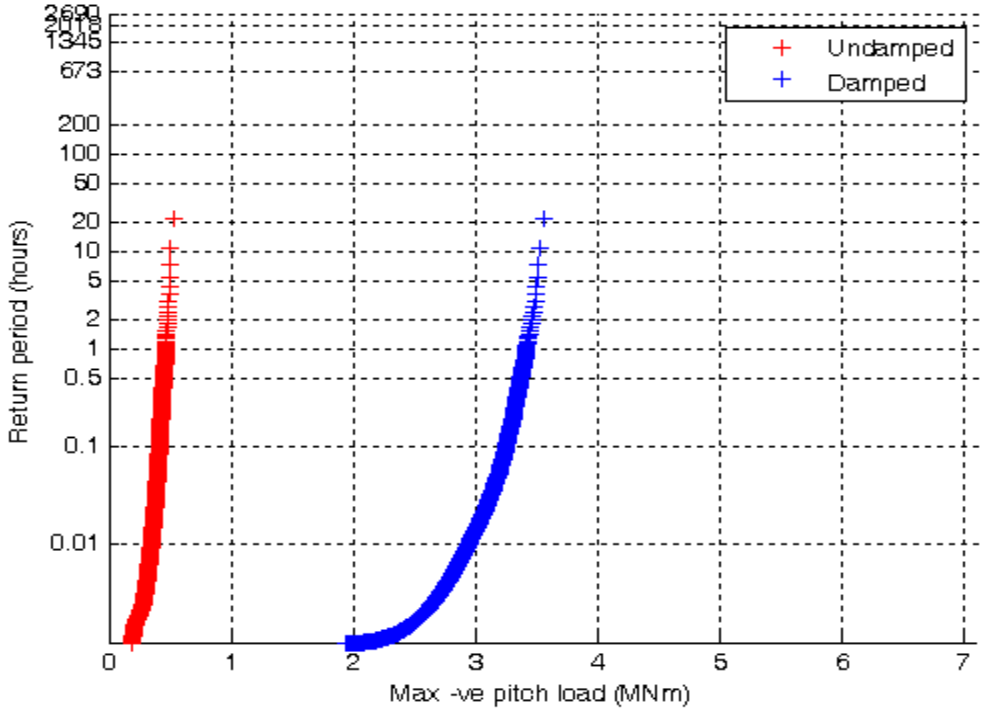

Figure 4h: Negative pitch extreme value analysis plots for 18m damped and undamped flap

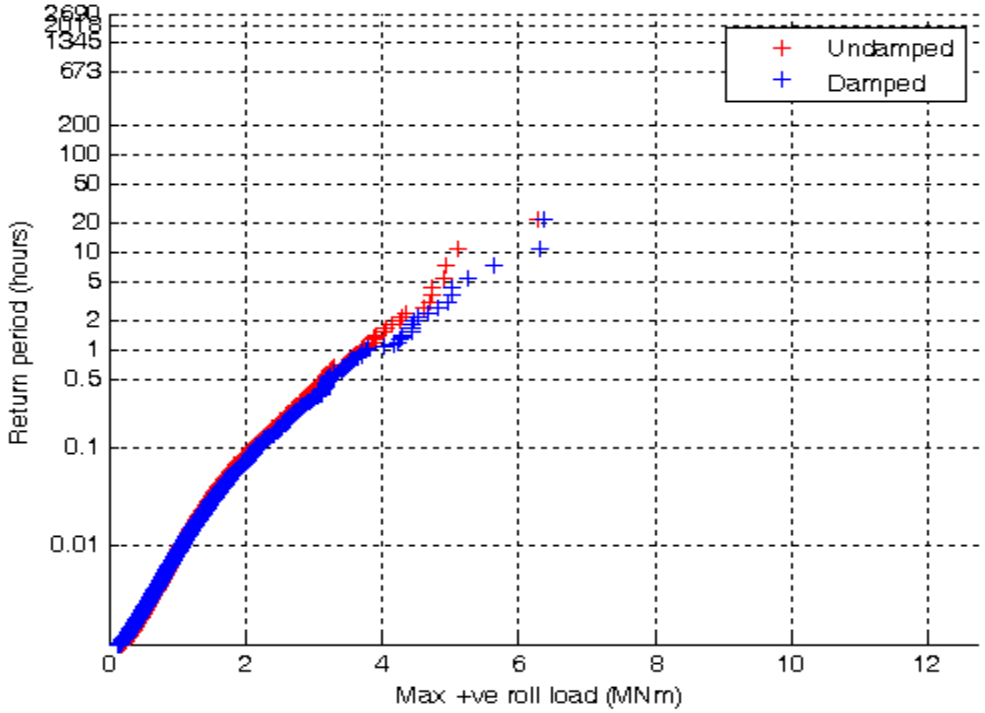

Figure 4i: Positive roll extreme value analysis plots for 18m damped and undamped flap

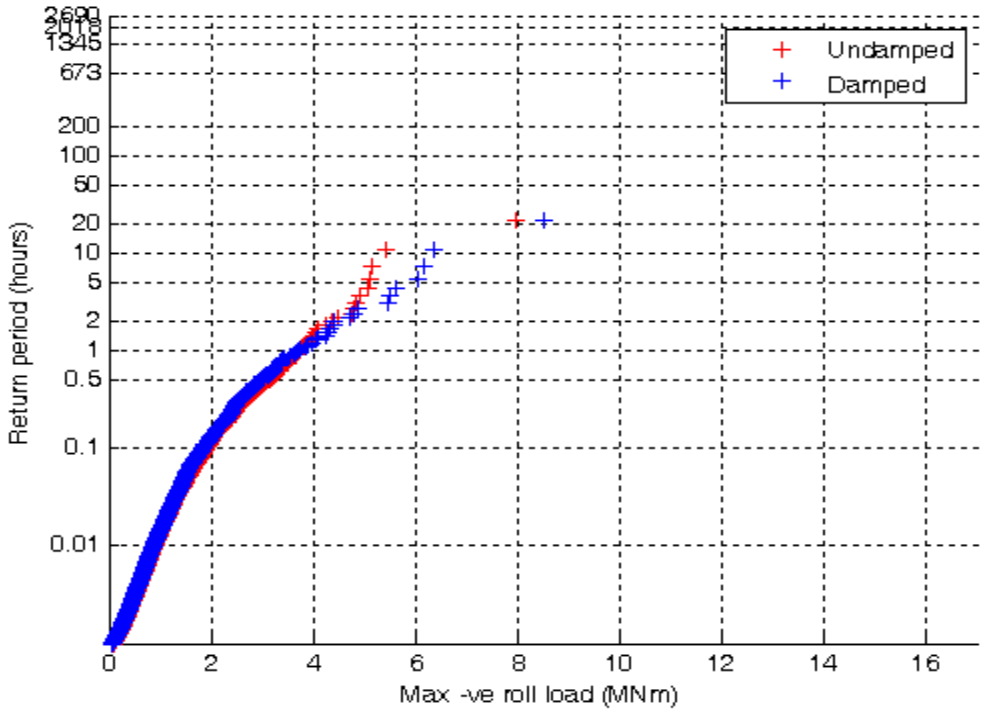

Figure 4j: Negative roll extreme value analysis plots for 18m damped and undamped flap

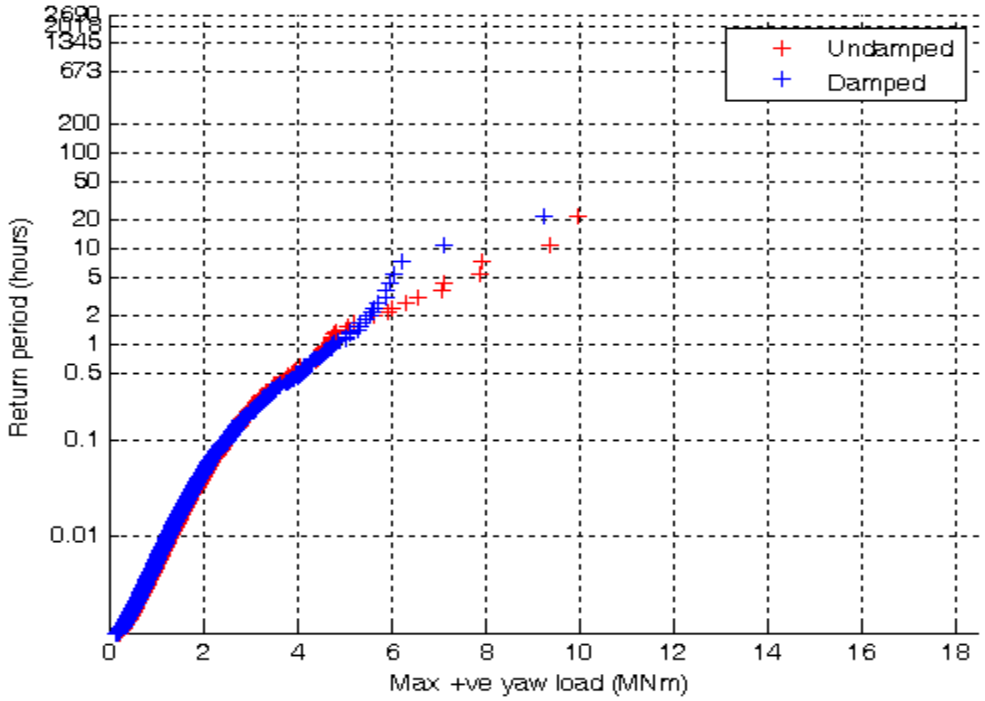

Figure 4k: Positive yaw extreme value analysis plots for 18m damped and undamped flap

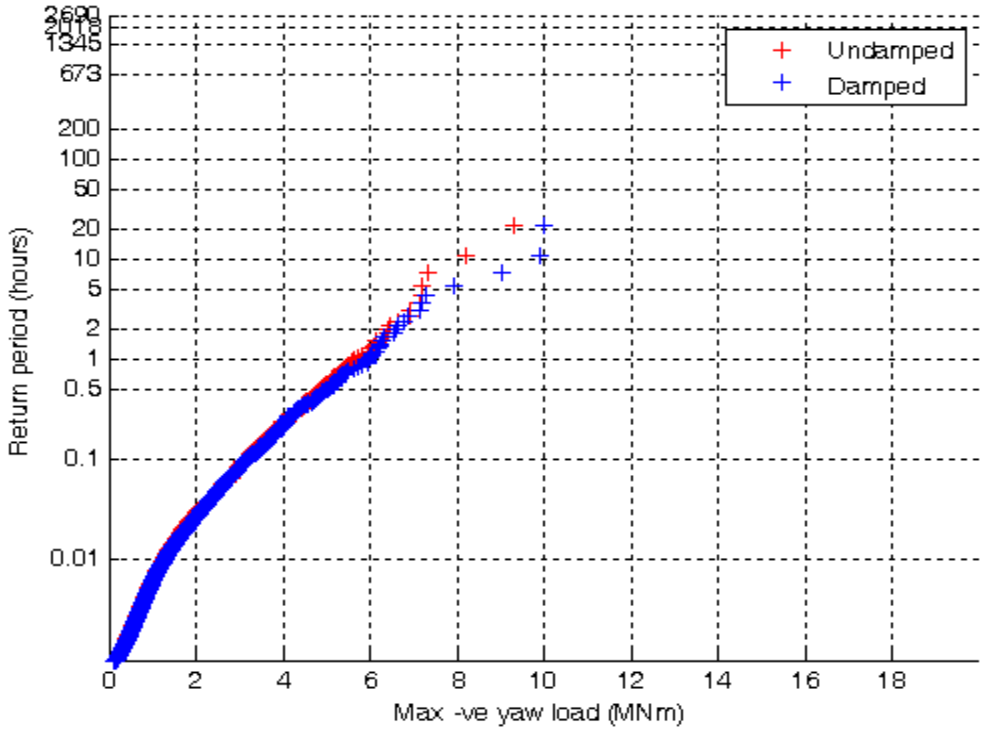

Figure 4l: Negative yaw extreme value analysis plots for 18m damped and undamped flap

APPENDIX 4: Return Period-24 meter wide flap

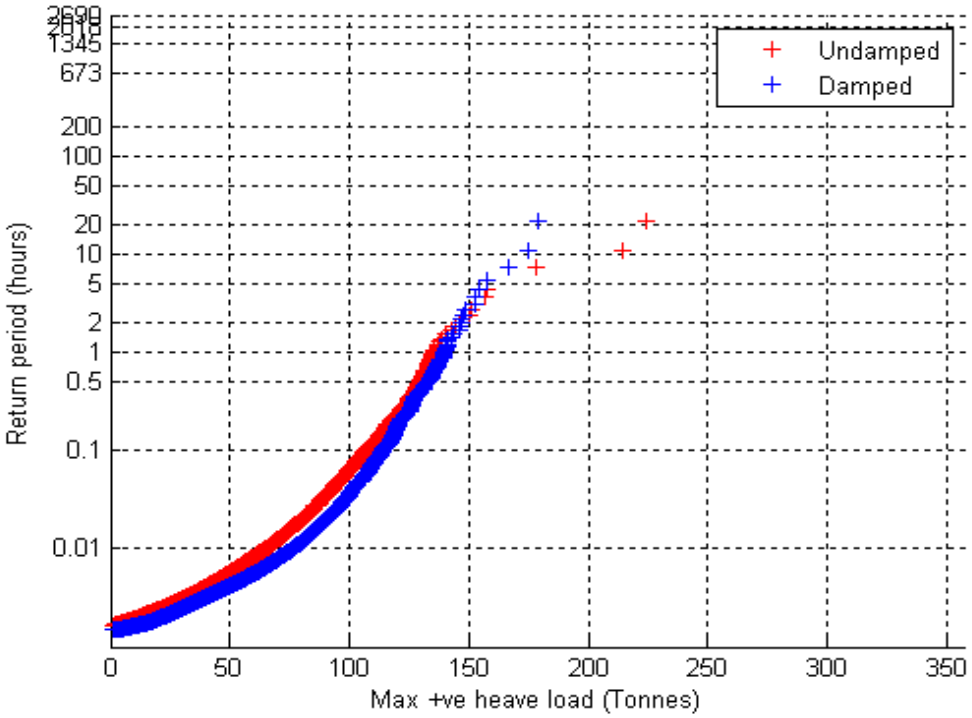

Figure 5a: Positive heave extreme value analysis plots for 24m damped and undamped flap

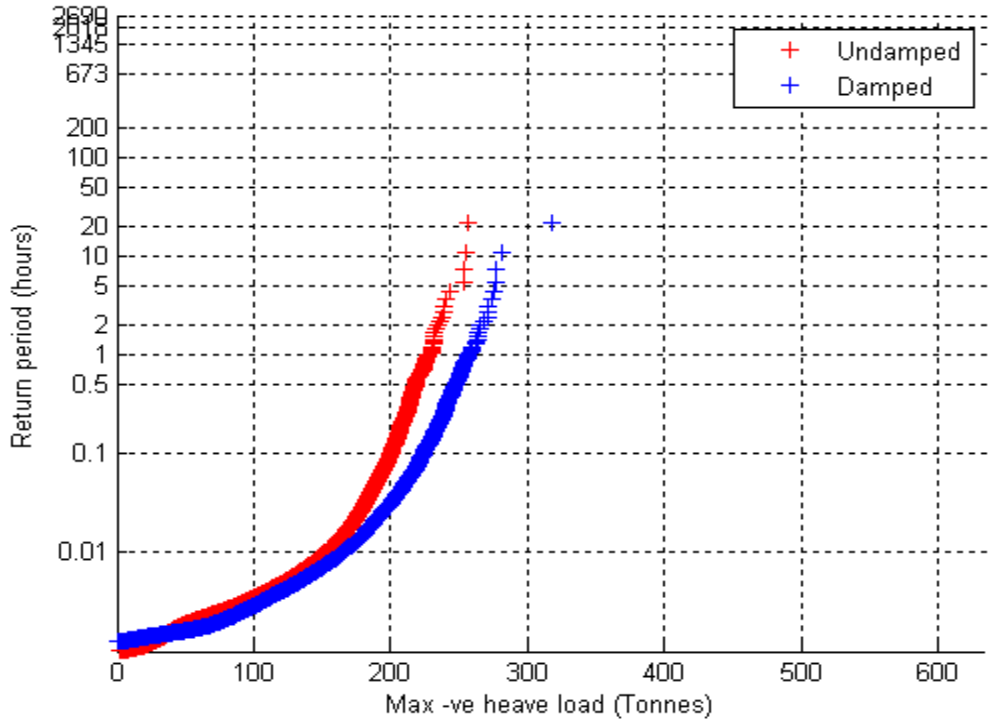

Figure 5b: Negative heave extreme value analysis plots for 24m damped and undamped flap

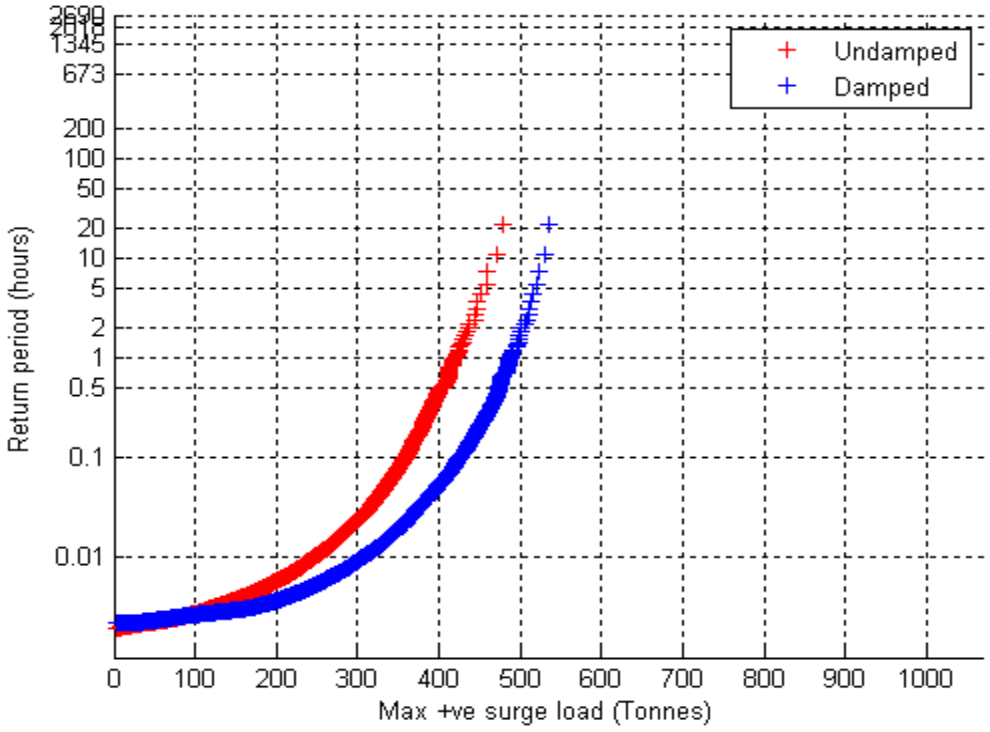

Figure 5c: Positive surge extreme value analysis plots for 24m damped and undamped flap

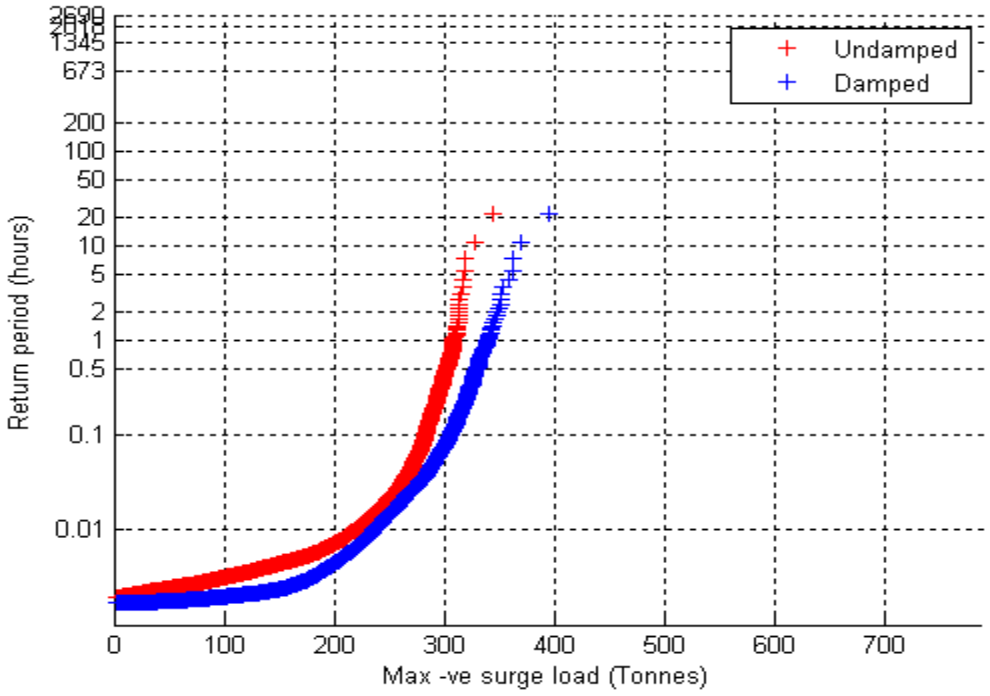

Figure 5d: Negative surge extreme value analysis plots for 24m damped and undamped flap

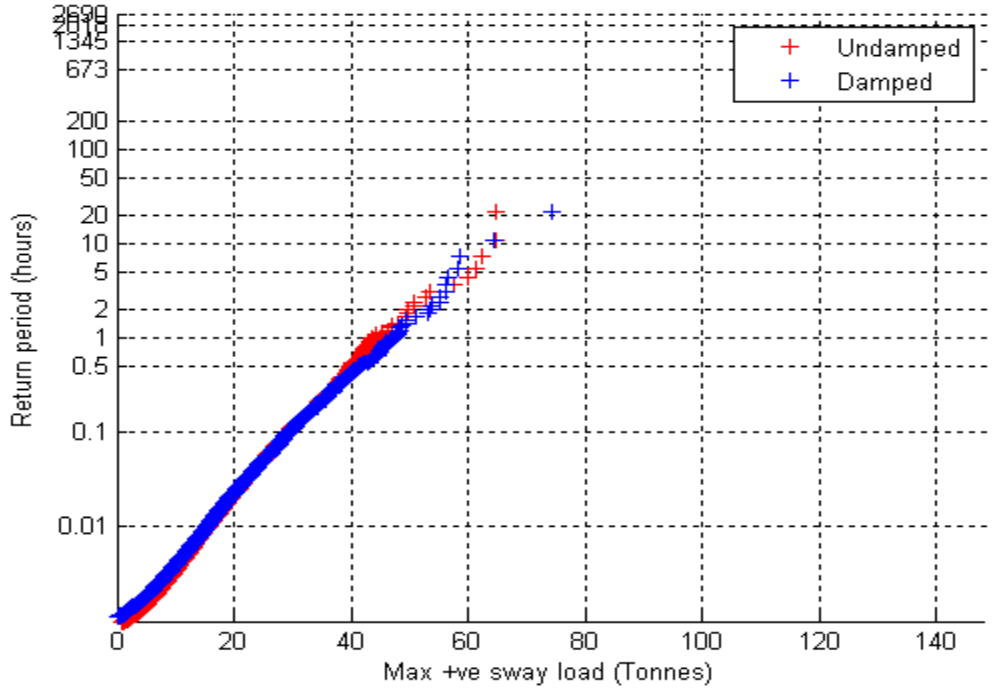

Figure 5e: Positive sway extreme value analysis plots for 24m damped and undamped flap

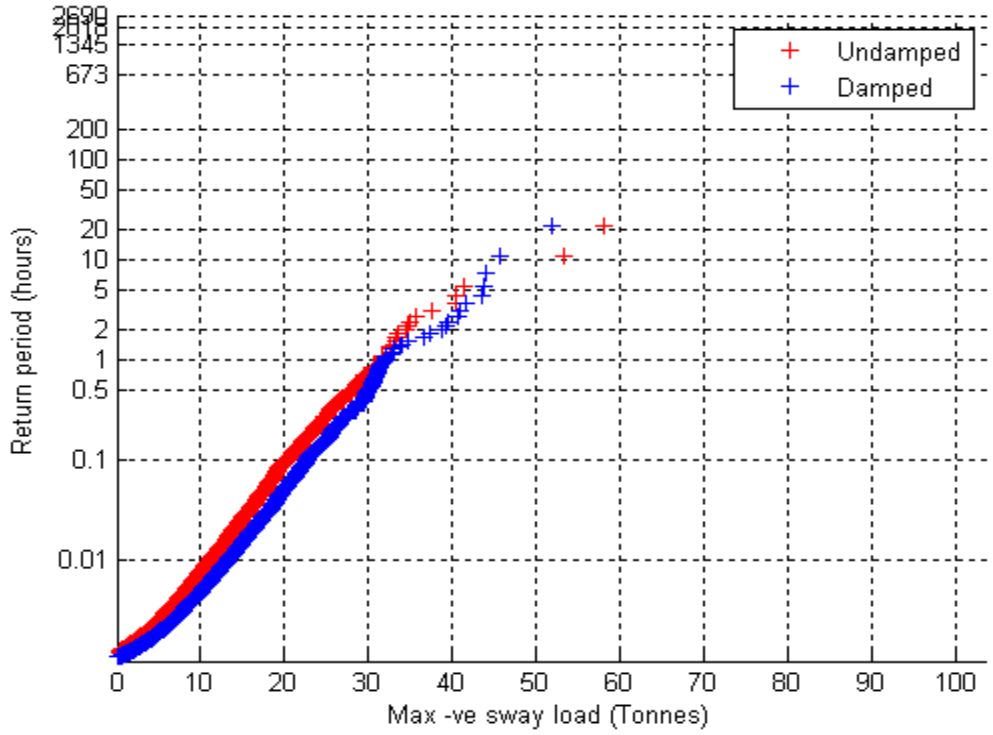

Figure 5f: Negative sway extreme value analysis plots for 24m damped and undamped flap

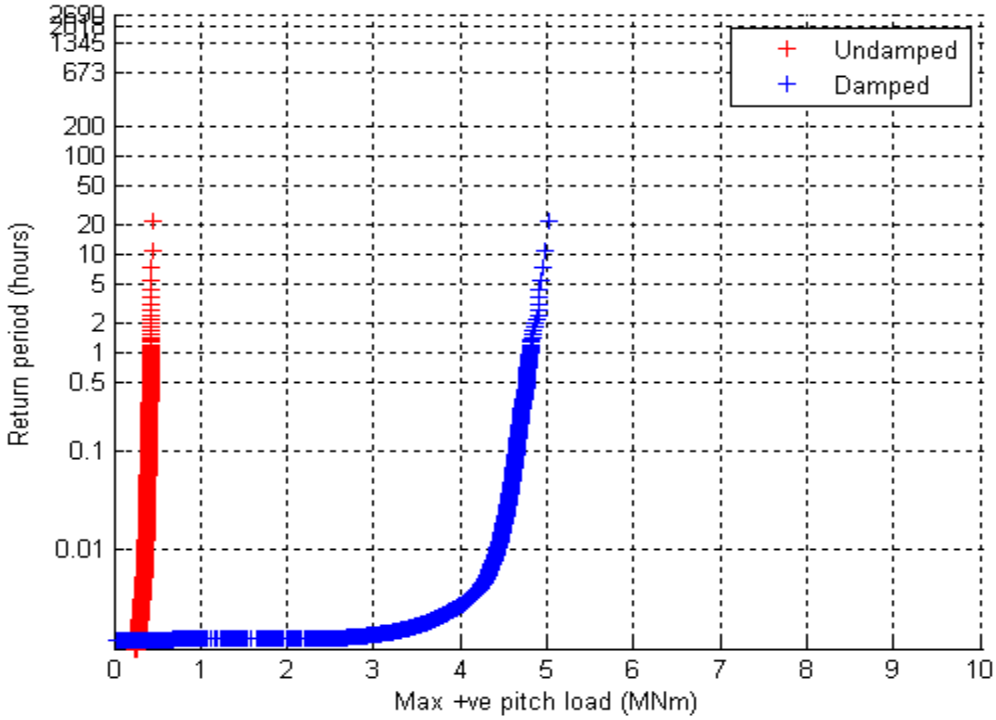

Figure 5g: Positive pitch extreme value analysis plots for 24m damped and undamped flap

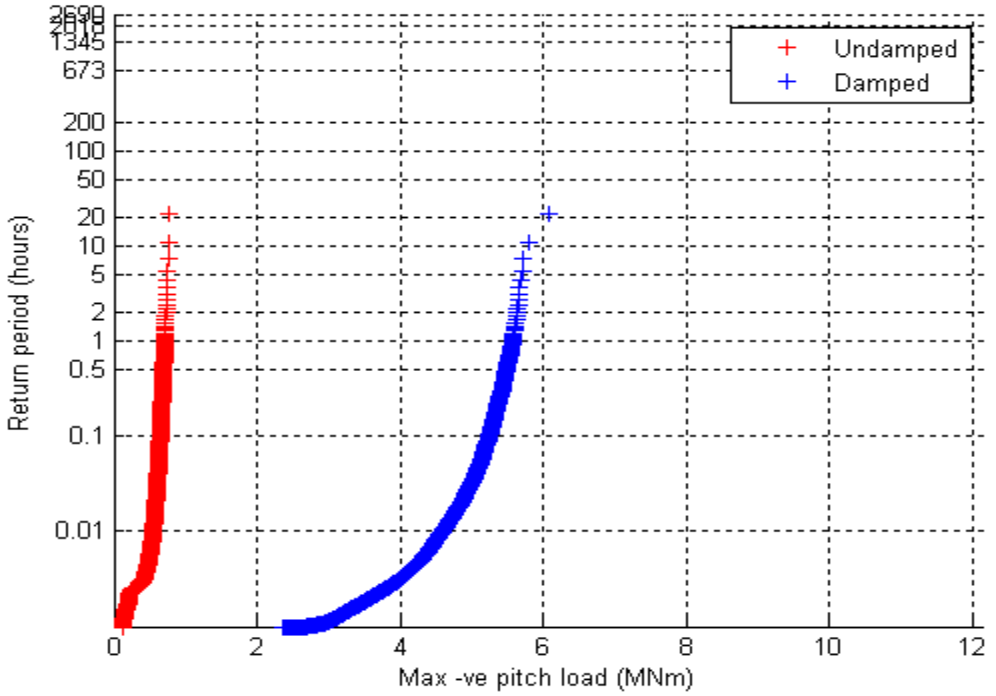

Figure 5h: Negative pitch extreme value analysis plots for 24m damped and undamped flap

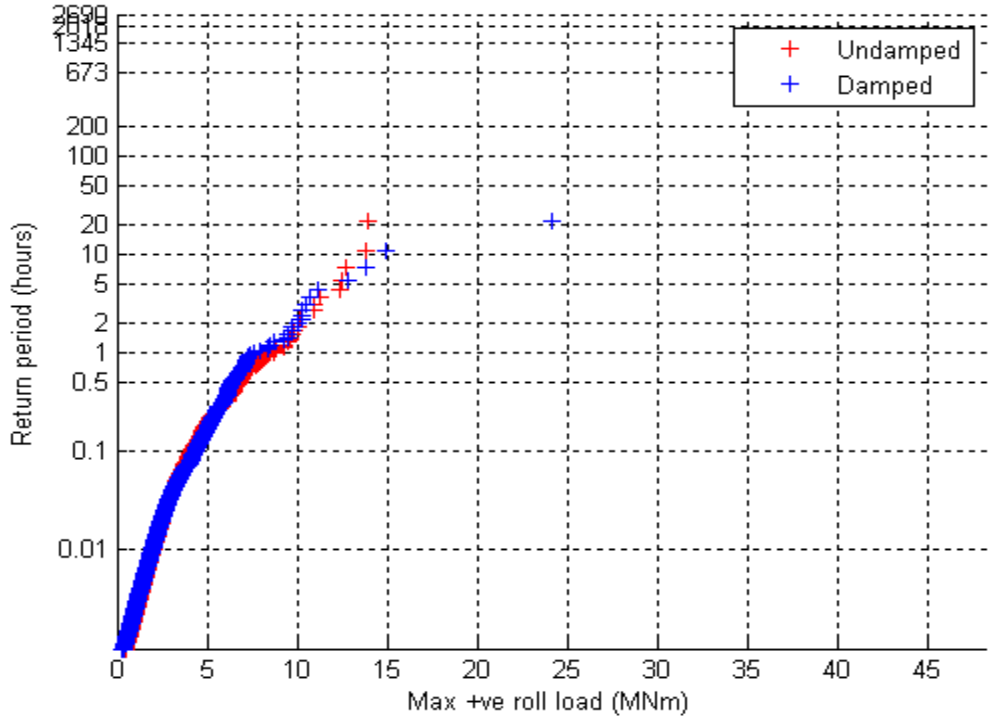

Figure 5i: Positive roll extreme value analysis plots for 24m damped and undamped flap

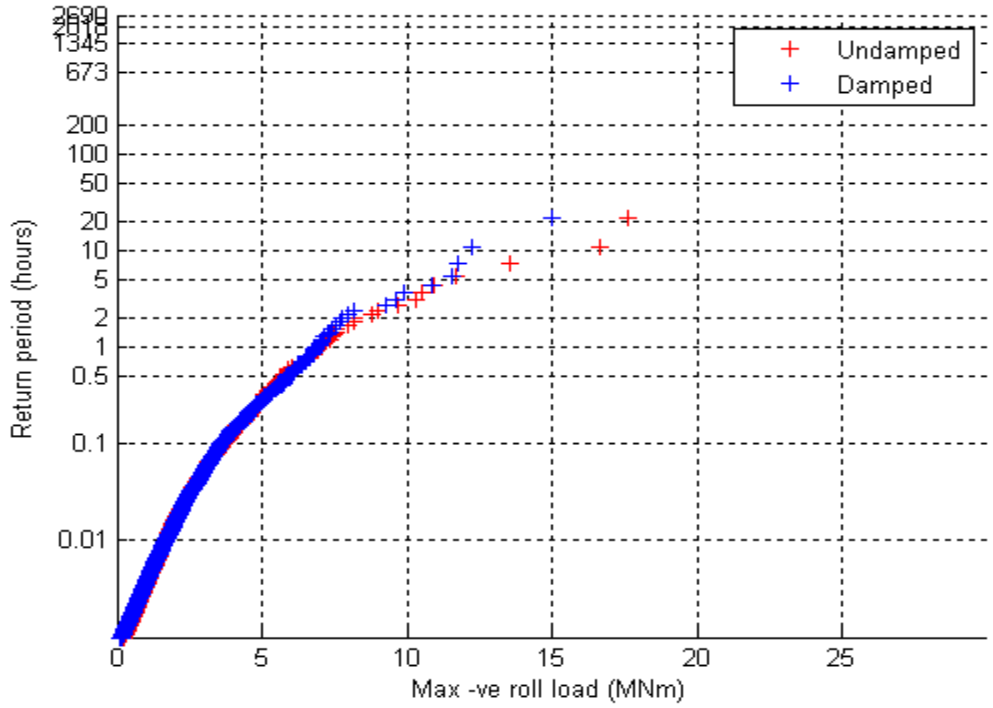

Figure 5j: Negative roll extreme value analysis plots for 24m damped and undamped flap

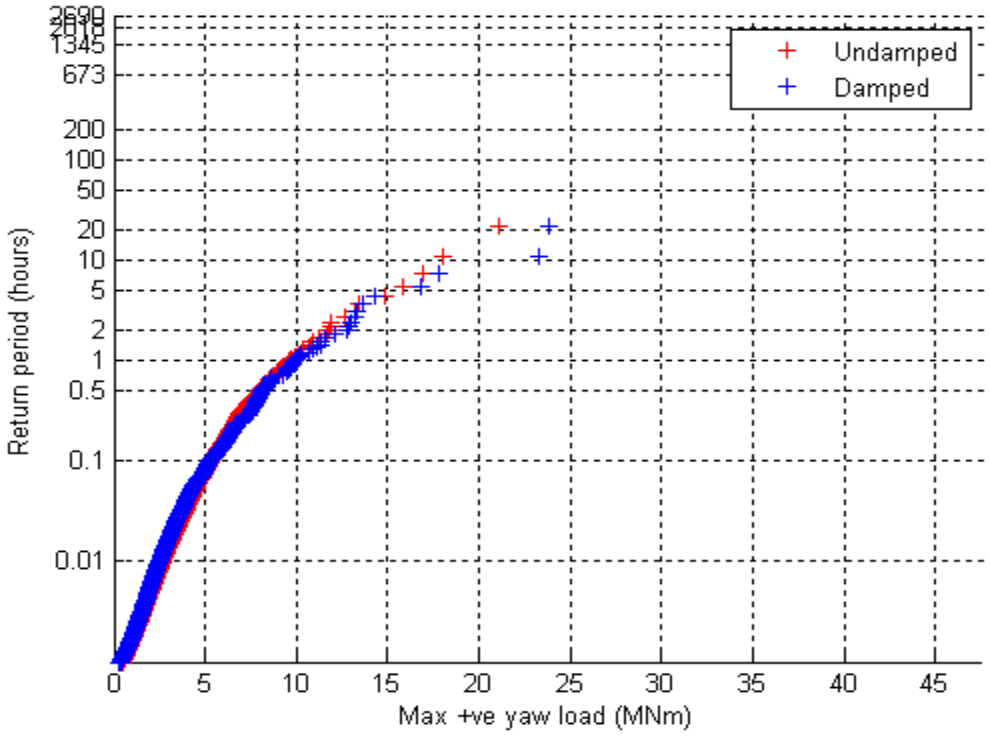

Figure 5k: Positive yaw extreme value analysis plots for 24m damped and undamped flap

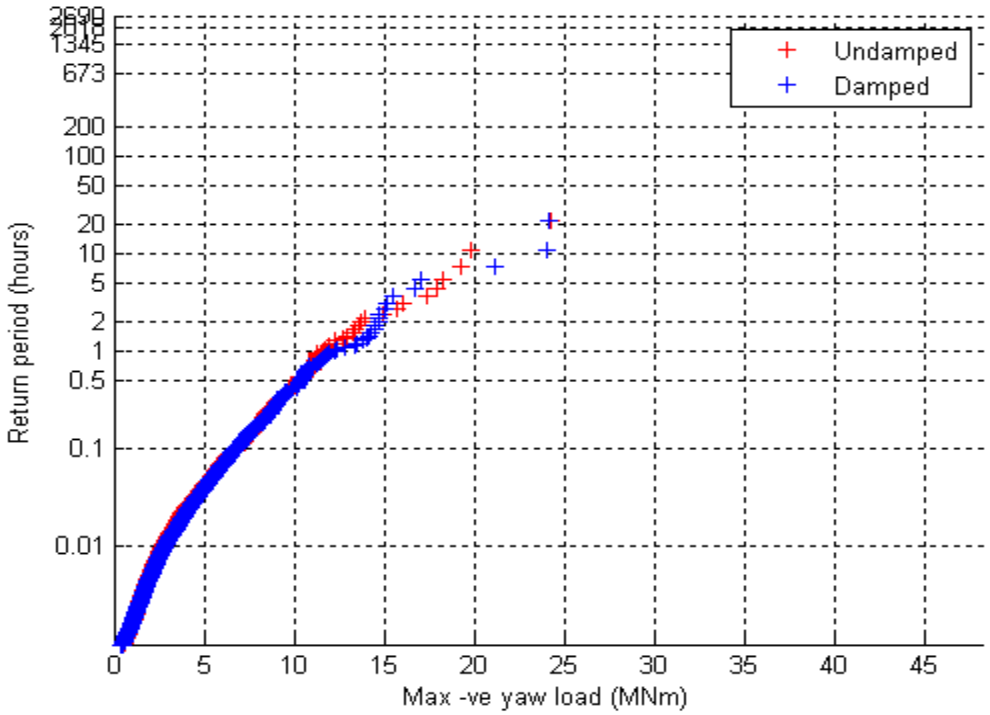

Figure 5l: Negative yaw extreme value analysis plots for 24m damped and undamped flap